INVESTIGATIONS ON METAMATERIALS BASED DUAL AND WIDE BAND MICROSTRIP PATCH ANTENNAS

Submitted in partial fulfilment of the requirements

for the award of the degree of

Doctor of Philosophy

By

Suman Nelaturi

(Roll No. 701355)

Under the Guidance of

Prof. N V S N Sarma

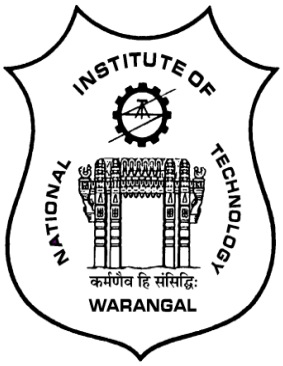

DEPARTMENT OF ELECTRONICS AND COMMUNICATION ENGINEERING

NATIONAL INSTITUTE OF TECHNOLOGY

WARANGAL – 506004, TELANGANA, INDIA

July-2018

INVESTIGATIONS ON METAMATERIALS BASED DUAL AND WIDE BAND MICROSTRIP PATCH ANTENNAS

Submitted in partial fulfilment of the requirements

for the award of the degree of

Doctor of Philosophy

By

Suman Nelaturi

(Roll No. 701355)

Under the Guidance of

Prof. N V S N Sarma

DEPARTMENT OF ELECTRONICS AND COMMUNICATION ENGINEERING

NATIONAL INSTITUTE OF TECHNOLOGY

WARANGAL – 506004, TELANGANA, INDIA

July-2018

APPROVAL SHEET

This thesis is entitled **"Investigations on Metamaterials based Dual and Wide Band Microstrip Patch Antennas"** by Mr. Suman Nelaturi is approved for the degree of **Doctor of philosophy**.

Examiners

Supervisor

Prof. N V S N Sarma

Department of Electronics & communication Engineering

NIT WARANGAL

Chairman

Prof. N Bheema Rao

Head, Department of Electronics & communication Engineering

NIT WARANGAL

Date:

Place: NIT Warangal

DECLARATION

I hereby declare that the matter embodied in this thesis entitled "**Investigations on Metamaterials based Dual and Wide Band Microstrip Patch Antennas**" is based entirely on the results of the investigations and the research work carried out by me under the supervision of **Prof. N V S N Sarma**, Department of Electronics and Communication Engineering, NIT Warangal, India. I declare that this work is original and has not been submitted in part or full elsewhere for the award of any degree or diploma to any other university.

I declare that this written submission represents my ideas in my own words and where others ideas or words have been included; I have adequately cited and referenced the original sources. I also declare that I have adhered to all principles of academic honesty and integrity and have not misrepresented or fabricated or falsified any idea/date/fact/source in my submission. I understand that any violation of the above will be cause for disciplinary action by the institute and can also evoke penal action from the sources which have thus not been properly cited or from whom proper permission has not been taken when needed.

Date: **(Suman Nelaturi)**

Place: (Roll No. 701355)

Department of Electronics and Communication Engineering

National Institute of Technology

Warangal – 506004, Telangana, India

CERTIFICATE

This is to certify that the thesis entitled "**Investigation on Metamaterials based Dual and Wide band Microstrip Patch Antennas**" which is being submitted by **Mr. Suman Nelaturi (Roll No. 701355)** in partial fulfilment for the award of the degree of **Doctor of Philosophy** to the Department of Electronics and Communication Engineering of National Institute of Technology Warangal, is a record of bonafide research work carried out by him under my supervision and has not been submitted elsewhere for any degree.

Prof. N V S N Sarma,
(Supervisor)
Dept. of ECE,
National Institute of Technology,
Warangal – 506004,
Telangana, India.

****

Dedicated to My Father

****

CONTENTS

ACKNOWLEDGEMENTS

First and foremost, I owe my deepest gratitude to my research supervisor, Prof. N. V. S. N Sarma, Professor, Department of Electronics and Communication Engineering, National Institute of Technology Warangal who has been my mentor not only in research, but for many other things in life for his help, kindness, patience, unwavering support and constant encouragement more than I could ever ask for throughout my years as a graduate student. He has been instrumental in often returning me to the correct point of view at various points during my research. His advice and guidance on matters both academic and non academic have proved invaluable time. I feel very thankful not only for the research guidance but also for the humanity shown on me.

I am also grateful to Dr. N. Bheema Rao, Head, Department of Electronics and Communication Engineering, for his invaluable assistance and suggestions that he shared during my research tenure.

I take this privilege to thank all my Doctoral Scrutiny Committee members, Prof. M. Sydulu, Professor of Department of Electrical & Electronics Engineering, and Prof. G. Radhakrishnamacharya, Professor of Department of Mathematics, Dr. L. Anjaneyulu, Professor of Department of Electronics and Communication Engineering, Dr. P. Sri Hari Rao, Associate Professor of Department of Electronics and Communication Engineering for their detailed review, constructive suggestions and excellent advice during the progress of this research work.

I am also very grateful to the former Heads of the ECE department Prof. N.V.S.N. Sarma, Dr. T. Kishore Kumar for their continuous support and encouragement. I would also like to thank all the faculty members of ECE department for their suggestions.

I thank Government of India and MHRD for financial support.

I also thank the team of Microwave wing headed by Mr. Rakesh Kumar Singh, Research Center Imarat, Hyderabad and M/s Cosmic Enterprises, Hyderabad in supporting the fabrication of Patch antennas.

I would like to acknowledge my biggest debt to my family members for their continuous support.

Suman Nelaturi

LIST OF FIGURES

LIST OF TABLES

LIST OF ABBREVIATIONS

RFID.....	Radio Frequency Identification
CP.....	Circular Polarization
LP……	Linear polarization
AR.....	Axial Ratio
WLAN.....	Wireless Local Area Network
Wi-MAX.....	Worldwide Interoperability for Microwave Access
GSM.....	*Global System for Mobile* Communications
GPS.....	*Global Positioning System*
VSWR.....	Voltage Standing Wave Ratio
PEC.....	Perfect Electric Conductor
PMC.....	Perfect Magnetic Conductor
RIS.....	Reactive Impedance Surface
HIS……..	High Impedance Surface
MUC……..	Mushroom Unit Cell
ENGTL……..	Epsilon Negative Transmission Line
MNGTL…….	Mu Negative Transmission Line
DNGTL……	Double Negative Transmission Line
UMTS.....	*Universal Mobile Telecommunications System*
ISM.	Industrial, Scientific and Medical
LTE.....	Long Term Evolution
HFSS.....	High Frequency Structure Simulator
IF.....	Indentation Factor
IA.....	Indentation Angle
ID.....	Indentation Depth
IR.....	Indentation Radius
IO.....	Iteration Order
HP.....	Horizontal Plane
VP.....	Vertical Plane
RHCP.....	Right Hand Circular Polarization

ABSTRACT

Studies on metamaterials based microstrip patch antennas are carried out for dual band and wide band operation. Metamaterials like CSRR, MUC, ENGTL VIAs and RIS are used to design compact dual band antennas and HIS is used to design miniaturized wide band antennas with linear polarization at all the bands. The edges of the square patch are replaced with fractal curves such as Minkowski, Koch, Poly and Semi circled to achieve circular polarization at patch mode band.

Initially the proposed antennas are designed using HFSS Electromagnetic Simulator and later simulation results are verified experimentally. A new class of compact dual band patch antennas based on CSRR is designed with good impedance and CP bandwidth at patch mode band and less bandwidth at left hand band. Another class of dual band patch antennas are investigated based on MUC which are producing good impedance bandwidth at both the bands. The third class of dual band patch antennas studied are based on ENGTL VIAs which are responsible for good return loss bandwidth at both the bands and good CP bandwidth at patch mode band. The fourth class of dual band patch antennas demonstrated is based on RIS which are compact in size and are able to produce good return loss bandwidth at both the bands and the CP bandwidth at patch mode band.

The antennas mentioned above all operate at 2.4 GHz and 3.4 GHz frequencies and are useful for Wi-Fi and Wi-MAX applications. The fifth class of patch antennas is for wide band operation based on HIS working at 2.4 GHz for Wi-Fi application. The obtained impedance bandwidth is 15% and the 3-dB axial ratio bandwidth is 4%.

The dual band and wide band antennas proposed in this thesis provide good impedance bandwidth at both the bands and good circular polarization bandwidth at patch mode band. These antennas are best suitable for handheld gadgets which support wireless applications. The ideas given in this thesis are useful to the design engineers who are working on compact dual band and wide band microstrip patch antennas.

Chapter 1

Introduction

Antennas are the most critical sub systems for the designers of wireless devices, which have experienced an exceptional quick growth. Some of the conventional radiating elements are wire antennas, travelling wave antennas, reflector antennas, log-periodic antennas, array antennas, etc. Several unwanted attributes of the conventional antennas are: long design line, disturb aerodynamic profile, etc. Furthermore, it is tough to design regular antennas to execute more than one function, such as multi frequency and dual-polarization. Antennas which do not obtrude from a surface are very much advisable for vehicles like airplanes, missiles, and spacecrafts which are undergoing rapid growth. This led to the invention of microstrip patch antenna.

The first microstrip patch radiator design is proposed and executed by Deschamps in the year 1953 [1]. These antennas are made up of a region of metallization assisted by a thin dielectric substrate above a ground plane and fed against the ground at suitable position. The structure of the patch can in principle be arbitrary, however, in practice: rectangle, square, triangle, circle, and annular ring are usual shapes. The four feeding methods that are used for patch antennas are microstrip line feed, coaxial probe feed, aperture-coupled feed and proximity coupled feed. These antennas can be used only in low power applications because of their low power handling capability, and normally for reception [2].

A Patch antenna which can cater multiple wireless applications is the most desirable one for recent wireless communication systems. During the initial days multiband antennas are designed using slits, slots, corner truncation and multi substrate technology. The low frequency band is designed first and the remaining higher bands will come after this with the help of added discontinuities. The dimensions of the patch antenna are calculated proportional to the lower frequency band which will demanded larger size of the patch antenna. But today manufacturers are looking for miniaturized multifunctional antennas to suit the small size available within the handheld wireless devices.

To minimize the size of the multi band patch antennas metamaterials are the perfect choice for the designers [3]. Metamaterials are the artificially made materials having

electromagnetic properties which are not existing in the nature. The backward wave propagation is the special property for these metamaterials. Due to this left handed nature of metamaterials the dimensions of the patch are chosen with reference to upper frequency band such that the size of the antenna becomes compact.

Metamaterials are of several types, out of which Epsilon Negative Materials (ENG), Permeability Negative Materials (MNG), Double Negative Materials (DNG) are the major categories [4]. Vertical metallic VIAs are the example materials for ENG type. Split Ring Resonators (SRRs) are the examples for MNG type. The materials under DNG category are Mushroom Unit Cell (MUC), Reactive Impedance Surface (RIS) and High Impedance Surface (HIS). In metamaterials terminology the frequency which is resonating with reference to patch length is called as patch mode band (n=+1) whereas the frequency with reference to metamaterial is called as left hand band (n=0).

Microstrip structure having conventional patch shapes with classical feed designs radiate linearly polarized electromagnetic waves. In such cases the receiving and transmitting antennas must be aligned properly to receive signals. To overcome the reflectivity, absorption, phasing issues, multi-path fading, and inclement weather problems and to make wave propagation independent of inclination of the transmitting and receiving antennas, Circularly Polarized (CP) antennas are preferred over linearly polarized antennas. To produce circular polarization, two orthogonal components of currents are required. These components must be equal in amplitude, but shifted in phase by ±90°. Circular polarization can be achieved with various feeding arrangements.

The requirements of two patch mode currents can be achieved by slightly disturbing the patch at proper location. In general the modification can be done by introducing slot or other truncated segment. So, generation of CP with single feed reduces the space occupied by the antenna and avoids the external polarizer. If asymmetry is inserted to the square patch in the corners, the antenna has to be fed along either of the sides. Else if the perturbation is introduced at the sides of the patch, the antenna should be fed along the diagonal. However, conventional designs yield low CP bandwidth (<1%). But, the modern handheld devices demand wider CP bandwidth (>1%) at multiple bands for secure data transmission. This can be accomplished using fractal shaped radiators.

To increase the CP bandwidth fractal concept can be attempted. The idea of fractal was first introduced by Benoit Mandelbrot in 1975 [5]. He has used the term “fractal” while

describing the complex shapes. A fractal is a mathematical set that displays repeating same pattern at different levels. If the repetitiveness is of same scale at different levels it is called self-similar fractal. If this property is different at various levels then it is known as self-affinity fractal.

So in this thesis an attempt is made to design dual band and wide band patch antennas with multifunctional capability using metamaterials and fractals for handheld devices.

For the design of dual band patch antennas the first attempt here is usage of Complementary Split Ring Resonators (CSRRs). CSRRs are the dual structures of Split Ring Resonators (SRRs) based on Babinet's principle. SRR is constructed with pair of enclosed loops having breaks in them at opposite ends. The loops are made of copper and have a small gap between them [6, 7 and 8].

You-Quan Li, Hui Zhang, Xi Chen, Nai-Chang Yuan and Yun-Qi Fu introduced CSRR loaded dual band rectangular patch antenna [9]. It is resonating at 4.04 GHz and 4.84 GHz with a 10-dB return loss bandwidth of <0.5% at both the bands. However the antenna is resonating with only Linear Polarization at both operating frequencies.

J X Niu proposed CSRR loaded dual band patch antenna [10]. The antenna is made up of two rectangular metal patches separated by small distance and a CSRR loaded in the ground plane. The antenna is resonating at 0.9 GHz and 1.8 GHz with the impedance bandwidth of 1% and 1.5%. However the antenna is resonating with Linear Polarization at both operating frequencies.

J. G. Joshi and Shyam Pattnaik came up with electrically small patch antenna based on SRR for single band of operation [11]. The antenna structure is composed of a rectangular patch along with two square SRRs. The operating frequency of the antenna is 9.51 GHz with 10-dB return loss bandwidth of 5.3%. However this antenna is limited to single band and bandwidth is also less.

Wenquan Cao et al reported a single band probe feed patch antenna [12]. The antenna structure is designed with a square patch and two CSRRs loaded in the ground plane. The resonating frequency of the antenna is 2 GHz with a 10-dB return loss bandwidth of less than 1%. However the antenna is designed for single band and bandwidth is also less.

Yuandan Dong and Tatsuo Itoh have presented dual band patch antenna [13]. The antenna structure consists of rectangular radiating patch loaded with two CSRRs and the radiating patch is placed above RIS, which is shown in the Fig. 1.1. The operating frequencies of the antenna are 2.41 GHz and 3.82 GHz respectively. However the 10-dB return loss bandwidth is dismal.

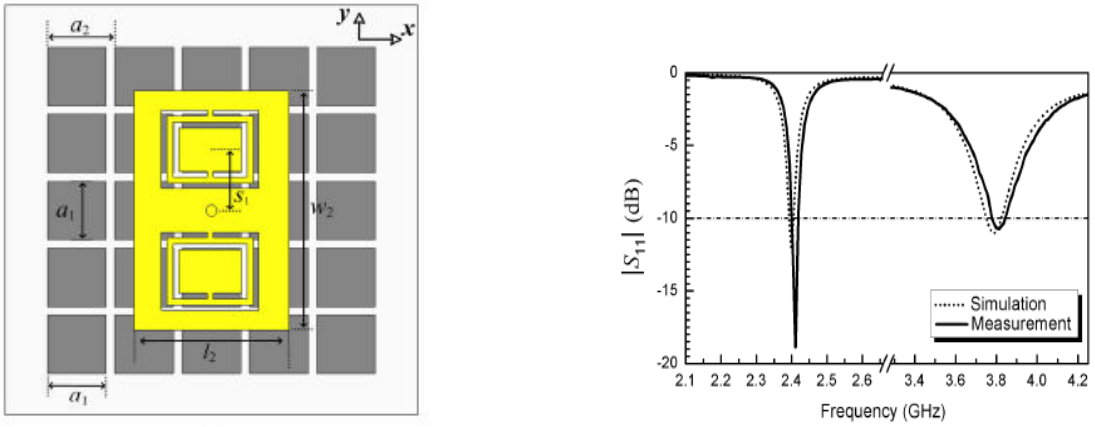

(a) (b)

Fig. 1.1 (a) Geometry of the CSRR loaded microstrip patch antenna over RIS (b) Reflection coefficient characteristics of the antenna

N. Ortiz, M. Sorolla and F. Falcone described line fed dual band patch antenna [14]. The antenna is made up of a rectangular patch loaded with CSRR, which is shown in the Fig. 1.2. The resonating frequencies of the antenna are 4.19 GHz and 4.808 GHz respectively. However, the size of the antenna is more and the impedance bandwidth is also less (<1%).

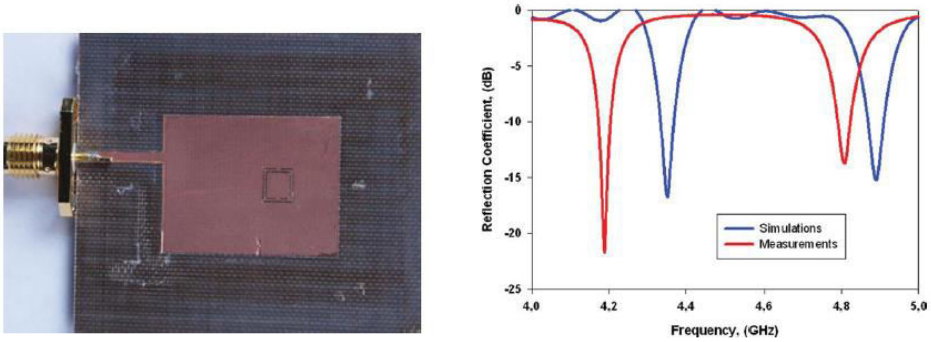

(a) (b)

Fig. 1.2 (a) Geometry of the CSRR loaded microstrip patch rectangular patch antenna (b) Return loss characteristics of the antenna

Y. Xie, L. Li, C. Zhu, and C. Liang analyzed dual band line feed square patch antenna [15]. The radiator is composed of a square radiating patch. Three CSRRs are loaded in the ground plane. The center frequencies of the patch antenna are 3.73 GHz and 5.23 GHz with the 10-dB return loss bandwidth of 1.2% and 1.5% respectively. However, only LP is realized at both the ends.

Jaegeun Ha, and Jaehoon Choi have attempted dual band patch antenna [16]. The antenna structure is designed with an inter digital capacitor loaded patch and the circular CSRR loaded in the ground plane. The resonating frequencies are 3.2 GHz and 3.8 GHz respectively. The 10-dB return loss bandwidth of the antenna is very less (<0.5%) at zeroth order frequency and 6.8% at patch mode frequency. However there is no resonance at zeroth order frequency and the bandwidth is also less at patch mode band.

Noelia Ortiz, Francisco Falcone, and Mario Sorolla investigated dual band patch antenna [17]. It is a rectangular radiating patch loaded with CSRR and the antenna is shown in the Fig. 1.3. The operating frequencies of the patch antenna are 4.19 GHz and 4.808 GHz respectively. The 10-dB return loss band width at zeroth order band is 1.2% and is 1.5% at patch mode band. However the size of the antenna is high and the patch mode bandwidth is also not of realizable width.

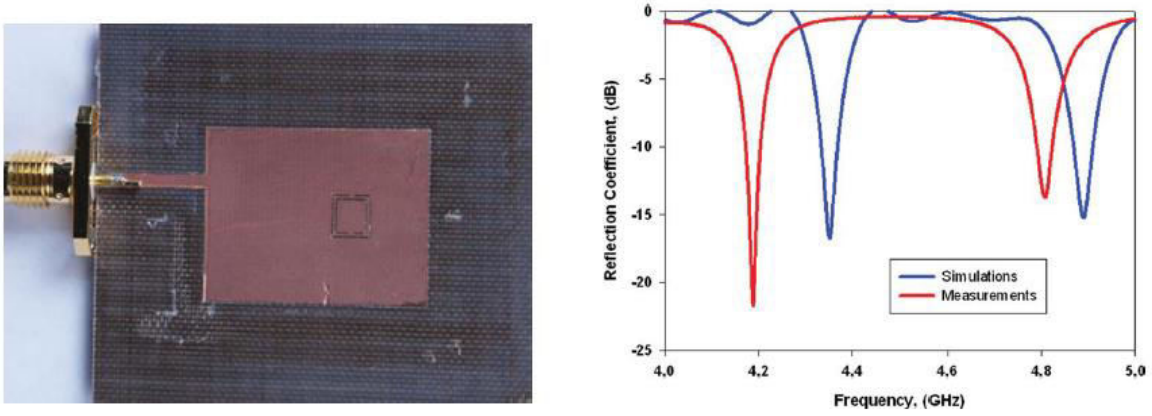

(a) (b)

Fig. 1.3 (a) Geometry of the CSRR loaded rectangular patch antenna (b) Return loss characteristics of the antenna

J. Malik and M. V. Kartikeyan nominated dual band patch antenna [18]. It has a square patch loaded with circular CSRR and L shaped slot etched ground plane. The resonating

frequencies of the patch are 3.5 GHz and 5.8 GHz respectively. The impedance bandwidth is around 200 MHz at both the bands which is minimal.

Yuandan Dong, Hiroshi Toyao, and Tatsuo Itoh introduced dual band patch antenna based on CSRR [19]. It is composed of a rectangular patch antenna loaded with two CSRRs and the ground plane is replaced by RIS. The operating frequency bands are 2.386 GHz and 2.958 GHz respectively. The 10-dB return loss bandwidth is 1.32% for the first band and 2.68% for the second band. However the structure is complex and the impedance bandwidth is also less.

S.C. Basaran, U. Olgun and K. Sertel discussed triple band patch antenna based on CSRR [20]. The antenna is constructed with a rectangular patch loaded with two CSRRs side by side and is fed by line feed. It is working at 2.4 GHz, 3.4 GHz and 5.8 GHz. However, the antenna is unable to produce 3-dB axial ratio bandwidth.

Debdeep Sarkar, Kushmanda Saurav, and Kumar Vaibhav Srivastava suggested dual band patch antenna based on CSRR [21]. The antenna is designed with a rectangular radiating patch loaded with two CSRRs at the top edge. It is fed by coaxial probe feed. The antenna is working at 3.4 GHz and 5.8 GHz frequencies with impedance bandwidth of around 5% at each band. However the antenna structure is complex and is not easy to design.

J. G. Liang, Z. J. Song, L. J. Yu, and X. F. Zhang demonstrated triple band patch antenna [22]. The antenna consists of two rectangular metallic patches and a triangular CSRR loaded ground plane. The operating frequency bands of the patch antenna are 4.45 GHz, 5.55 GHz and 7.35 GHz respectively. The 10 dB impedance bandwidth of the antenna are 130 MHz, 350MHz and 110MHz respectively. However the antenna is suitable for only one application among the three bands of handheld wireless devices.

Noelia Ortiz, Juan Carlos Iriarte, Gonzalo Crespo and Francisco Falcone examined dual band patch antenna [23]. The antenna is made up of a rectangular patch antenna loaded with circular CSRR and is shown in the Fig. 1.4. The resonant frequency bands of the antenna are 4.95 GHz and 5.3 GHz respectively. The return loss bandwidth of the antenna is 1.2% at lower band and 1.5% at upper band. However the size of the antenna is more and the bandwidth at patch mode band is not sufficient.

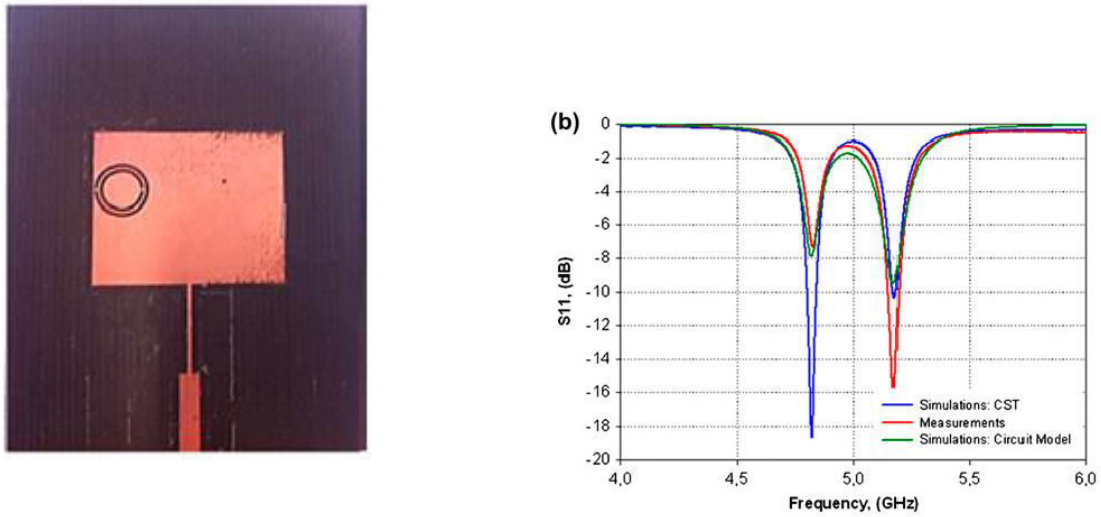

(a) (b)

Fig. 1.4 (a) Geometry of the CSRR loaded rectangular patch antenna (b) Reflection coefficient characteristics of the antenna

Wael Ali, Ehab Hamad, Mohamed Bassiuny and Mohamed Hamadallah suggested triple band patch antenna [24]. The antenna is constructed with a rectangular line feed patch and the ground plane with two circular CSRRs and one square CSRR. The structure and the return loss characteristics are shown in the Fig. 1.5. The operating frequencies of the patch antenna are 2.45 GHz, 3.56 GHz and 5.62 GHz respectively. However the impedance bandwidth is quite small.

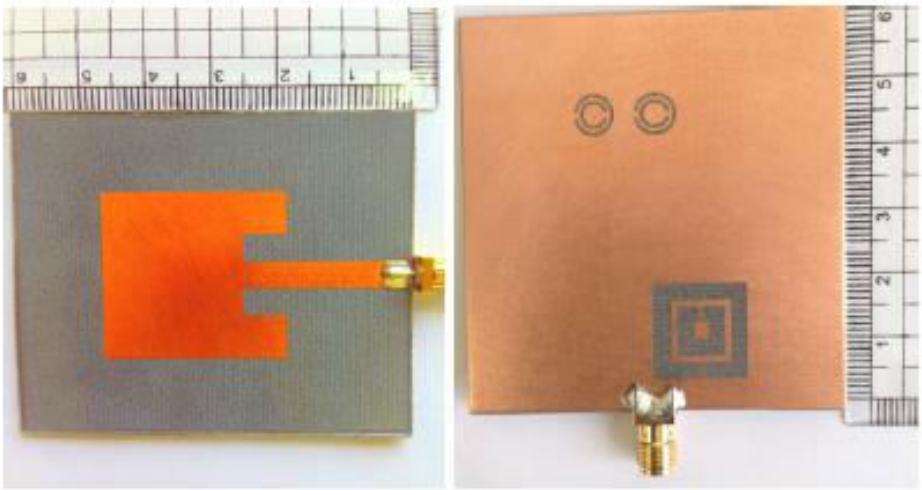

(a)

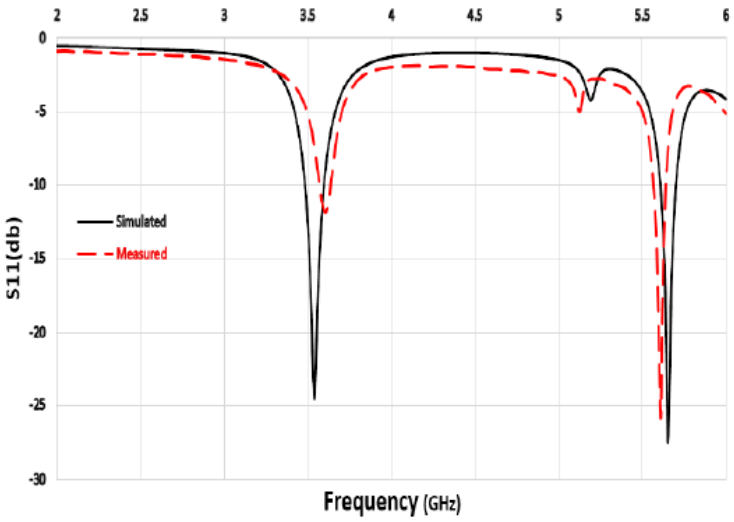

(b)

Fig. 1.5 (a) Top and bottom views of Line feed rectangular patch antenna (b) Return loss characteristics

Mohamed A. Bassiuny, Ehab K. I. Hamad, Wael A. Aly, and Mohamed Z. M. Hamdallah designed dual band antenna [25]. The antenna structure consists of a rectangular patch antenna and circular CSRR loaded ground plane. The structure along with return loss characteristics are shown in the Fig. 1.6. The 10-dB return loss bandwidth of the patch is 119.2 MHz at lower band and 45 MHz at upper band. However, the antenna is suffering from low impedance bandwidth.

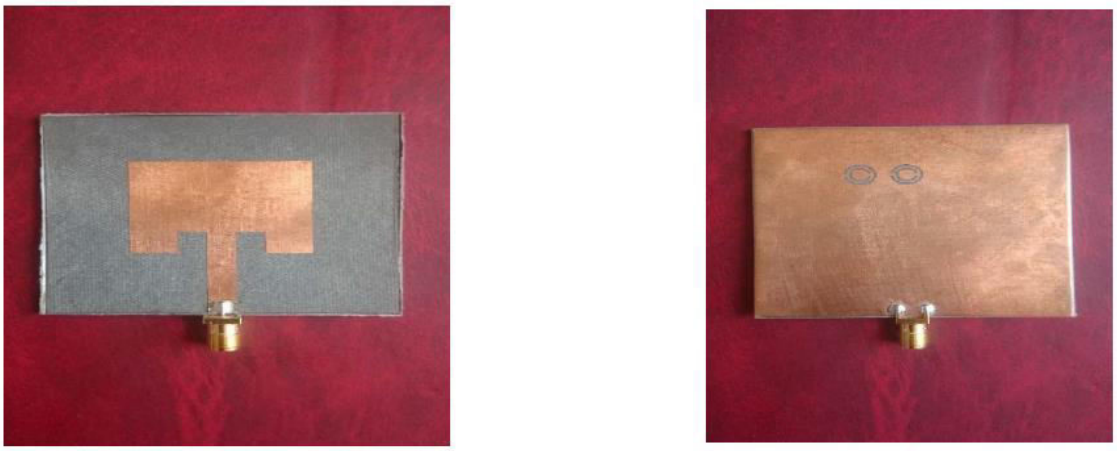

(a) (b)

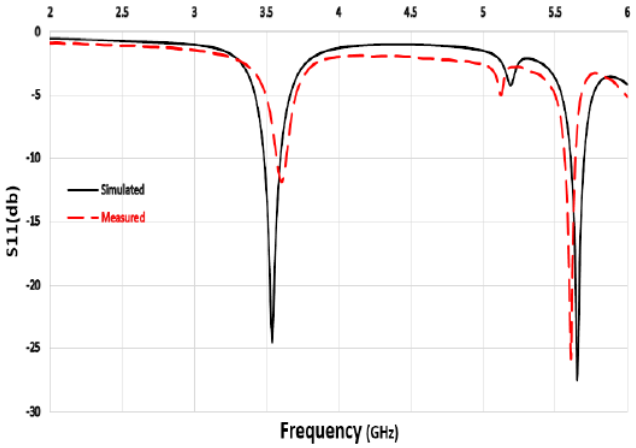

(c)

Fig. 1.6 Rectangular patch antenna (a) Top view (b) Bottom view (c) Return loss characteristics

Ming-Chun Tang, Hao Wang, Li Guo, Xiaoping Zeng, Hong Liu, and Youbing Pang discussed dual band patch antenna based on SRR [26]. The antenna is made up of a circular radiating patch surrounded by a circular SRR and is shown in the Fig. 1.7. The operating frequencies of the patch are 1.602 GHz and 4.63 GHz respectively. Though realized bandwidth at upper band is 4.3% the lower band has very narrow bandwidth.

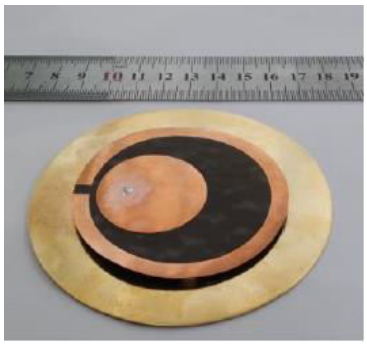

(a)

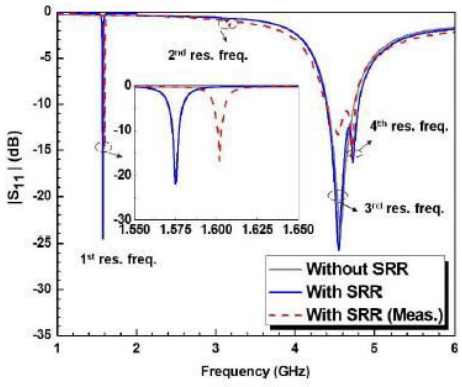

(b)

Fig. 1.7 (a) Circular patch antenna surrounded by Circular SRR (b) Return loss characteristics

The antennas mentioned above [6] – [26] are single feed dual band microstrip antennas based on CSRR. The return loss bandwidth at both the bands is very low (<1%). In some of those antenna structures, CSRR is loaded into the patch as well as

into the ground plane. However, the 3-dB axial bandwidth at patch mode band of most these approaches is very narrow (<1%) and minimum AR value is also not close to 0-dB.

To achieve good impedance bandwidth at both the bands and CP bandwidth at patch mode band the second attempt is made using of MUCs. According to Victor Veselago the materials for which both the parameters permittivity (ε) and permeability (μ) are negative are known as Double Negative materials. Mushroom Unit Cells and Inter digital capacitors are the best examples for these types of materials. These materials produce the shunt inductance due to current carrying copper wire and the series capacitance due to gap between the radiating surface and ground plane [27 and 28].

Francisco Javier Herraiz Martinez, Vicente Gonzalez-Posadas, Luis Enrique Garcia-Munoz and Daniel Segovia-Vargas proposed dual band patch antenna [29]. The antenna consists of a square patch radiator loaded with four MUCs. The operating frequencies of the patch are 1.81 GHz and 2.20 GHz respectively. The impedance bandwidth is less than 1%. However the antenna is suffering from high size and low bandwidth.

Jiang Xiong, Hui Li, Yi Jin, and Sailing He demonstrated dual band patch antenna based on DNG materials like Mushroom Unit Cell [30]. The antenna is loaded with MNG as well as DNG materials. The antenna is working at 0.9 GHz and 1.8 GHz with negligible impedance bandwidth. However the structure is too complex.

Yuandan Dong, Hiroshi Toyao, and Tatsuo Itoh investigated dual band patch antenna based on Mushroom Unit Cell [31]. The antenna consists of a rectangular patch antenna loaded with four MUCs and implemented over RIS. The antenna is operating at 2.4 GHz and 3 GHz frequencies with impedance bandwidth of less than 2% at each band. However the antenna is suffering from low impedance bandwidth.

Cherl-Hee Lee, Jonghun Lee, Dong-Sik Woo and Kang-Wook Kim presented line feed single band patch antenna [32]. The structure is made up of three U- shaped slot loaded MUCs. The operating frequency of the patch is 9.37 GHz. The 10-dB return loss bandwidth is 450 MHz. However the antenna is unable to produce dual band operation.

Seung Tae Ko, Byung Chul Park, and Jeong Hae Lee described probe feed dual band patch antenna [33]. The structure consists of corner truncated square patch antenna loaded with four triangular MUCs. The antenna is working at the center frequencies 3.03 GHz and 3.77 GHz with impedance bandwidth of 3.63% and 0.5% respectively. But the antenna is suffering from poor bandwidth at second band.

Nasimuddin, Xianming Qing, and Zhi Ning Chen discussed probe fed single band CP patch antenna [34]. The antenna is constructed with a square patch antenna loaded with four MUCs. The operating frequency of the patch antenna is 1.61 GHz with a return loss bandwidth of 90MHz. However the antenna is unable to resonate at second band and even the bandwidth at resonant frequency is less.

Kushmanda Saurav, Debdeep Sarkar and Kumar Vaibhav Srivastava have studied the dual band patch antenna [35]. The structure consists of a square patch antenna loaded with modified MUC. The antenna and the return loss characteristics are shown in the Fig. 1.8. The center frequencies of the antenna are 2.31 GHz and 2.56 GHz with an impedance bandwidth of 3.5% and 1.97%. However the antenna is suffering from low bandwidth at each band.

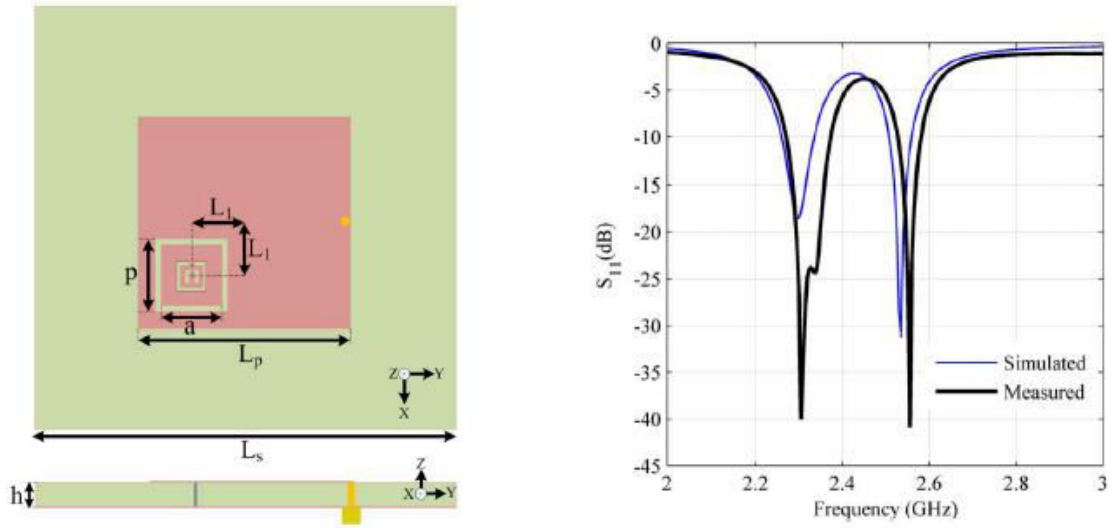

(a) (b)

Fig. 1.8 (a) Square patch antenna loaded with modified MUC (b) Return loss characteristics

Seung Tae Ko and Jeong Hae Lee demonstrated single band coaxial probe feed patch antenna [36]. The patch structure is made up of a rectangular patch antenna loaded with a rectangular

MUC. The resonant frequency of the patch is 5.75 GHz with impedance bandwidth of 3.3%. However the antenna is unable to produce dual band operation and wide bandwidth.

Binfeng Zong, Guangming Wang, Cheng Zhou, and Yawei Wang introduced dual band patch antenna [37]. The antenna consists of a square patch antenna loaded with four MUCs, which is shown in the Fig. 1.9. The operating frequencies of the patch antenna are 2.76 GHz and 5.23 GHz with a return loss bandwidth of 1.44% and 3.05% respectively.

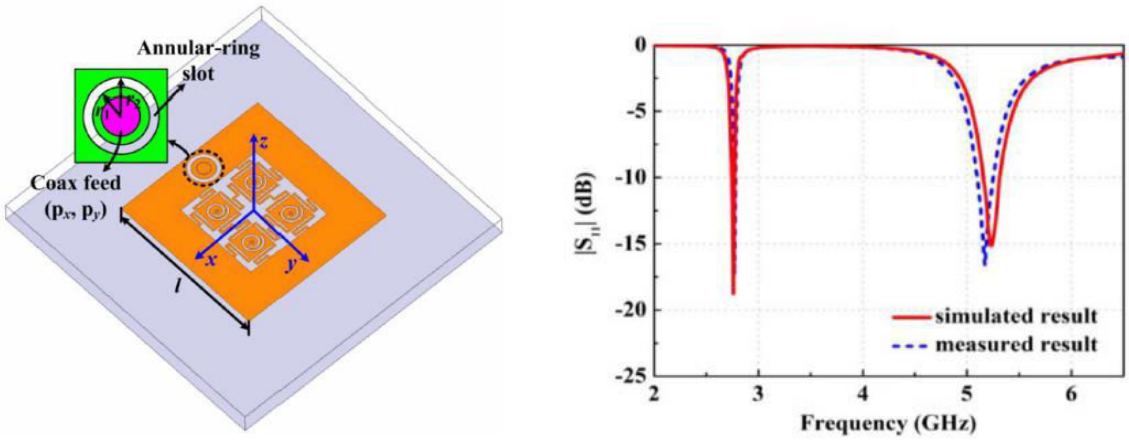

(a) (b)

Fig. 1.9 (a) Square patch antenna loaded with modified MUC (b) Return loss characteristics

Xi-Wang Dai, Tao Zhou, and Guan-Feng Cui examined double band patch antenna [38]. The circular patch antenna is surrounded by MUCs. The resonant frequencies of the patch are 4.01 GHz and 5.24 GHz respectively. The antenna geometry and the return loss characteristics are shown in the Fig. 1.10. The impedance bandwidth of the antenna is 0.75% at lower band and is 20% at upper band. But the antenna size is more and bandwidth at lower band is less.

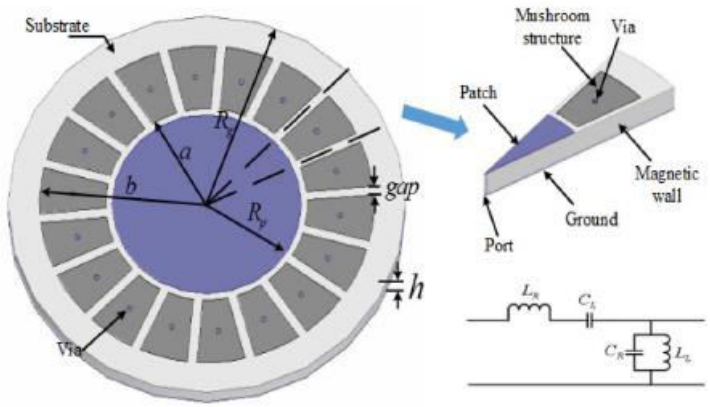

(a)

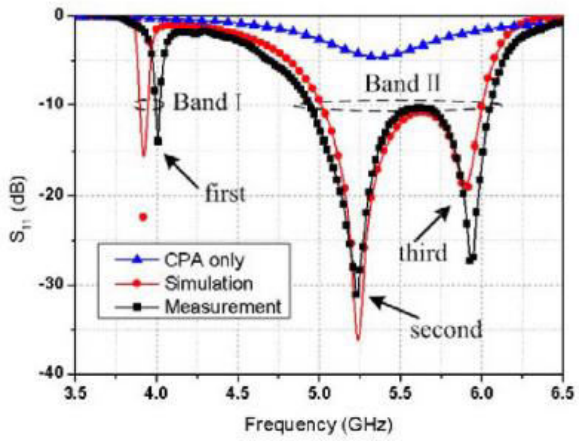

(b)

Fig. 1.10 (a) Square patch antenna loaded with modified MUC (b) Return loss characteristics

Yan sen, Ping Jack and Vandenbosch designed dual band patch antenna [98]. The antenna structure consists of rectangular patch antenna loaded with two rectangular Mushroom Unit Cells. The antenna structure and the return loss characteristics are shown in the Fig. 1.11. The antenna is operating at 2.4 GHz and 5.2 GHz frequencies respectively. However the antenna is suffering from low impedance bandwidth at both the bands.

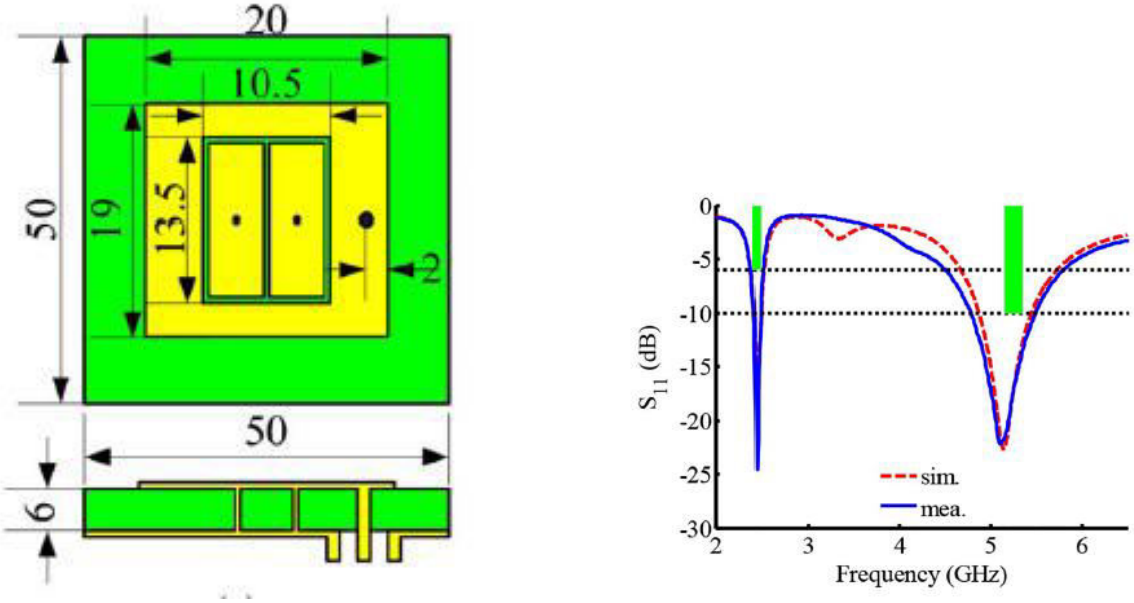

(b) (b)

Fig. 1.11 (a) Rectangular patch antenna loaded with MUCs (b) Return loss characteristics

The antennas discussed above [29] – [38] and [98] are MUC based single feed dual band microstrip antennas. The return loss bandwidths at both the bands are very low (<2%). In most of those antenna structures, MUC is loaded into the patch. However, the 3-dB axial ratio bandwidth at patch mode band of most these approaches is very narrow (<1%) and minimum AR value is also not close to 0-dB.

The third attempt to improve the CP bandwidth at patch mode band is to load with VIAs. According to Victor Veselago the second quadrant materials are known as Epsilon Negative materials where the permittivity (ε) is negative and the permeability (μ) is positive for these materials and the examples are vertical metallic VIAs inserted between radiating surface and the ground plane. These materials produce the shunt inductance and the radiation pattern at the frequency which is produced due to current at these materials is dipolar [39, 40, 41 and 42].

Hangfei Tang and Xiaopeng Zhao proposed single band circular patch antenna [43]. A circular radiating patch loaded with four vertical metallic VIAs along the circumference of the antenna. The resonant frequency of the patch antenna is 5.17 GHz with the return loss bandwidth of 116 MHz. However the antenna is unable to produce another band.

S. Yoo and S. Kahng presented double band patch antenna [44]. The antenna consists of a circular patch antenna capacitively coupled to a circular ring MUC. The structure along with the return loss characteristics are shown in the Fig. 1.12. The operating frequencies of the patch are 2.2 GHz and 2.5 GHz respectively. The impedance bandwidth of the patch is not mentioned for both the bands. However the size of the antenna is more to get the proposed result.

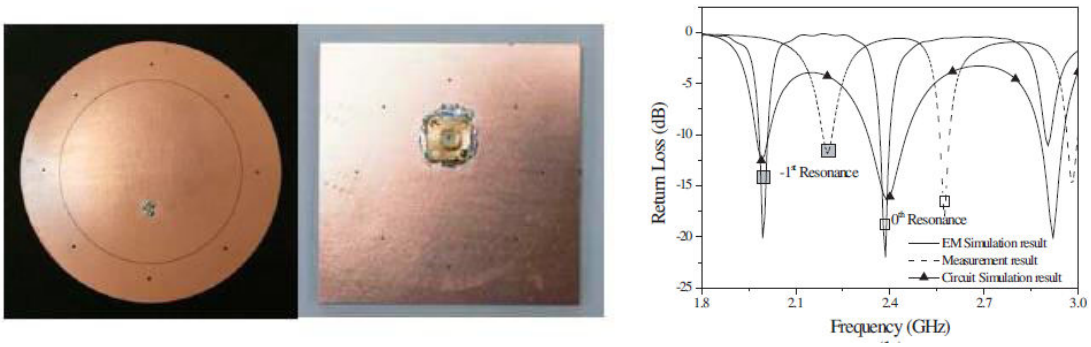

(a) (b)

Fig. 1.12 (a) Structure of the circular patch antenna (b) Return loss characteristics

Quanwen Hou, Yahong Liu, and Xiaopeng Zhao investigated dual band and wide band patch antenna [45]. A circular patch antenna loaded with four metallic VIAs. The antenna structure and the return loss characteristics are shown in the Fig. 1.13. The center frequencies of the dual band patch antenna are 5.25 GHz and 6.05 GHz. The impedance bandwidth of the antenna at both the bands is less.

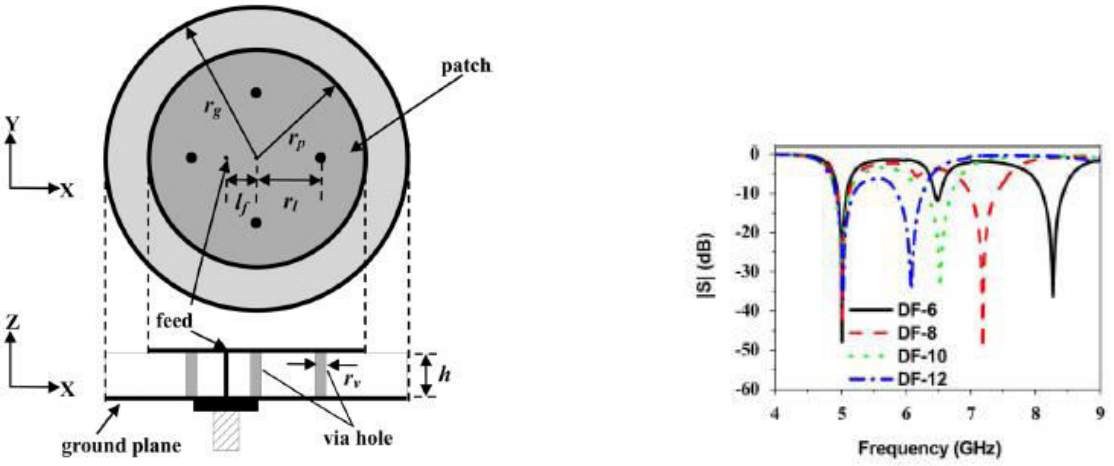

(a) (b)

Fig. 1.13 (a) Structure of the circular patch antenna (b) Return loss characteristics

Mohammad Saeed Majedi, Amir Reza Attari described dual band dual polarized single probe feed patch antenna [46]. The antenna structure is made up of a rectangular radiating patch loaded with two metallic VIAs and is shown in the Fig. 1.14. The resonating frequencies of the antenna are 2.52 GHz and 3.74 GHz respectively. However the antenna is unable to produce good bandwidth at both the bands.

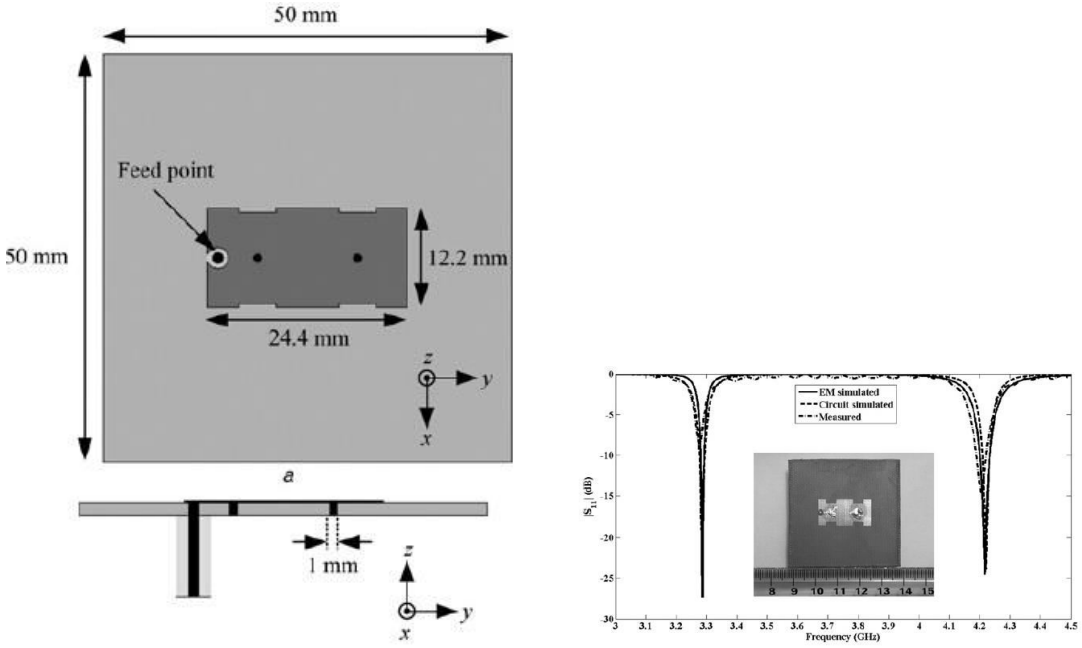

(a) (b)

Fig. 1.14 (a) Structure of the VIAs loaded rectangular patch antenna (b) Return loss characteristics

Y.T. Wan, F.S. Zhang, D. Yu and F.C. Ren have studied dual band patch antenna [47]. A circular radiating patch is loaded with circular metallic cylinder. The operating frequencies of the antenna are 2.504 GHz and 3.289 GHz respectively. The impedance bandwidth of the antenna is 58 MHz at lower band and is 173 MHz at upper band. However the antenna is suffering from less bandwidth.

Youngtaek Hong, Jinpil Tak and Jaehoon Choi discussed dual band patch antenna [48]. A semi circular patch is coupled to a semi circular MUC. The resonant frequencies of the antenna are 2.5 GHz and 5.8 GHz. The impedance bandwidth of the antenna at lower band is 140 MHz and at upper band is 935 MHz. However the antenna is too bulky.

Seyed Amir Hossein Saghanezhad, and Zahra Atlasbaf examined CPW fed dual band patch antenna [49]. The antenna structure consists of a rectangular patch antenna loaded with ‘u’ shaped metallic VIAs. The resonating frequencies of the antenna are 2.7 GHz and 6.3 GHz respectively. The 10-dB return loss bandwidth of the antenna is 23.2% at lower band and is 7.9% at upper band. However the gain of the antenna at both the bands is less. The antenna size is also very large.

Jose L. Jimenez Martina and Vicente Gonzalez Posadasa investigated the probe feed dual band patch antenna [50]. The antenna is made up of a circular patch antenna loaded with cylinder. The antenna structure and return loss characteristics are shown in the Fig. 1.15. The operating frequencies of the antenna are 1.3 GHz and 1.9 GHz respectively. However the impedance bandwidth of the antenna at both the bands is very less.

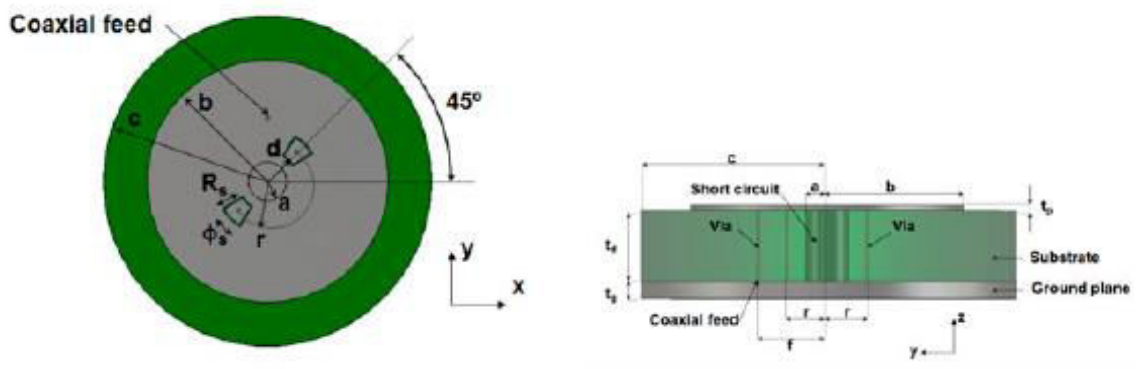

(a) (b)

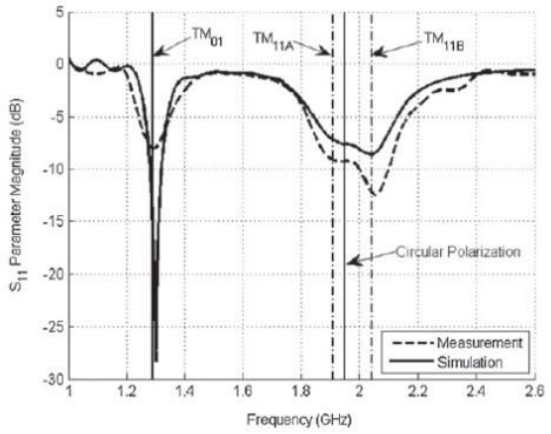

(c)

Fig. 1.15 Structure of the circular patch antenna loaded with VIAs and cylinder (a) Top view (b) Bottom view (c) Return loss characteristics

Soumen Banerjee, Biswarup Rana and Susanta Kumar Parui designed dual band patch antenna [51]. The antenna is composed of a triangular patch antenna loaded with multiple vertical VIAs. The antenna is operating at 4 GHz and 9 GHz with negligible impedance bandwidth. However the impedance bandwidth is low at both the bands.

Wen-Quan Cao came up with probe feed dual band patch antenna [52]. The patch structure consists of a circular patch antenna loaded with four metallic VIAs and four parasitic elements along the circumference of the patch, which is shown in the Fig. 1.16 along with return loss characteristics. The resonating frequencies of the antenna are 4.42 GHz and 5.74 GHz. The impedance bandwidth of the antenna is 5.1% at lower band and is 1.9% at upper band respectively. However the antenna size is more compared to conventional patch antenna which will produce the same frequency bands.

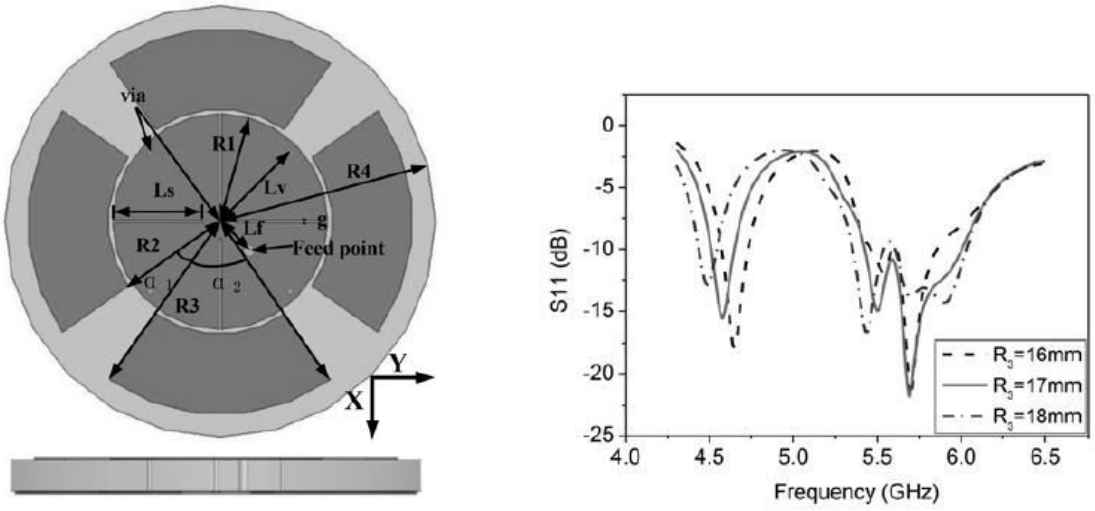

(a) (b)

Fig. 1.16 (a) Structure of the circular patch antenna loaded with four VIAs and four parasitic elements (b) Return loss characteristics

Xiao Zhang and Lei Zhu reported single band probe feed patch antenna [53]. The patch is made up of a square patch antenna loaded with a slot and two metallic VIAs. The operating frequency of the antenna is 3.65 GHz. However the size of the antenna is more and bandwidth is less.

Arpan Pal, Amit Mehta, Dariush Mirshekar-Syahkal and Hisamatsu Nakano designed single band patch antenna [54]. The patch structure is loaded with multiple vertical VIAs. The antenna is working at 2.4 GHz with less impedance bandwidth. Further the antenna is unable to produce dual band operation.

Wen-quan Cao, Qian-qian Wang, Bang-ning Zhang and Wei Hong proposed capacitive probe fed dual band patch antenna [55]. The antenna geometry and return loss characteristics are shown in the Fig. 1.17. The patch structure is made up of a circular radiating patch loaded

with four slits and four metallic VIAs. The resonating frequencies of the antenna are 4.72 GHz and 5.78 GHz. The impedance bandwidth of the antenna is 4.8% at lower band and is 23% at upper band. However the size of the antenna is more.

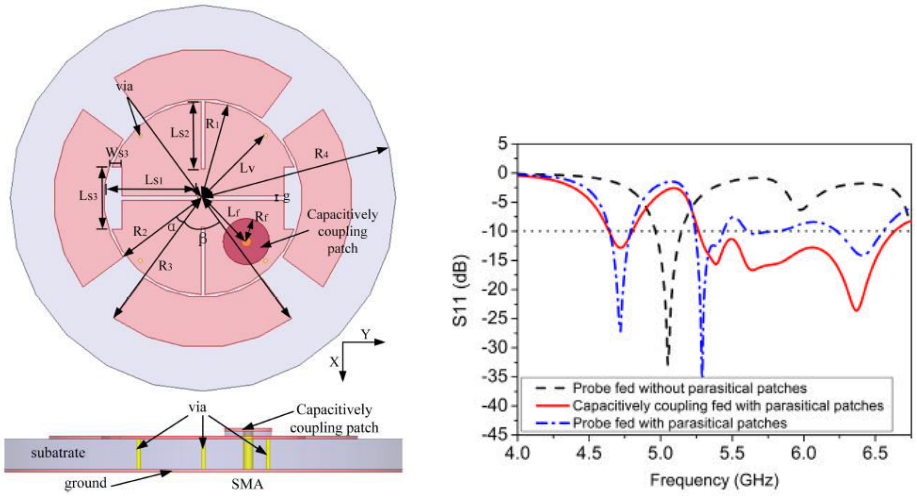

(a) (b)

Fig. 1.17 (a) Structure of the capacitively coupled circular patch antenna (b) Return loss characteristics

E Guo Juhua Liu and Yunliang Long presented single band probe feed yagi antenna [56]. The antenna consists of a rectangular active patch antenna loaded with metallic VIAs, MUCs as reflectors and another rectangular patch loaded with VIAs which acts as director. The resonating frequency of the antenna is 5.14 GHz. The impedance bandwidth of the antenna is 11.5%. However the antenna is unable to produce second band.

Ankang Liu, Yilong Lu, Ling Huang investigated probe fed single band patch antenna [57]. The antenna is made up of a circular patch antenna loaded with metallic VIAs and capacitively coupled MUCs. The operating frequency of the antenna is 5.9 GHz with an impedance bandwidth of 6.38%. However the structure is complex and bandwidth is small.

The antennas reported above [46] – [57] are single feed dual band microstrip antennas based on vertical metallic VIAs. In most of those antenna structures, VIAs are inserted between the patch and ground plane. However, the 10-dB return loss bandwidth at both the bands and the 3-dB axial bandwidth at patch mode band of most of these approaches are good and minimum AR value is also close to 0-dB but the size is large.

To design compact antennas with good impedance and CP bandwidths implementation of patch antennas over RIS is attempted. Reactive Impedance Surface is constructed using periodic arrangement of planar metallic patches (cells) which are kept under the patch radiator. The reflection phase of the single metallic patch lies between perfect electric conductor and perfect magnetic conductor (180^0 reflection phase and 0^0 reflection phases). The required frequency of operation needs to be kept in the inductive impedance region [58, 59, 60 and 61]

Yuandan Dong, Hiroshi Toyao, and Tatsuo Itoh came up with probe fed dual band patch antenna which is shown in the Fig. 1.18 along with its return loss characteristics [62]. The antenna structure consists of a square radiating patch loaded with four MUCs. The operating frequencies of the antenna are 2.4 GHz and 2.9 GHz. The impedance bandwidth of the antenna at the upper band is 4.62%. However the antenna size is more and bandwidth at lower band is less.

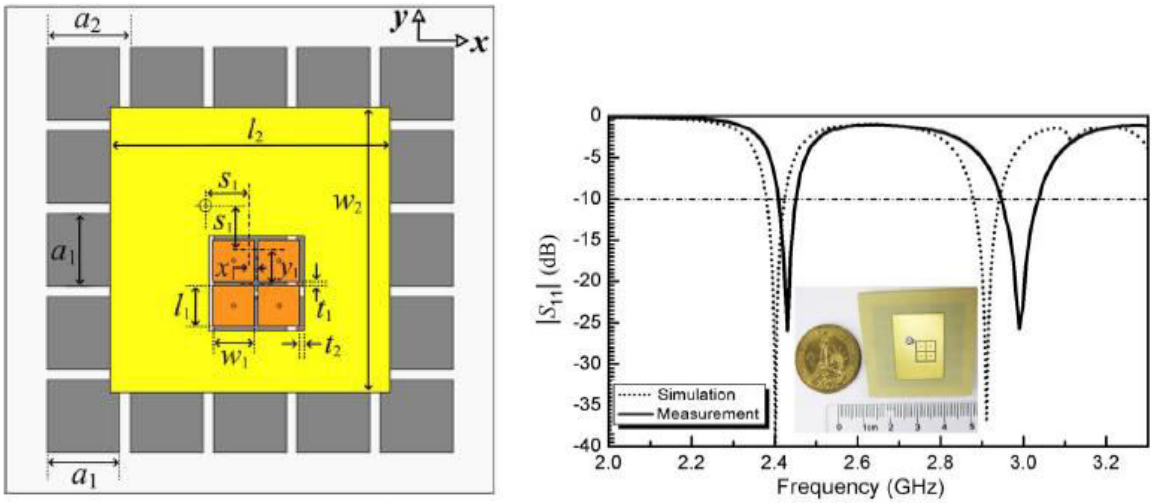

(a) (b)

Fig. 1.18 (a) Structure of the rectangular patch antenna (b) Return loss characteristics

Hsing-Yi Chen and Yu Tao proposed dual band probe fed patch antenna [63]. The antenna structure and return loss characteristics are shown in the Fig. 1.19. The antenna is made up of u-shaped slot loaded rectangular patch antenna placed on RIS. The resonating bands of the antenna are 2.44 GHz and 5.77 GHz respectively. The impedance bandwidth of the antenna is 3.2% at lower band and is 1.7% at upper band. However the size of the antenna is more and the bandwidth at both the bands is less.

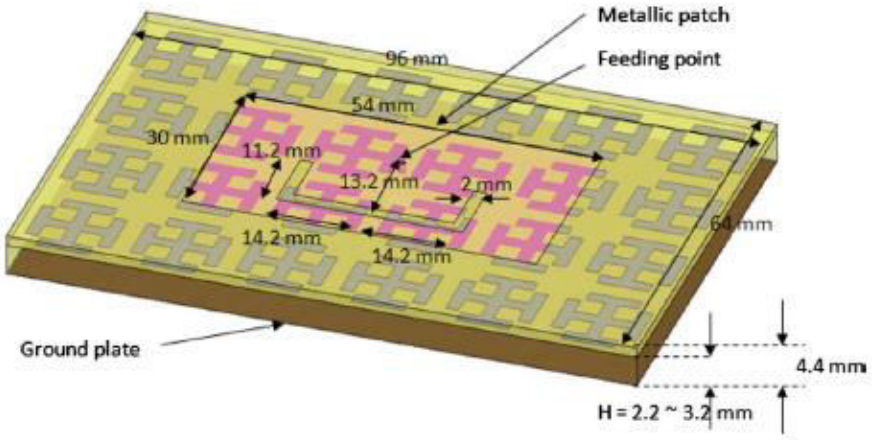

\

(a)

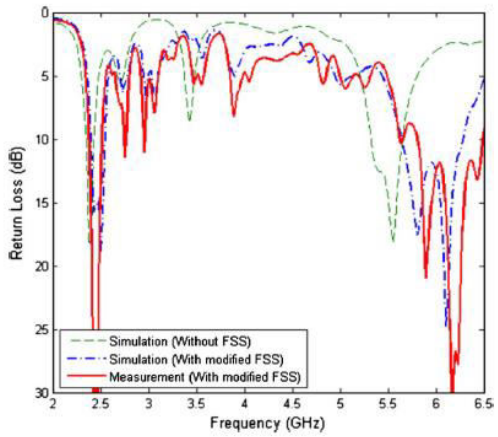

(b)

Fig. 1.19 (a) Structure of the rectangular patch antenna (b) Return loss characteristics

L. Bernard, G. Chertier and R. Sauleau presented single band probe fed patch antenna [64]. It is constructed with a slot loaded patch antenna placed on RIS. The operating frequency of the antenna is 2.3 GHz with an impedance bandwidth of 14%. However the antenna is unable to produce second band.

Kush Agarwal, Nasimuddin, and Arokiaswami Alphones reported a probe fed single band patch antenna [65]. The antenna is composed of cross slot loaded radiating patch antenna placed on RIS. The operating frequency of the antenna is 2.5 GHz with an impedance bandwidth of 5.2%. However the antenna is unable to produce second band.

Kush Agarwal, and Sanjib Kumar Panda described probe fed single band patch antenna [66]. The antenna structure consists of a corner truncated patch antenna placed on RIS. The operating frequency of the antenna is 2.42 GHz with an impedance bandwidth of 5.78%. However the antenna size is more and the antenna is unable to produce another band.

He-Xiu Xu, Guang-Ming Wang, Jian-Gang Liang, Mei Qing Qi, and Xi Gao examined dual band patch antenna [67]. The antenna geometry and return loss characteristics are shown in the Fig. 1.20. The patch structure is made up of metamaterial loaded patch antenna placed on RIS. The resonating frequencies of the antenna are 2.86 GHz and 3.11 GHz respectively. The impedance bandwidth of the antenna is 1.75% at lower band and is 2.57% at upper band. However the antenna is unable to produce more bandwidth at both the bands.

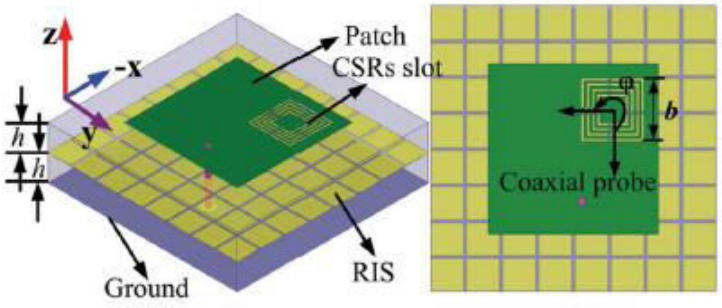

(a)

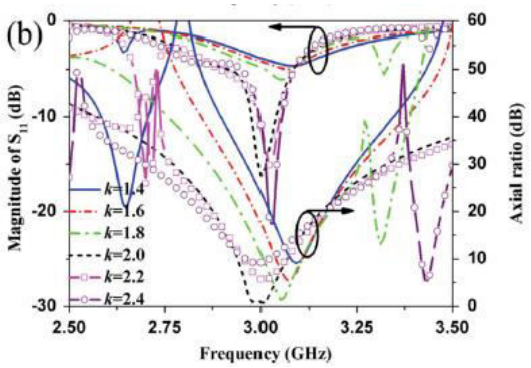

(b)

Fig. 1.20 (a) Structure of the rectangular patch antenna (b) Return loss characteristics

Kush Agarwal, Nasimuddin and Arokiaswami Alphones studied triple band patch antenna [68]. The geometry and return loss characteristics are shown in the Fig. 1.21. The antenna is designed with three different patch antennas placed on RIS. The operating frequencies of the antenna are 1.176 GHz, 1.227 GHz and 1.575 GHz. The impedance bandwidth of the antenna

is 1.45% at first band, is 3.68% at second band and is 5.16% at third band. However the antenna structure is complex.

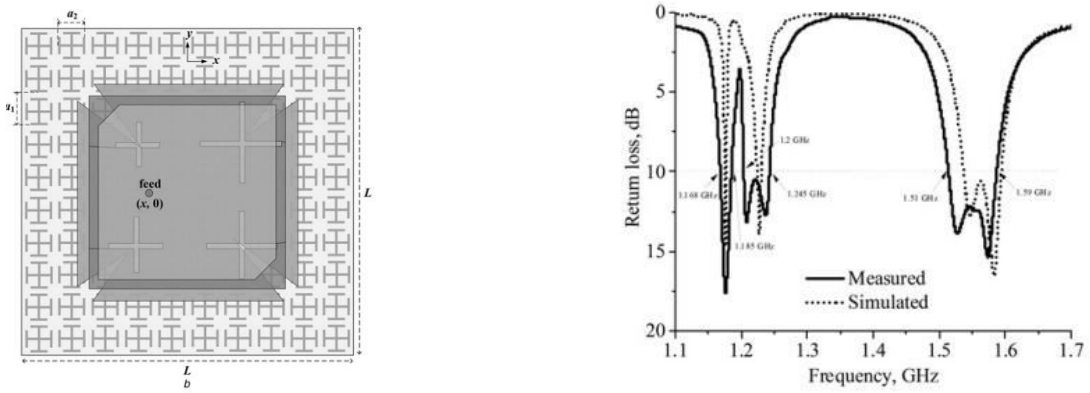

(a) (b)

Fig. 1.21 (a) Structure of the rectangular patch antenna (b) Return loss characteristics

Tong Cai, Guang-Ming Wang, Xiao-Fei Zhang, and Jun-Peng Shi investigated line fed single band patch antenna [69]. The patch is constructed with a rectangular patch loaded with Hilbert shaped curves which is placed on Hilbert curve shaped RIS. The antenna structure along with return loss characteristics is shown in the Fig. 1.22. The resonating frequency of the antenna is 3.52 GHz with an impedance bandwidth of 3.61%. However the antenna is unable to produce second band.

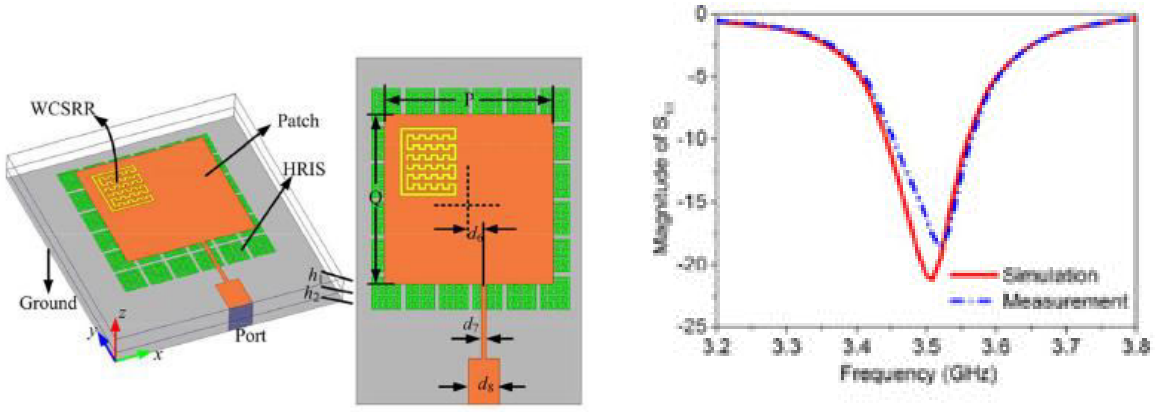

(a) (b)

Fig. 1.22 (a) Structure of the rectangular patch antenna (b) Return loss characteristics

Son Xuat Ta and Ikmo Park reported single band probe fed patch antenna [70]. The structure is formed with corner truncated patch antenna placed between RIS and the ground plane. The operating frequency of the antenna is 6.09 GHz with an impedance bandwidth of 45.6%. However the antenna is too complex and is unable to produce the second band.

Galaba Sai Rajesh, Venkata Kishore K and Vijay Kumar presented multiband patch antenna [71]. The antenna structure consists of square, hexagon and star shaped patch antennas placed on RIS where the RIS elements are constructed by loading circular CSRR. The presented antenna structures and their return loss characteristics are shown in the Fig. 1.23. The operating bands of the antenna are 3.29 GHz, 5.11 GHz, 5.4 GHz, 5.9 GHz, 6.62 GHz and 8.1GHz. However the bandwidth at each band is less.

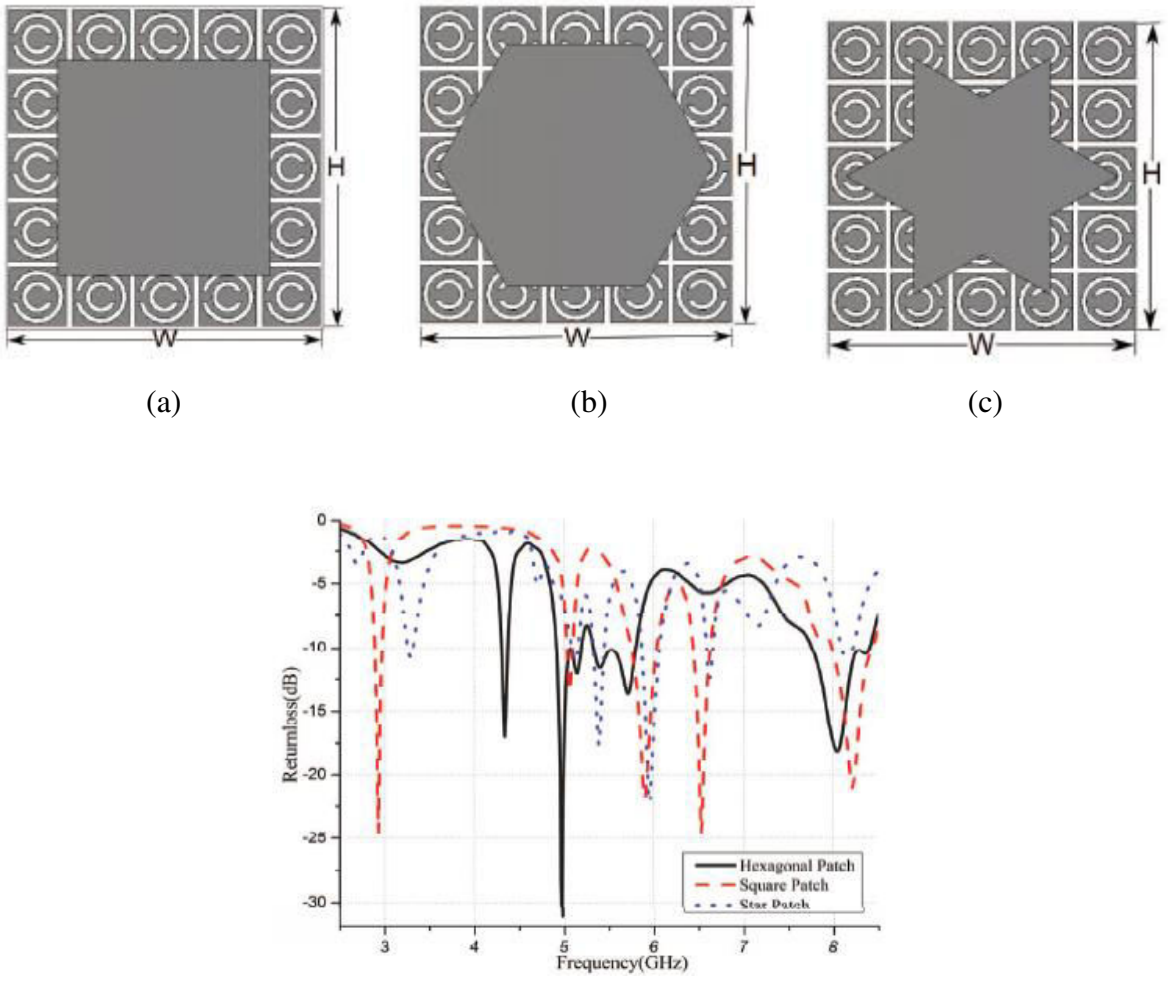

(a) (b) (c)

(d)

Fig. 1.23 Structure of the (a) rectangular patch antenna (b) Hexagon patch antenna (c) Star shaped patch antenna (d) Return loss characteristics

N. Nasimuddin, Zhi Ning Chen, and Xianming Qing proposed single band probe fed patch antenna [72]. The antenna is made up of rectangular slotted patch antenna placed on RIS with

rectangular ring cells. The operating frequency of the antenna is 4.1 GHz with an impedance bandwidth of 36%. However the antenna is unable to generate second band.

Junyi Ren, Shuxi Gong, and Wen Jiang demonstrated single band metamaterial absorber based on RIS [73]. The antenna contains a circular patch antenna coupled with dual ring metamaterial absorber. The antenna is working at 5.8 GHz. However the antenna structure is complex.

Krashnkant Gupta and Binod Kumar Kanaujia reported single band probe feed patch antenna [74]. The patch is formed with a rectangular patch antenna loaded with slot placed on RIS. The operating bandwidth of the antenna is 319 MHz at 2.8 GHz. However the antenna is suffering from producing second band.

C. Ren, L. Bernard and R. Sauleau investigated single band patch antenna [75]. The antenna structure is made up of a square patch implemented over RIS. The antenna is resonating at 2.4 GHz. However the antenna is unable produce another band.

S. Jarchi, J. Rashed Mohassel and R. Faraji Dana introduced single band patch antenna [76]. The patch antenna is designed with a square radiating patch implemented over RIS. The antenna is analyzed using Greens function to achieve compactness. However the CP bandwidth of the antenna is negligible.

The antennas enumerated above [62] – [76] are RIS based single feed single band and dual band microstrip antennas. In most of those antenna structures, RIS is used as ground plane for basic patch antenna. However, the dimensions of these antennas are small but the 10-dB return loss bandwidth at both the bands and the 3-dB axial bandwidth at patch mode band of most these approaches are not good.

High Impedance Surface is constructed using periodic arrangement of planar Mushroom Unit Cells which are kept under the patch radiator. There is small dissimilarity between RIS and HIS in the frequency of operation. For HIS at the resonant frequency the parallel LC circuit leads to very high impedance which is theoretically infinity and for RIS at other frequencies the net impedance is either inductive or capacitive. Also, the magnetic field tangential component is zero at the surface [77 and 78].

Lina Moustafa and Bernard Jecko proposed single band patch antenna [79]. The antenna consists of double layer EBG separated by small distance. The operating frequency of the antenna is 11.8 GHz with an impedance bandwidth of 17%. However the antenna structure is too complex.

W. Q. Cao and Z. D. Song presented single probe feed dual band patch antenna [80]. The antenna is made up of a corner truncated square patch antenna placed on HIS. The HIS is made of 5x5 periodic MUCs. The presented antenna structure and its return loss characteristics are given in the Fig. 1.24. The antenna is operating at 3.735 GHz and 4.195 GHz bands. The impedance bandwidth at lower band is 2.4% and at upper band is 3.1%. However the impedance bandwidth at patch mode band is poor.

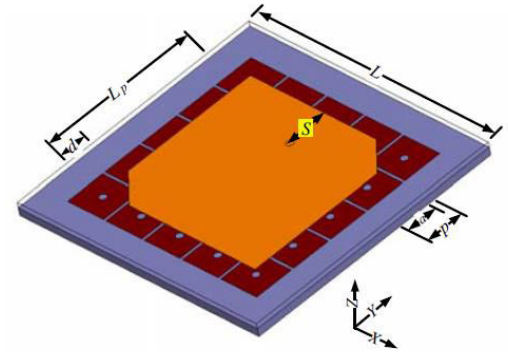

(a)

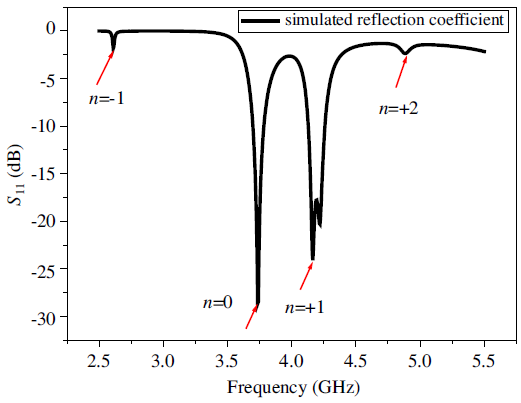

(b)

Fig. 1.24 (a) Geometry of the rectangular patch antenna on HIS (b) Return loss characteristics

A. Ameelia Roseline, K. Malathi and A.K. Shrivastav described coaxial probe fed single band patch antenna [81]. The antenna structure comprises of a square patch antenna surrounded by spiral EBG. The described antenna structure and the return loss

characteristics are shown in the Fig. 1.25. The patch antenna is resonating at 2.36 GHz with an impedance bandwidth of 11.4%. However the antenna is suffering from small bandwidth.

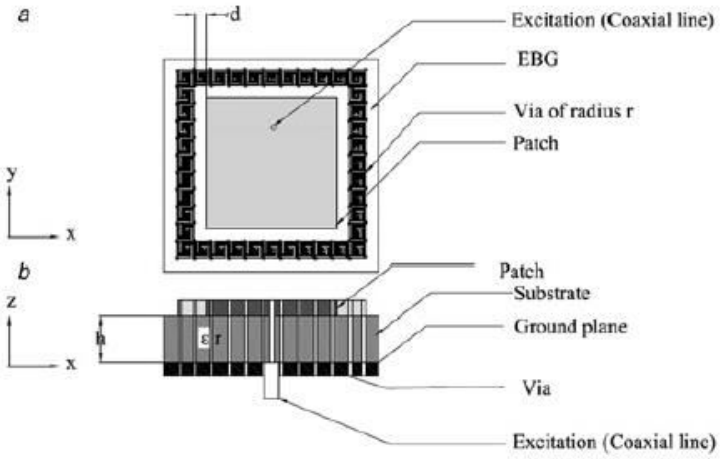

(a)

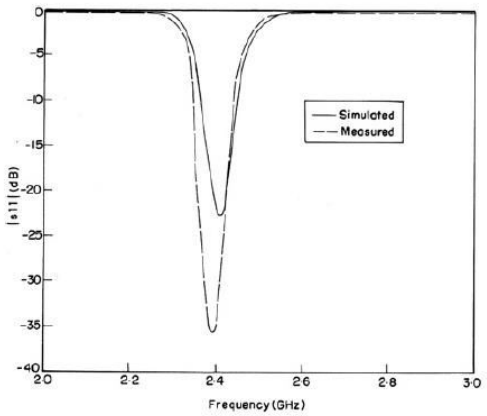

(b)

Fig. 1.25 (a) Structure of the rectangular patch antenna (b) Return loss characteristics

Filippo Costa and Peter M. de Maagt demonstrated a single band probe fed patch antenna [82]. The antenna contains a dipole antenna placed on HIS. The number of MUCs is varied to observe the effect of HIS on dipole antenna. The operating frequency of the antenna is 1.3 GHz with an impedance bandwidth of 23%. However the size of the HIS is more and number of MUCs are also more.

Julien Sarrazin, Anne-Claire Lepage, and Xavier Begaud reported single band patch antenna [83]. The antenna is designed with a rectangular patch which is fed by coaxial probe feed technique. The antenna is operating at 2.4 GHz with 5% impedance bandwidth. However the antenna structure is complex and is unable to produce good CP bandwidth.

Marzieh SalarRahimi, J. Rashed-Mohassel, and M. Edalatipour discussed the dual band patch antenna [84]. The antenna structure is made up of circular patch antenna surrounded by MUCs. The antenna is working at 1.7 GHz and 2.5 GHz. However the antenna is suffering to produce good return loss bandwidth and CP bandwidth at patch mode band.

Wenquan Cao and Xiaofei Pan introduced probe fed triple band patch antenna [85]. The antenna contains a corner truncated square patch antenna placed on HIS. The HIS is constructed from spiral slot loaded MUCs which is shown in the Fig. 1.26. The operating frequencies of the antenna are 1.33 GHz, 1.88 GHz and 2.412 GHz. The 10-dB return loss bandwidth is 1.88% at first band, is 3.24% at second band and is 10.03% at third band. However the antenna is suffering from small bandwidth at patch mode band.

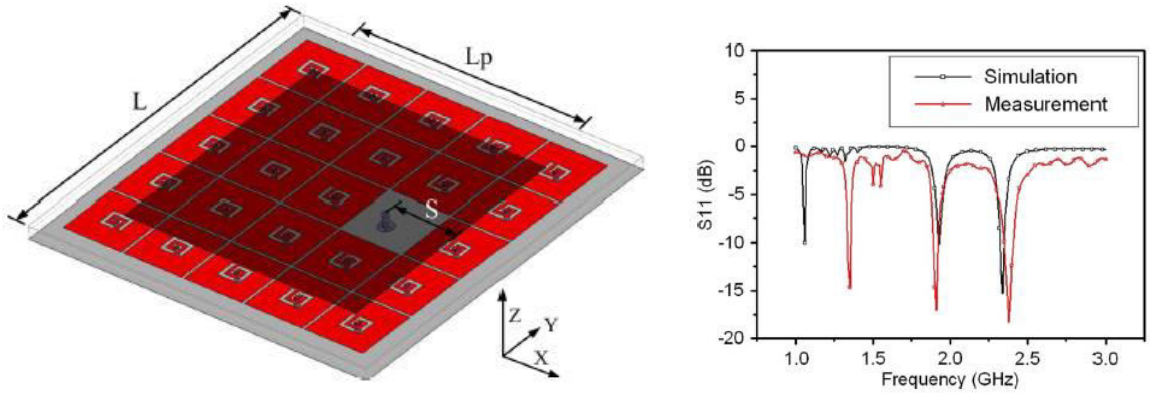

(a) (b)

Fig. 1.26 (a) Structure of the rectangular patch antenna over HIS (b) Return loss characteristics

Soham Ghosh, Thanh-Ngon Tran, and Tho Le-Ngoc nominated probe fed single band MIMO antenna [86]. They formed the antenna with a square patch placed on HIS. The operating frequency of the antenna is 2.5 GHz. However the impedance bandwidth is small.

Wei Liu, Zhi Ning Chen, and Xianming Qing designed broadband patch antenna [87]. The antenna structure consists of 4x4 MUCs fed by microstrip line through a cut slot onto the ground plane. The antenna structure along with return loss characteristics are shown in the Fig. 1.27. The antenna is working at 5 GHz frequency with an impedance bandwidth of 25%. However the antenna is too complex.

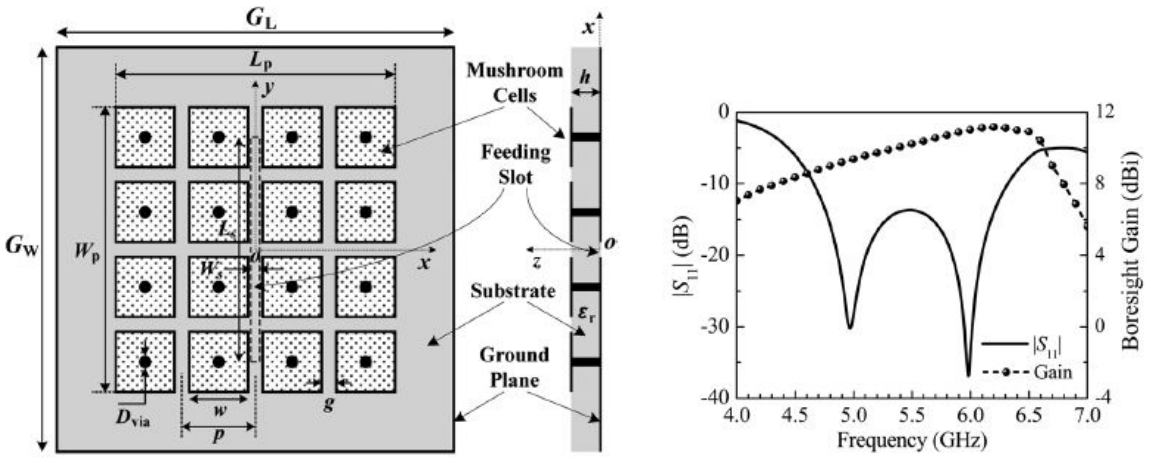

(a) (b)

Fig. 1.27 (a) Structure of the aperture coupled patch antenna (b) Return loss characteristics

Naveen Jaglan and Samir Dev Gupta addressed single band patch antenna [88]. The antenna structure is made up of a square patch antenna surrounded by MUCs. The operating frequency of the antenna is 5.2 GHz. However the impedance bandwidth is poor for this antenna.

Karthik T. Chandrasekaran, Muhammad Faeyz Karim, Nasimuddin, Arokiaswami Alphones worked on triple band patch antenna [89]. The antenna consists of CRLH structure based on HIS and a rectangular patch. The antenna is resonating at 2.34 GHz, 3.73 GHz and 5.55 GHz. However the antenna is suffering from poor bandwidth at patch mode band.

The antennas investigated above [84] – [89] are HIS based single feed wide band microstrip antennas. In most of those antenna structures, HIS is used as ground plane for basic patch antenna. The 10-dB return loss bandwidths as well as the 3-dB axial ratio bandwidth at patch mode band of most of these approaches are good. However the size of the antenna is more and structures are complex.

After a comprehensive literature survey it is understood that the metamaterials can be used to design compact dual band and wide band patch antennas with good return loss bandwidth at both the bands. And the CP bandwidth at patch mode can be improved by using fractal curves at the edges of the conventional square patch antenna. The motivation to

choose the metamaterials is that the left handed nature of them which gives compactness to the designs.

1.1 Introduction to Metamaterials and Fractal curves

1.1.1 Metamaterials

The investigation of artificial materials or metamaterials started at the end of 19th century. In the year 1967 Russian physicist Victor Veselago described Negative-index materials and demonstrated that these materials could transmit light. He illustrated that the phase velocity and direction of Poynting vector are anti-parallel. This is opposite to wave propagation in naturally occurring materials. In the year 1999 John Pendry demonstrated practical way to design metamaterials. Metamaterials are artificial materials having electromagnetic properties which are not existing in the nature especially with a negative refractive index. According to Victor Veselago materials are classified into four categories based on the parameters permittivity (ε) and permeability (μ) which is shown in the Fig 1.28 [97].

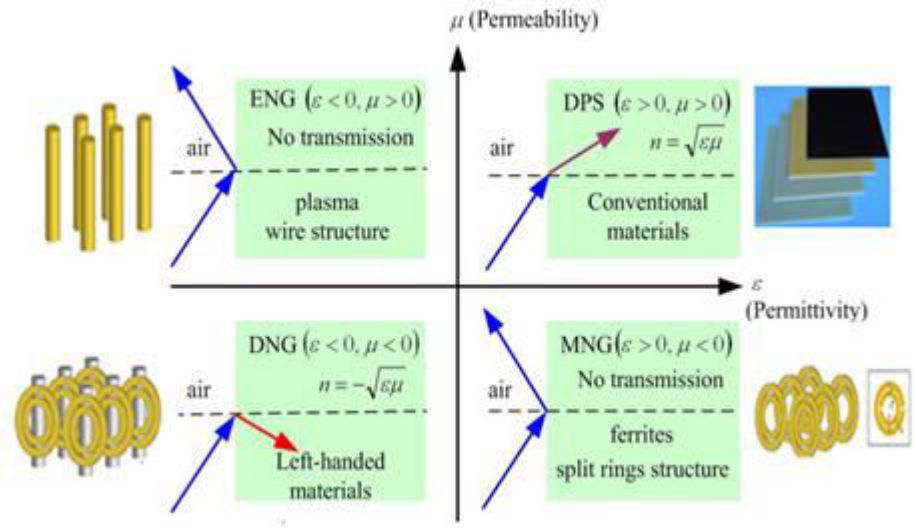

(a)

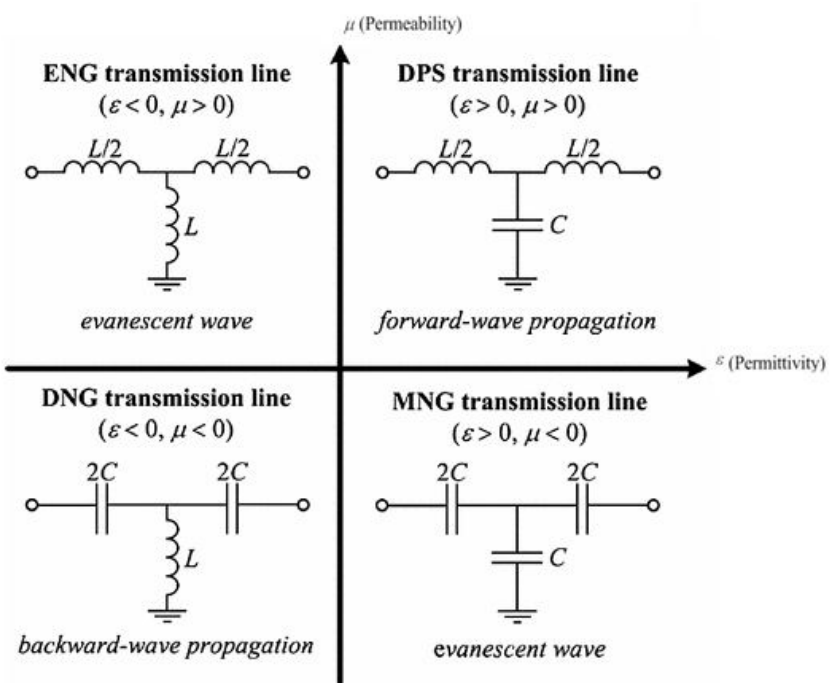

(b)

Fig. 1.28 Metamaterials (a) Classification based on μ and ε (b) equivalent circuit diagrams

1.1.2 DPS materials

From the Fig. 1.28, the first quadrant materials are known as Double Positive materials where the permittivity (ε) and the permeability (μ) are positive. The examples for these types of materials are generally available dielectric materials. The refractive index is positive for these types of materials and the waves follow right hand rule to propagate in the forward direction.

1.1.3 ENG materials

From the Fig. 1.28, the second quadrant materials are known as Epsilon Negative materials where the permittivity (ε) is negative and the permeability (μ) is positive for these materials and the examples are vertical metallic VIAs inserted between radiating surface and the ground plane. These materials produce shunt inductance and the radiation pattern due to current at these materials is similar to that of dipole antenna.

ENG TL unit cell model is constructed using the combination of series inductance (L_R), shunt capacitance (C_R), shunt inductance (L_L) as shown in the Fig. 1.29 [46]. The relationship

between the phase constant and the angular frequency is obtained using Bloch Floquet theory, According to them the propagation constant of an ENG TL is given by $\gamma = \sqrt{ZY}$ Where z is per unit length impedance and y is per unit length admittance [46].

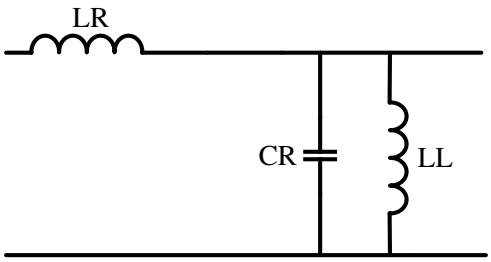

Fig. 1.29 Equivalent circuit diagram of ENG TL

The special property of ENGTL is that the wavelength is infinite at zeroth order frequency. The propagation constant of both ENGTL from Bloch Floquet theory is given by

$$\beta_{ENGTL} d = \arccos(1 - 0.5 * \frac{(w^2 - w_{sh}^2)}{w_R^2})$$

Where β is the phase constant for Bloch waves and d is the length of the unit cell and

$$w_R = \frac{1}{\sqrt{L_R C_R}} \quad \text{and} \quad w_{sh} = \frac{1}{\sqrt{L_L C_R}}$$

1.1.4 DNG materials

From the Fig. 1.28, the third quadrant materials are known as Double Negative materials where the permittivity (ε) is and the permeability (μ) both are negative for these materials. The examples are Mushroom Unit Cells and Inter Digital Capacitors. These materials produce shunt inductance due to current carrying copper wire and the series capacitance due to gap between the radiating surface and ground plane.

DNG TL unit cell is shown in Fig. 1.30 [97], where L_R is per unit length series inductance and C_R is per unit length shunt capacitance in which both are due to patch and L_L is the shunt inductance due to VIA and C_L is series capacitance due to the gap between radiating patch and MUC.

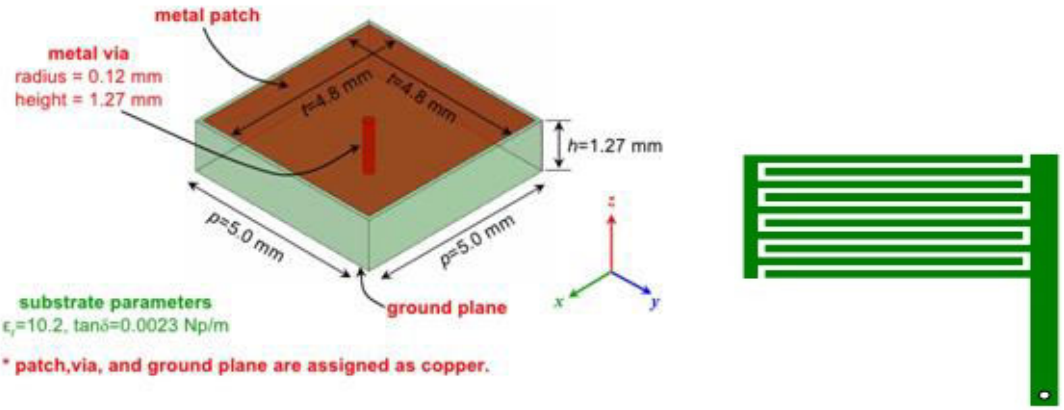

(a) (b)

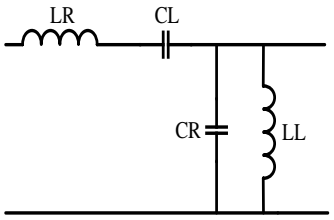

(c)

Fig. 1.30 Structures of (a) Mushroom Unit Cell (b) Inter digital capacitor (c) Equivalent circuit diagram of DNG TL unit cell

The special property of DNGTL is that the wavelength is infinite at zeroth order frequency (zeroth order resonance is independent of the wavelength) [46]. The propagation constant of DNGTL from Bloch Floquet theory is given by

$$\beta_{DNGTL} d = \arccos(1 - 0.5 * (\frac{w^2}{w_R^2} - \frac{w_L^2}{w_{se}^2} - \frac{w_L^2}{w_{sh}^2} + \frac{w_L^2}{w^2}))$$

Where β is the phase constant for Bloch waves and d is the length of the unit cell and

$$w_{se} = \frac{1}{\sqrt{L_R C_L}} \qquad w_L = \frac{1}{\sqrt{L_L C_L}}$$

$$w_R = \frac{1}{\sqrt{L_R C_R}} \qquad w_{sh} = \frac{1}{\sqrt{L_L C_R}}$$

From the above equation, it is observed that the phase constant is dependent on four different angular frequencies. Those are patch mode frequency (w_R) or n=+1 mode, zeroth

order frequency (w_{sh}) or n=0 mode, w_{se} or n=-1 mode and w_L or n=+2 mode respectively. The proposed antenna is resonating at two frequencies only those are patch mode band and zeroth order band. The phase constant is negative for n=0 mode and positive for the n=+1 mode.

1.1.5 MNG materials

From the Fig. 1.28, the fourth quadrant materials are known as permeability Negative materials where the permittivity (ε) is positive and the permeability (μ) is negative for these materials and the examples are SRRs (Split Ring Resonators). A single cell SRR has a pair of enclosed loops with splits in them at opposite ends. SRR is constructed with pair of enclosed loops with breaks in them at opposite ends. The loops are made of copper and have a small gap between them. The dual of SRR is CSRR (Complementary Split Ring Resonator).

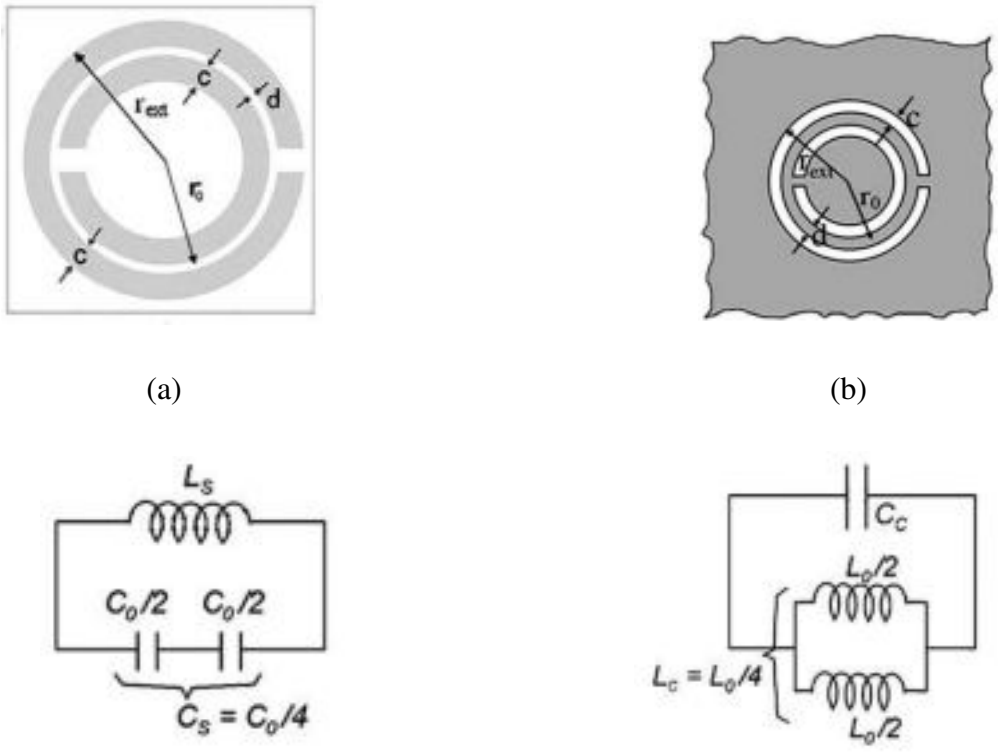

Fig. 1.31 Topologies of (a) SRR (b) CSRR equivalent circuit diagrams of (c) SRR (d) CSRR

The two topologies of Split Ring Resonator (SRR) and CSRR are shown in the Fig. 1.31 [7] According to Babinet's principle CSRR is the dual structure of the SRR in which the

roles of metal and air are interchanged, and also the role of electric and magnetic field components. The SRR can act as magnetic dipole that can be excited by an external magnetic flux where the CSRR can act as electric dipole that can be excited by external electric field. The equivalent circuit diagram of SRR and CSRR are shown in the Fig. 1.31, where the C_0 is the total capacitance between the rings, L_0 is the total inductance, L_s is the series inductance of the SRR, Lc is the shunt inductance, Cc is the shunt capacitance and C_s is the series capacitance of the lower and upper halves of the SRR. The resonant frequency of the SRR is given by

$$f_0 = \frac{1}{2\pi(C_s L_s)}.$$

Based on duality concept of SRR and CSRR the resonant frequency of CSRR is same as the resonant frequency of SRR.

1.1.6 Reactive Impedance Surface (RIS)

Reactive Impedance Surface is constructed using periodic arrangement of planar metallic patches (cells) which are kept under the patch radiator as shown in the Fig 1.32 [97]. The reflection phase of the single metallic patch lies between perfect electric conductor and perfect magnetic conductor (180^0 reflection phase and 0^0 reflection phases). The desired frequency of operation must to be kept in the inductive impedance region.

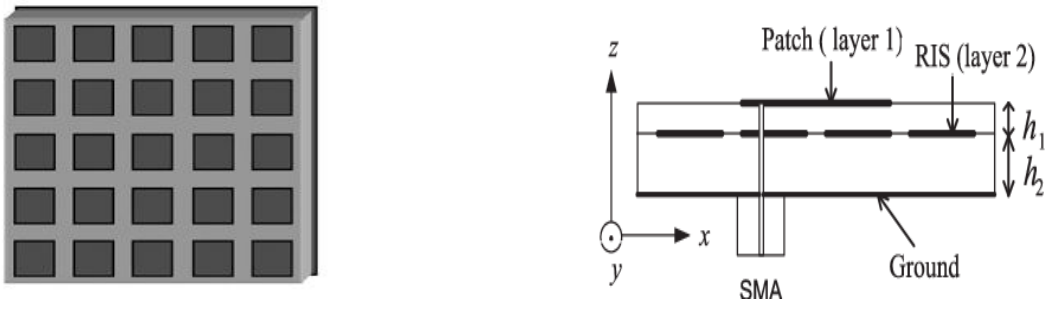

(a) (b)

Fig. 1.32 Reactive Impedance Surface (a) Top view (b) Side view

The advantages of RIS are

1. Impedance matching over a wide bandwidth
2. Radiation efficiency is good

3. Reduced size at the same resonant frequency
4. Front to back ratio will be improved

1.1.7 High Impedance Surface (HIS)

High Impedance Surface is constructed using periodic arrangement of planar Mushroom Unit Cells which are kept under the patch radiator as shown in the Fig 1.33 [96]. The small dissimilarity between RIS and HIS is their resonant frequency. For HIS at the resonant frequency the parallel LC circuit leads to very high impedance which is theoretically infinity and for RIS at other frequencies the net impedance is either inductive or capacitive. Also, the magnetic field tangential component is zero at the surface.

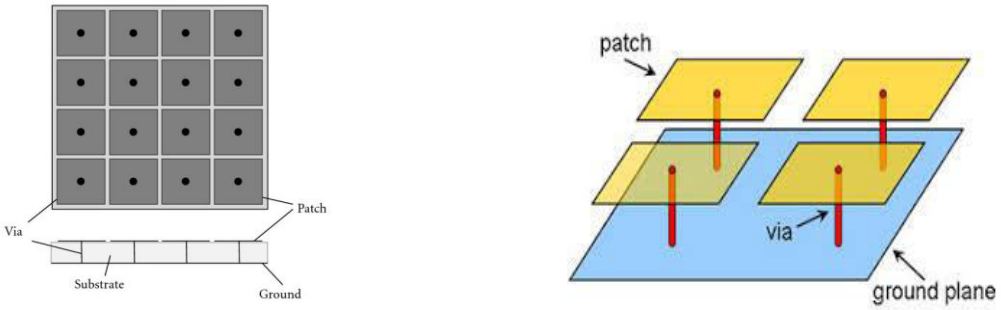

(a) (b)

Fig. 1.33 High Impedance Surface (a) Top view (b) Side view

1.1.8 Fractals Curves

Fractals are first proposed in the early stages of 17th century but graphically defined and executed by Karl Weierstrass in the year 1872. Fractal curves are self repetitive and space filling curves which are used to design compact antennas. Fractals are often formed by iterative process. A fractal is a repetitive design to increase the length of a material that can receive or transmit electromagnetic radiation within a given total surface area or volume.

Fractal curves are characterized by two parameters: Iteration Order (IO) and Indentation Factor (IF). The IF is different for different types of fractals. For example, the IF for the Minkowski fractal curve is Indentation Depth (ID) where Dx and Dy are the IDs along x- and y- axes, and for the Koch fractal curves the same is Indentation Angle (IA) where θx

and θy are the IAs along x- and y- axes. The IAs of Koch fractal curves are shown in the Fig. 1.34 [99].

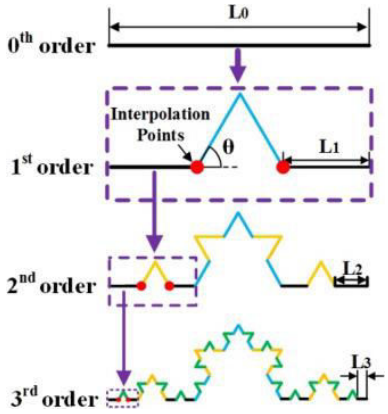

Fig. 1.34 Generation of Koch fractal curve

In the case of Koch fractal curves, the equal IA (θx1=θx2=θy1=θy2) along four sides of the square patch antenna results in LP at upper frequency band. CP radiation can be obtained by placing different IAs along each side of the patch (θx1≠ θx2≠ θy1≠ θy2) or (θx1= θx2= θx ≠ θy1= θy2 =θy) where the high bandwidth can be obtained when IAs along same axis are equal and are another along the perpendicular axis.

In the case of Minkowski fractal curves, the equal ID (Dx1=Dx2=Dy1=Dy2) along four sides of the square patch antenna results in linear polarization (LP) at upper frequency band which is shown in the Fig. 1.35 [100]. CP radiation can be obtained by loading different IDs along each side of the square patch (Dx1≠ Dx2≠ Dy1≠ Dy2) or (Dx1= Dx2= Dx ≠ Dy1= Dy2 =Dy) where the high bandwidth can be obtained when IDs along same axis are equal and are not equal along the perpendicular axis.

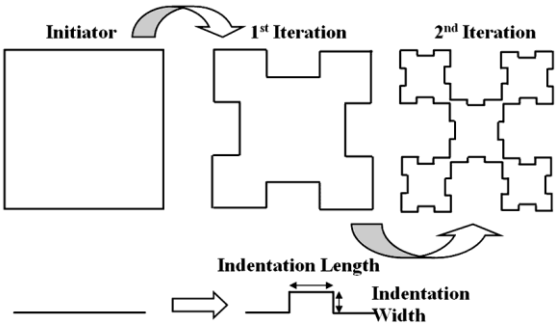

Fig. 1.35 Generation of Minkowski fractal curve

The poly fractal boundary patch antenna can be obtained by using the combination of both Koch and Minkowski fractal curves. The edges of the square patch are replaced by Koch fractal curve along x- axis and Minkowski fractal curve along y- axis.

This thesis mainly focuses on the issue of getting dual band and wide band with good return loss bandwidth at both the bands and CP radiation at patch mode band. In order to accomplish this, metamaterials and fractal curves are being used. To show the effectiveness of the proposed antennas, several types of metamaterials and fractal curves have been used. Ansoft HFSS Electromagnetic Simulator is used for simulating the antennas. The simulated results have been verified experimentally and a good agreement is obtained.

1.1.9 Motivation and Objectives:

Considering the merits and demerits of the published literature the author arrived at the conclusion that there is a strong need to realize dual band antennas with a bandwidth of greater than 1% at both the bands. Also to have CP bandwidth at least at upper band with bandwidth greater than 1% suitable for Wi-Fi and WiMAX applications. The existing works can provide bandwidths sufficient for applications on the hand held devices but the designers of hotspots and routers are looking for wider bandwidths to support more bandwidth and also for nascent applications.

In this direction the author has arrived at following objectives.

To be able to provide at least two bands of operation for the antennas used for simple applications.

To improve the bandwidth to at least 1% at both the bands while maintaining CP at second band.

To enhance the bandwidths at both the bands to at least 4% required for modern routers.

While maintaining the performance same as previous chapters a higher degree of compactness which is desirable for ultrathin systems is desirable.

To show the advantages of blending fractals as well as metamaterials another aspect of design i.e. simple wide band antenna design such that the bandwidth realized is greater than 15% with high degree of compactness.

1.1.10 The outline of the thesis is as follows.

First chapter contains introduction to microstrip antennas for dual band and wide band operation and their applications and challenges. The concept behind metamaterials is explained and several antennas proposed by earlier researchers using this are discussed. A

comprehensive review of dual and wide band antennas, their advantages and motivation to take up this work is quoted.

In Chapter 2, dual band patch antennas based on CSRR are proposed. The impedance bandwidth at patch band is good (> 5%) and at left hand band the same is less (< 0.5%). These antennas are useful for systems operating at Wi-Fi and Wi-MAX standards (IEEE 802.11 and IEEE 802.16). The best performing antennas are fabricated and tested experimentally.

In Chapter 3, dual band patch antennas based on MUC with good impedance bandwidth at both the bands are proposed. These antennas are fabricated and their performance is measured. Here, feed point location and the dimensions of the fractal slot are optimized for dual band operation. Various dual band antennas are proposed using different fractal boundary curves and their performance is compared with measured data.

In Chapter 4, ENGTL based dual band patch antennas with good return loss bandwidth at both the bands and CP bandwidth at patch mode band are proposed. The best resulting antennas are fabricated and tested. Close match is observed between the measured and simulated results.

In Chapter 5, dual band patch antennas based on RIS with good return loss bandwidth at both the bands and CP bandwidth at patch mode band are proposed. Here, several fractal boundary antennas with square and fractal RIS elements are designed. Best performing antennas are fabricated and experimentally tested. Close agreement between measured and simulated results is observed.

In Chapter 6, wide band patch antennas based on HIS with enhanced 3-dB axial ratio bandwidth are proposed. Here, several fractal boundary antennas with square and fractal HIS elements are designed. The antenna which is showing good radiation properties is manufactured and tested.

At the end conclusions are given in Chapter 7 for the proposed method of dual band patch antennas based on CSRR, MUC, ENGTL, RIS and wide band patch antennas based on HIS. The practical applications of proposed dual band antennas and the scope for future work are also mentioned.

Chapter 2

Compact Dual Band Microstrip Patch antennas based on Complementary Split Ring Resonator

The ongoing improvements in the field of wireless communications have expanded the requirement for multiband and multifunctional antennas. The essential requirements of recent communication systems have additionally inspired an extended interest for ease and more miniaturized antennas. The benefit of the multi-band antennas is to have the capacity to coordinate several frequencies on one single antenna, making it helpful for several ranges. In this way, multifunctional antennas are exceptionally appealing in wireless communications. For the purpose of proper transmission between the transmitting and receiving antennas in any orientation circular polarization is also becoming more and more attractive. In perspective of these viewpoints, minimal circularly polarized antennas with multi-band activities will be more helpful in the future wireless communication systems.

The majority of the dual band antennas existing in the literature are utilizing line fed and probe fed CSRR (Complementary Split Ring Resonators) loaded rectangular patch antennas. However, a large portion of these structures are linearly polarized. Some dual band antennas exist in using multi layer design, yet the produced 3-dB CP bandwidths are extremely narrow (<1%) at patch mode band, which is not meeting the prerequisites of present day communication systems.

Here, in the present work dual band dual polarized antennas are demonstrated utilizing the CSRRs and different fractal curves. By using asymmetrical fractal curves as boundaries of a square patch and embedding a square CSRR at right bottom corner of the patch, dual band operation with LP at lower band and CP at upper band is obtained.

In this section three new antennas are studied for dual band operation where lower band is resonating with LP and upper band is resonating with CP with a single probe feed based on CSRR and fractal curves. They are:

(1) CSRR based dual band Minkowski fractal boundary antenna

(2) CSRR based dual band Koch fractal boundary antenna

(3) CSRR based dual band Poly fractal boundary antenna

2.1 CSRR based dual band Minkowski fractal boundary antenna

The geometry of the proposed antenna is shown in the Fig.2.1. Rogers RT/Duroid 5880 substrate with dielectric constant 2.2 and thickness 3.2 mm is used. CSRR is etched from the patch to get dual band operation. The dimensions of the proposed antenna are listed in Table 2.1.

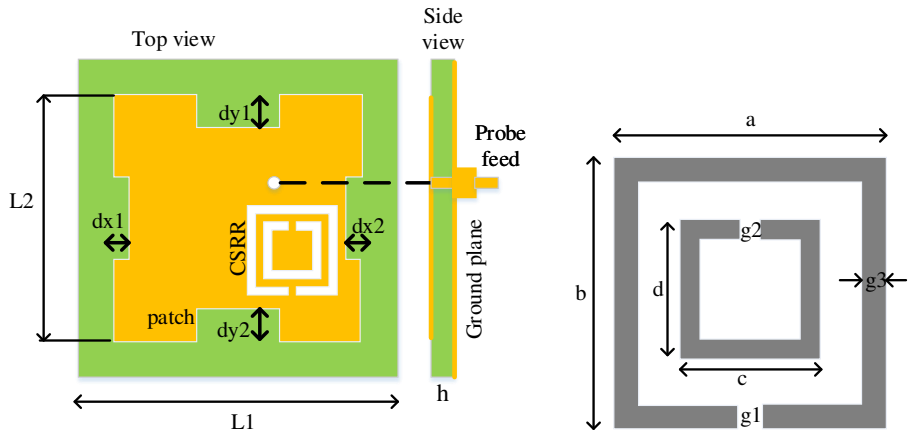

Fig. 2.1 Geometry of the proposed Minkowski fractal boundary patch antenna

Table 2.1: Parameter values in mm

parameter	Value in mm
L1	37
L2	27
h	3.175
a	10
b	10
c	9
d	9
g1	0.4
g2	0.4
g3	0.4
dx1=dx2	1
dy1=dy2	3.5

Simulation Results

Operation of the proposed design can be understood by considering an evolution of patch antenna design shown in Fig. 2.2.

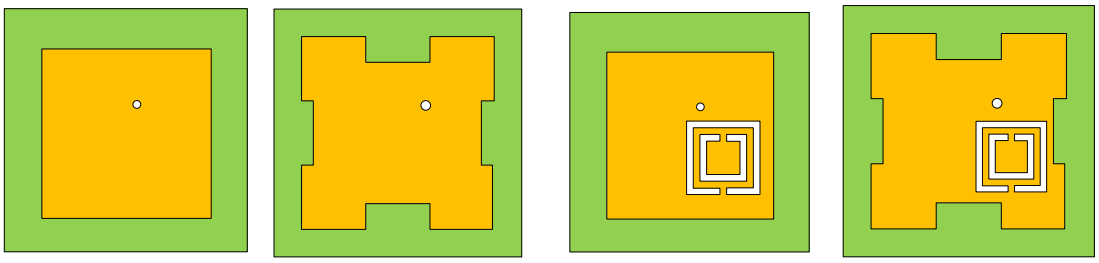

Ant1 Ant2 Ant3 Ant4

Fig. 2.2 Evolution of the proposed antenna

Initially the square patch Ant1 is chosen as reference which is resonating at 3.4 GHz with linear polarization. Minkowski fractal curves are introduced along edges of the square patch Ant1 to get Ant2 which results in CP. Ant3 can be obtained by introducing CSRR in the patch which results in double band operation with Linear Polarization. Ant4 represents the dual band dual polarization version achieved by introducing Minkowski fractal curves to the edges of Ant3. Finally Ant4 is the proposed antenna with dual band dual polarization.

The simulated return loss characteristics of all proposed antennas are shown in the Fig. 2.3. The circular polarization bandwidth at patch mode can be achieved by inserting Minkowski fractal curves along the edges of the patch. The 10-dB return loss bandwidth of all resonating frequencies is listed in Table 2.2.

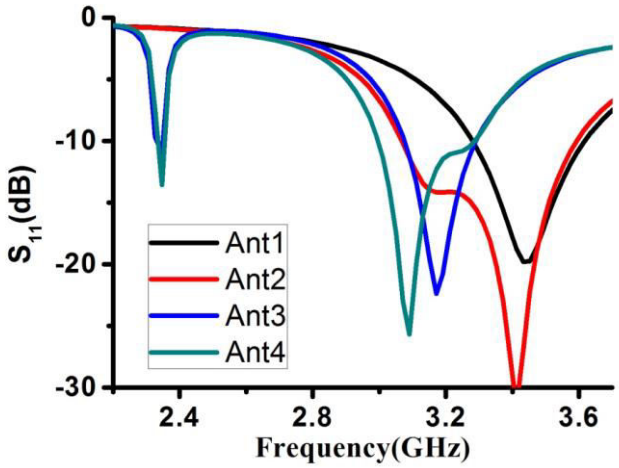

Fig. 2.3 Return loss characteristics of the proposed antennas

Table 2.2: Impedance bandwidth of the simulated antennas

Antenna	10-dB return loss bandwidth		AR bandwidth
	at left hand band	at patch mode band	At patch mode band
Ant1	---	9.27% (3.29- 3.61 GHz)	----
Ant2	---	15.06% (3.07- 3.57 GHz)	
Ant3	Resonance at 2.4 GHz	5.66% (3.09- 3.27 GHz)	
Ant4	Resonance at 2.4 GHz	8.22% (3.01- 3.27 GHz)	

To understand the operational mechanism of the proposed antenna, the HFSS simulated current distribution on patch ant 8 at each frequency band is shown in the Fig. 2.4.

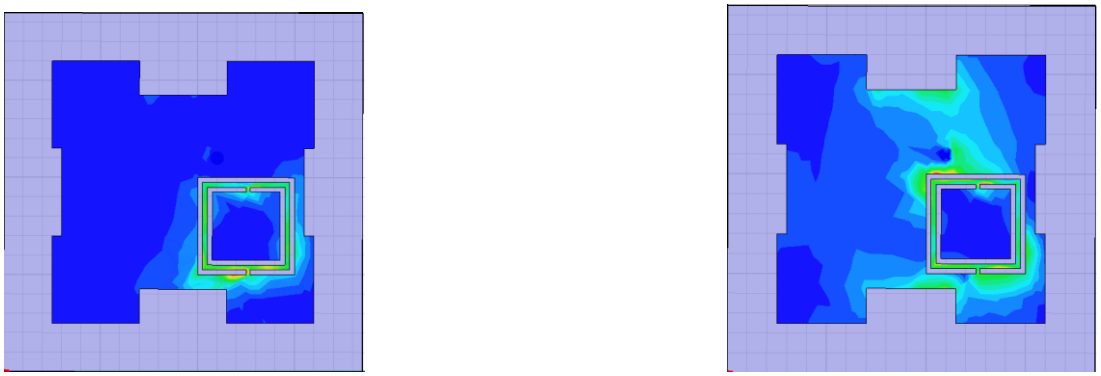

(a) (b)

Fig. 2.4 Surface current distribution at (a) 2.4 GHz (b) 3.4 GHz

The lower resonating frequency (2.4 GHz) is mainly due to strong surface current distribution at CSRR. The upper resonating frequency (3.2 GHz) is mainly because of current at Minkowski fractal edges of the patch.

2.2 CSRR based dual band Koch fractal boundary antenna

The geometry of the proposed antenna is shown in the Fig.2.5. Rogers RT/Duroid 5880 substrate with dielectric constant 2.2 and thickness 3.175 mm is used. CSRR is etched from the patch to get dual band operation. The dimensions of the proposed antenna are listed in Table 2.3.

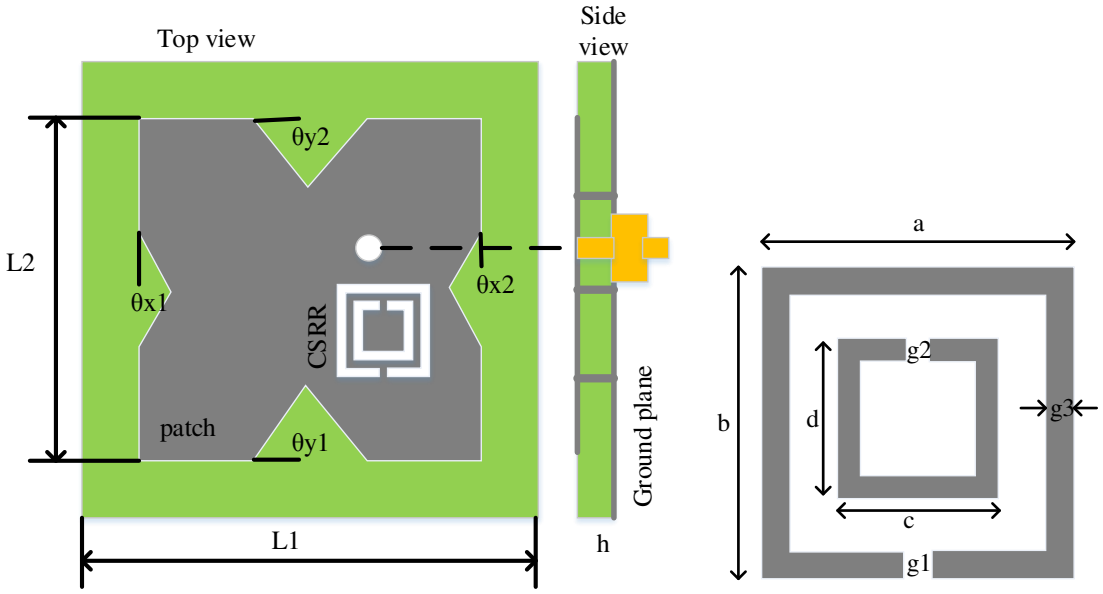

Fig. 2.5 Geometry of the proposed Koch fractal boundary patch antenna

Table 2.3: Parameter values in mm

parameter	Value in mm
L1	37
L2	27
h	3.175
a	10
b	10
c	9
d	9
g1	0.4
g2	0.4
g3	0.4
θx1= θx2	30^0
θy1= θy2	60^0

Simulation Results

The development of the proposed design can be understood by considering an evolution of patch antenna design shown in Fig. 2.6.

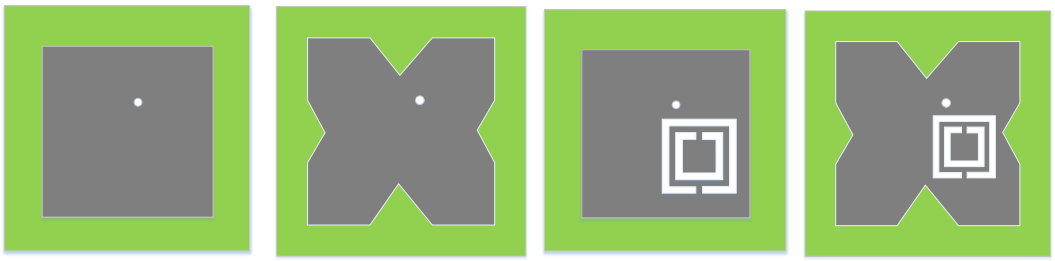

Ant1 Ant2 Ant3 Ant4

Fig. 2.6 Evolution of the proposed antenna

Initially, the square patch Ant1 is chosen as a reference which is resonating at 3.4 GHz with linear polarization. Poly fractal curves are introduced along edges of the square patch Ant1 to get Ant2 which results in CP. Ant3 can be obtained by introducing CSRR in the patch which results in double band operation with Linear Polarization. Ant4 represents the dual band dual polarization version achieved by introducing poly fractal curves to the edges of Ant3. Finally, Ant4 is the proposed antenna with dual band dual polarization.

The simulated return loss characteristics of all identified antennas are shown in the Fig. 2.7. The circular polarization bandwidth at patch mode can be achieved by inserting poly fractal curves along the edges of the patch. The 10-dB return loss bandwidth of all resonating frequencies is listed in Table 2.4.

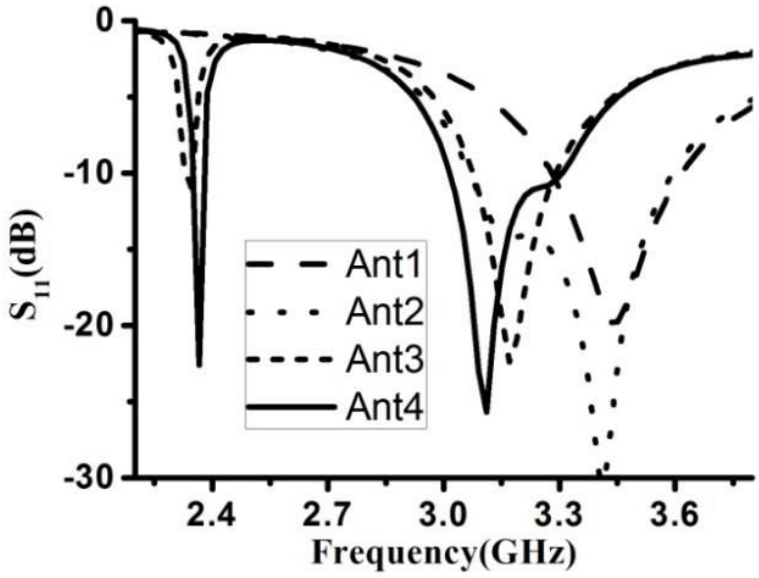

Fig. 2.7 Return loss characteristics of the proposed antennas

Table 2.4: Impedance bandwidth of the simulated antennas

Antenna	10-dB return loss bandwidth		AR bandwidth at patch mode band
	at left hand band	at patch mode band	
Ant1	---	9.27% (3.29- 3.61 GHz)	------
Ant2	---	15.06% (3.07- 3.57 GHz)	
Ant3	Resonance at 2.4 GHz	5.66% (3.09- 3.27 GHz)	----
Ant4	Resonance at 2.4 GHz	8.22% (3.03- 3.29 GHz)	2.5% (3.15- 3.23 GHz)

To understand the operational mechanism of the proposed antenna, the HFSS simulated current distribution on patch Ant4 at each frequency band is shown in the Fig. 2.8.

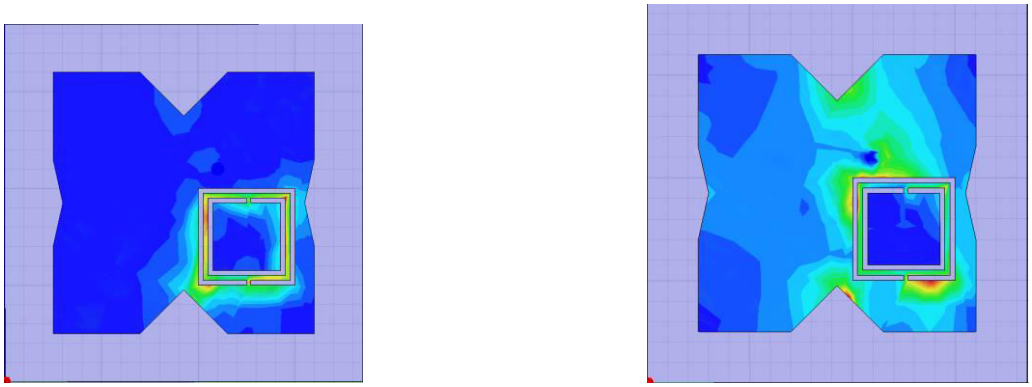

(a) (b)

Fig. 2.8 Simulated Surface current distribution at (a) 2.4 GHz (b) 3.3 GHz

The lower resonating frequency (2.4 GHz) is mainly due to strong surface current distribution at CSRR where as the upper resonating frequency (3.3 GHz) is due to current at poly fractal edges of the patch.

2.3 CSRR based dual band poly fractal boundary antenna

The geometry of the proposed antenna is shown in the Fig.2.9. Rogers RT/Duroid 5880 substrate with dielectric constant 2.2 and thickness 3.175 mm is used. CSRR is etched from the patch to get dual band operation. The dimensions of the proposed antenna are listed in Table 2.5.

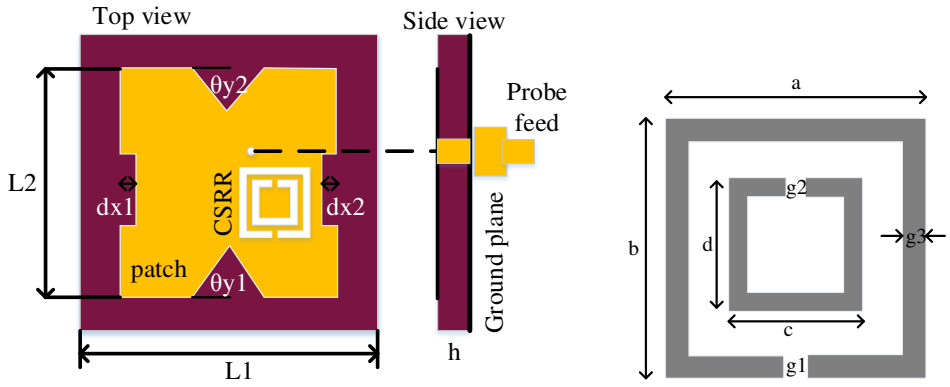

Fig. 2.9 Geometry of the proposed Poly fractal boundary patch antenna

Table 2.5: Parameter values in mm

parameter	Value in mm
L1	37
L2	27
h	3.175
a	10
b	10
c	9
d	9
g1	0.4
g2	0.4
g3	0.4
dx1=dx2	1
θy1= θy2	60

Simulation Results

The development of the proposed design can be understood by considering an evolution of patch antenna design shown in Fig. 2.10.

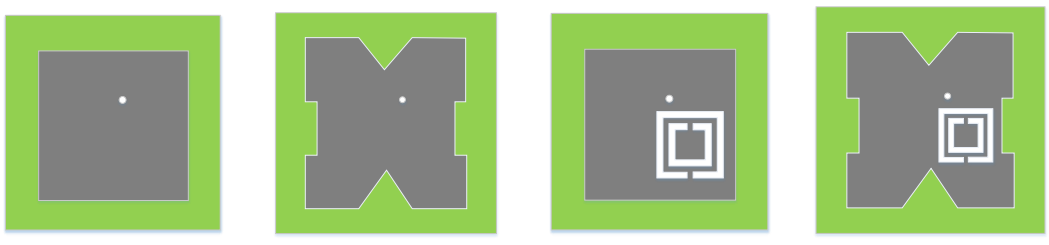

Ant1 Ant2 Ant3 Ant4

Fig. 2.10 Evolution of the proposed antenna

Initially, the square patch Ant1 is chosen as a reference which is resonating at 3.4 GHz with linear polarization. Poly fractal curves are introduced along edges of the square patch Ant1 to get Ant2 which results in CP. Ant3 can be obtained by introducing CSRR in the patch which results in double band operation with Linear Polarization. Ant4 represents the dual band dual polarization version achieved by introducing poly fractal curves to the edges of Ant3. Finally, Ant4 is the proposed antenna with dual band dual polarization.

The simulated return loss characteristics of all aforementioned antennas are shown in the Fig. 2.11. The circular polarization bandwidth at patch mode can be achieved by inserting poly fractal curves along the edges of the patch. The 10-dB return loss bandwidth of all resonating frequencies is listed in Table 2.6.

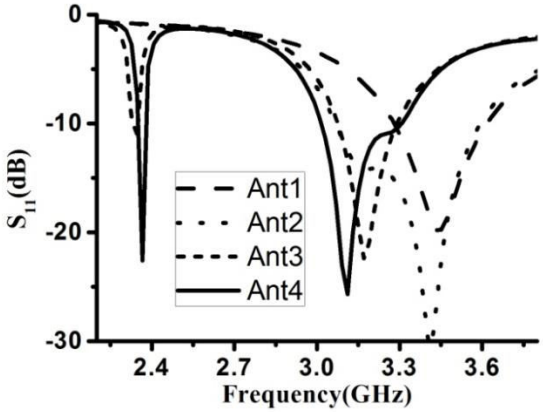

Fig. 2.11 Return loss characteristics of the proposed antennas

Table 2.6:Impedance bandwidth of the simulated antennas

Antenna	10-dB return loss bandwidth		AR bandwidth at patch mode band
	at left hand band	at patch mode band	
Ant1	---	9.27% (3.29- 3.61 GHz)	------
Ant2	---	15.06% (3.07- 3.57 GHz)	
Ant3	Resonance at 2.4 GHz	5.66% (3.09- 3.27 GHz)	
Ant4	Resonance at 2.4 GHz	8.22% (3.03- 3.29 GHz)	2.5% (3.15- 3.23 GHz)

To understand the operational mechanism of the proposed antenna, the HFSS simulated current distribution on patch Ant4 at each frequency band is shown in the Fig. 2.12

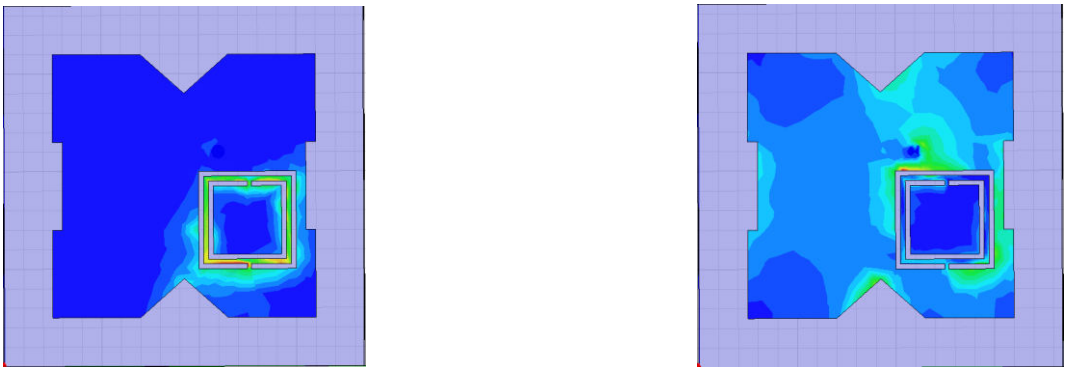

(a) (b)

Fig. 2.12 Simulated Surface current distribution at (a) 2.4 GHz (b) 3.3 GHz

The lower resonating frequency (2.4 GHz) is mainly due to strong surface current distribution at CSRR where as the upper resonating frequency (3.3 GHz) is due to current at poly fractal edges of the patch. The simulated radiation efficiency of the proposed antenna is shown in the Fig 2.13. The radiation efficiency of the proposed antenna is 96.5% at lower resonating frequency (2.4 GHz) and is 98.75% at upper resonating frequency (3.4 GHz).

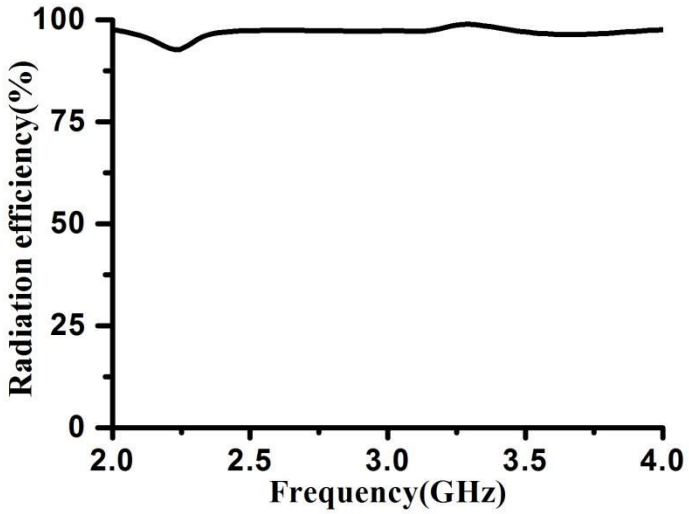

Fig 2.13 Simulated radiation efficiency characteristics of the proposed antenna

2.4 Experimental Results

The proposed antenna (Ant4) fabricated on Rogers RT/Duroid substrate with dimensions 37x37x3.175 mm^3 is shown in Fig. 2.14. The return loss characteristics are measured using Agilent 8719A microwave network analyzer. Radiation pattern measurements are taken in an anechoic chamber having the physical dimensions of 22.5 x 12.5 x 11.5 m^3 and with the operating frequency range of 400 MHz to 18 GHz.

(a) (b)

Fig. 2.14 Fabricated prototype (a) top view (b) bottom view

The measured return loss characteristics along with simulated data are given in Fig. 2.15. Measured results are in close agreement with simulated data. The slight kink at upper resonating band indicates the possibility of circular polarization radiation.

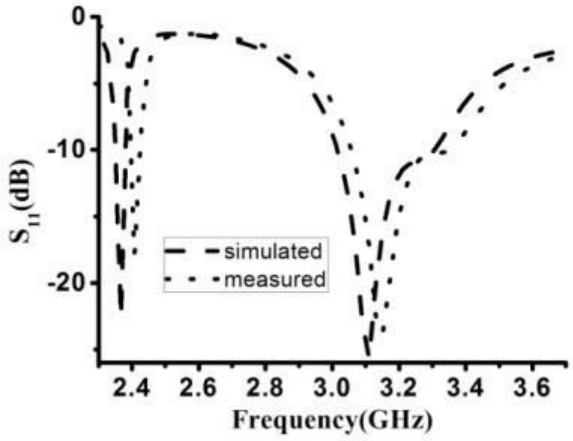

Fig. 2.15 Return loss characteristics of the fabricated antenna

The 10-dB return loss bandwidth is 8.22% (3.01- 3.27 GHz) at upper resonating frequency band due to current at patch edges and <1% (resonance at 2.4 GHz only) at lower left handed resonance frequency band because of current at CSRR respectively. The Axial ratio characteristics are given in Fig. 2.16. The measured 3-dB axial ratio bandwidth at the upper resonating frequency is 2.50% (3.15- 3.23 GHz). The minimum Axial Ratio value of 0.3 dB occurred at the center frequency. The radiation patterns of the proposed antenna at the lower and upper resonating bands (2.4 GHz and 3.2 GHZ) are shown in the Figs. 2.17 & 2.18 respectively. The gain of the proposed antenna is given in Fig. 2.19.

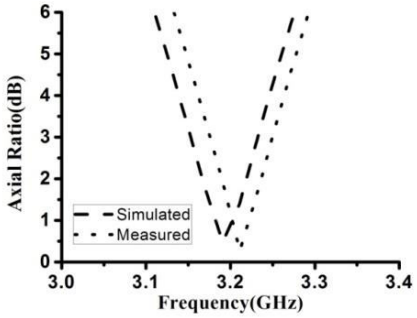

Fig. 2.16 Axial Ratio characteristics of the proposed antenna

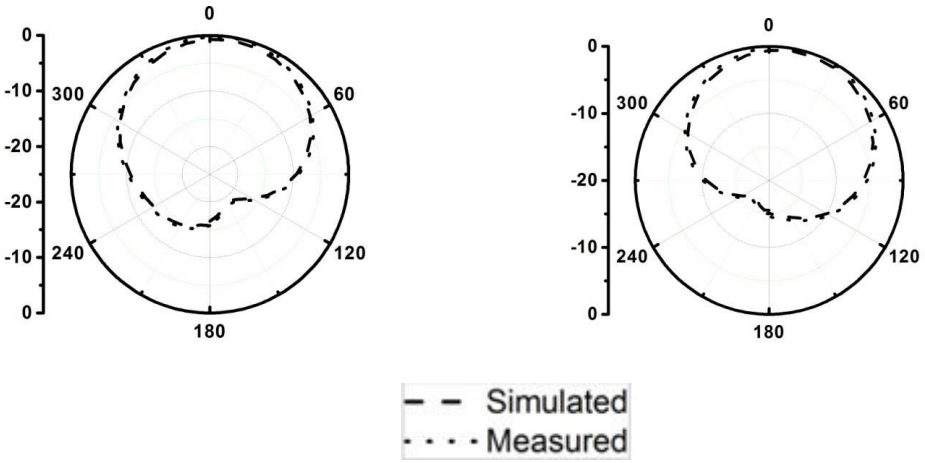

(a) (b)

Fig. 2.17 Simulated and measured radiation characteristics of the proposed antenna at 2.4 GHz (a) E plane (b) H plane

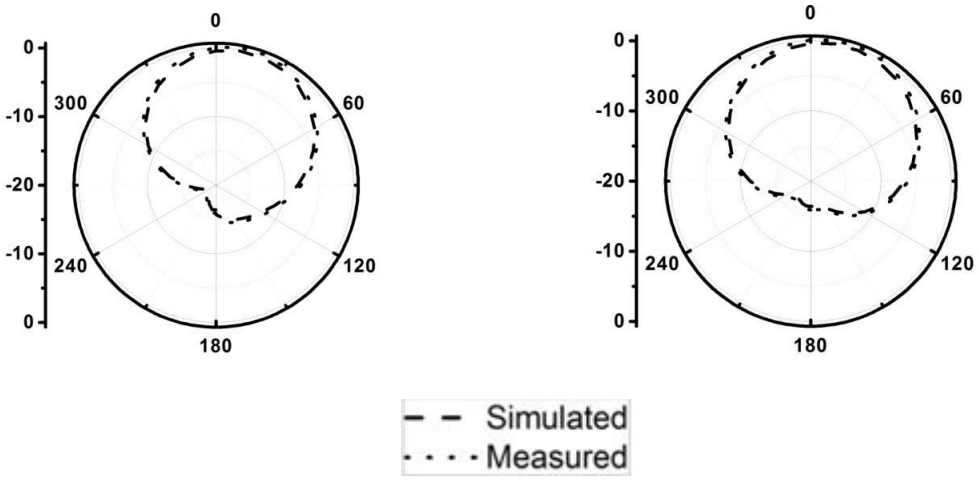

(a) (b)

Fig. 2.18 Simulated and measured radiation characteristics of the proposed antenna at 3.2 GHz (a) E plane (b) H plane

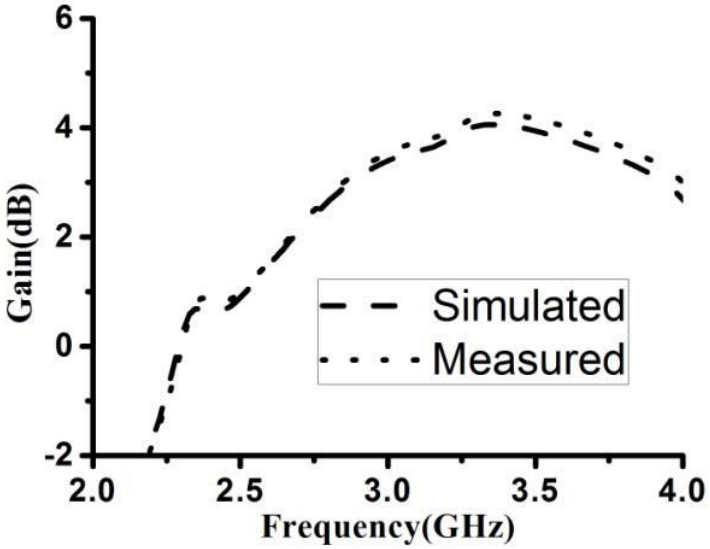

Fig. 2.19 Gain characteristics of the proposed antenna

Comparison between the results of the proposed antenna and the antennas which already exist in the literature are given in the Table 2.7. The proposed antenna is more compact and producing wide bandwidth compared to remaining antennas listed in Table 2.7.

Table 2.7 Comparison between the proposed antenna and the existing literature

	Antenna size (mm^2)	Substrate size (mm^3)	Resonant frequency (GHz), 10-dB return loss bandwidth (%)	
			At lower band	At upper band
prop	27x27	37x37x3.175	2.4, --	3.2, 8.22
[14]	18.43x23.68		4.1, -	4.8, -
[17]	18.43x23.68		4.1, -	4.8, -
[23]	16.8	32.62x3	1.6, -	4.5, -
[8]	20x16	30x50x1.6	2.9, -	3.6, -
[10]		58x23x1.5	0.917, 1	1.854, 1.5
[15]	17.7x17.5		3.73, 1.2	5.25, 1.5
[16]	19x19	40x35x1.57	6.8, --	
[11]	5x0.5		9.51, --	
[26]	16.8	32.62x3	1.62,-	4.53, -

2.5 Conclusions

Dual band patch antennas with embedded square CSRR at right bottom corner are presented. Various fractal antennas using Minkowski, Koch and poly curves are studied for dual band operation. By varying the feed point position dual band antennas which resonate at 2.4 GHz, 3.4 GHz are designed. The 3-dB CP bandwidths obtained at upper bands are more than 2%. These antennas are useful for systems operating at Wi-Fi and Wi-MAX standards IEEE 802.11 and IEEE 802.16. These antennas are fabricated and performance is measured. A good comparison is obtained.

Here dual band operation for the devices requiring small bandwidths to have voice communication or audio transmission is presented. However, high bandwidth is desirable at left hand band for video or data transmission. To realize this, another variety of metamaterials i.e. DNG materials are attempted in the next chapter.

Chapter 3

Compact Dual Band Microstrip Patch Antennas Based on Mushroom Unit Cell

The present-day handheld devices are required to operate with various standards thus forcing them to operate at separate frequency bands. Instead of using several antennas, a single Microstrip Patch Antenna (MPA) which operates for WLAN, Wi-Fi and WiMAX applications with less size and wider bandwidth at each operating frequency is the most suitable candidate for daily life wireless portable devices. In a conventional dual-band or multi-band, MPAs the dimensions of the radiating patch are taken with reference to the lowest frequency band which requires more size. Then the current on the patch is perturbed to obtain resonance at higher frequency band. Moreover, they offer only linear polarization at both the bands with narrow bandwidth. But modern devices need to provide good circular polarization at WiMAX band to avoid orientation problems.

Metamaterials are a good choice in designing novel antennas because of their artificial electromagnetic properties. These materials will support backward wave propagation, due to which left-handed bands (zeroth order or negative order modes) are produced. Metamaterials or left-handed materials are classified into Epsilon Negative materials (ENG), Permeability negative materials (MNG) and Double negative materials (DNG). These materials can be realized by using metallic VIAs, Split Ring Resonators (SRRs) and the combination of both these.

The pioneers in this area analyzed the Composite Right/ Left Handed transmission lines (CRLH TL) based on transmission line theory. MUC loaded patch antenna for single-band dual band and multiband antennas are presented so far. In all these antennas, the gain and bandwidth are low whereas the size is high. The novelty of the proposed antenna is to embed metamaterials and fractal curves into the conventional MPA. By the adoption of the metamaterials concept, the designer can identify an antenna for high-frequency operation first

with less size and then embed metamaterial structure for lower frequency band (this is reverse order compared to previous methods).

In this section three new antennas are studied for dual band operation where lower band is resonating with LP and upper band is resonating with CP with a single probe feed based on Mushroom Unit cell and fractal curves. They are:

(1) MUC based dual band Minkowski fractal boundary antenna
(2) MUC based dual band Koch fractal boundary antenna
(3) MUC based dual band Poly fractal boundary antenna

3.1 MUC based dual band Minkowski fractal boundary antenna

The geometry of the Minkowski fractal boundary patch antenna is shown in Fig. 3.1. The radiating patch is slotted at the right bottom corner to load MUC. The dimensions of the slot are 10x10 mm^2. Square MUC having a metallic patch with a side length of 9.5 mm and a VIA with 0.3 mm radius is loaded into the patch. The series capacitance due to the gap between patch and MUC and shunt inductance due to VIA are the main cause for getting zeroth order band (left-hand band). The dimensions of the proposed antenna are indicated in Table 3.1.

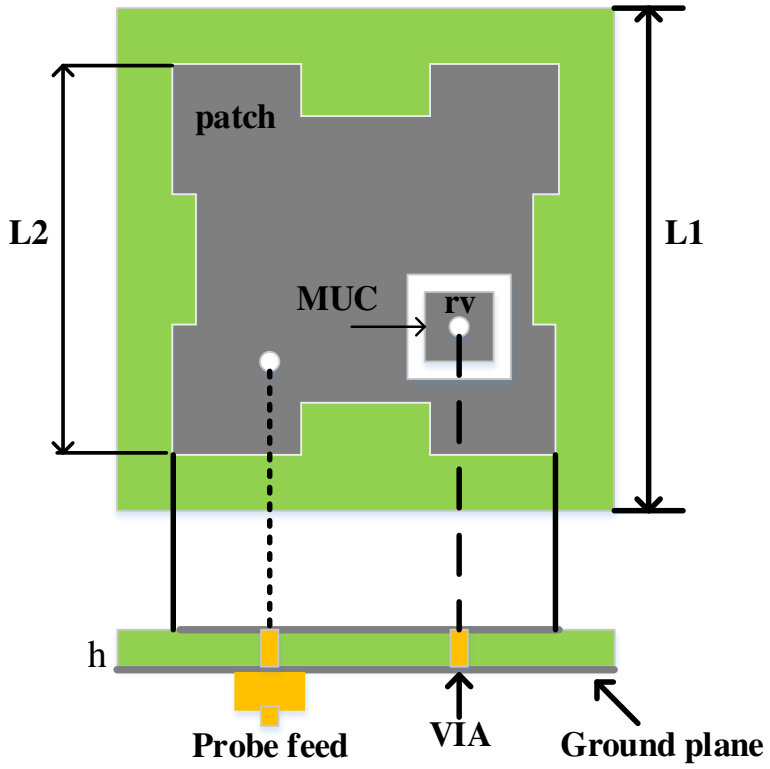

(a)

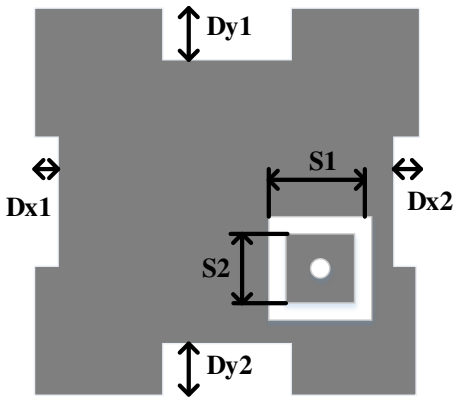

(b)

Fig. 3.1 Geometry of (a) DNGTL based patch antenna (b) Structure of Minkowski fractal patch

Table 3.1: parameter values

Parameter	Value in mm
L_1	37
L_2	27
S_1	10
S_2	9.5
Dx1=Dx2	1
Dy1=Dy2	3
H	3.175
r_v	0.3

The layout of the proposed antenna can be understood by considering an evolution of patch antenna layout shown in Fig. 3.2. To begin with, the rectangular patch Ant1 is selected as a reference that is resonating at 3.5 GHz with linear polarization (LP). The CP at this single band may be received by changing edges of the square patch with Minkowski fractal curves which results in Ant2. Ant3 is completed by using inserting MUC alongside the lowest right nook of Ant1 to provide two bands with LP. Ultimately, Ant4 may be designed by using loading MUC in Ant2 to bring about twin-band patch antenna with first band LP and the second band with CP. The simulated Return Loss (RL) characteristics of the presented Minkowski fractal boundary patch antenna are shown in the Fig. 3.3.

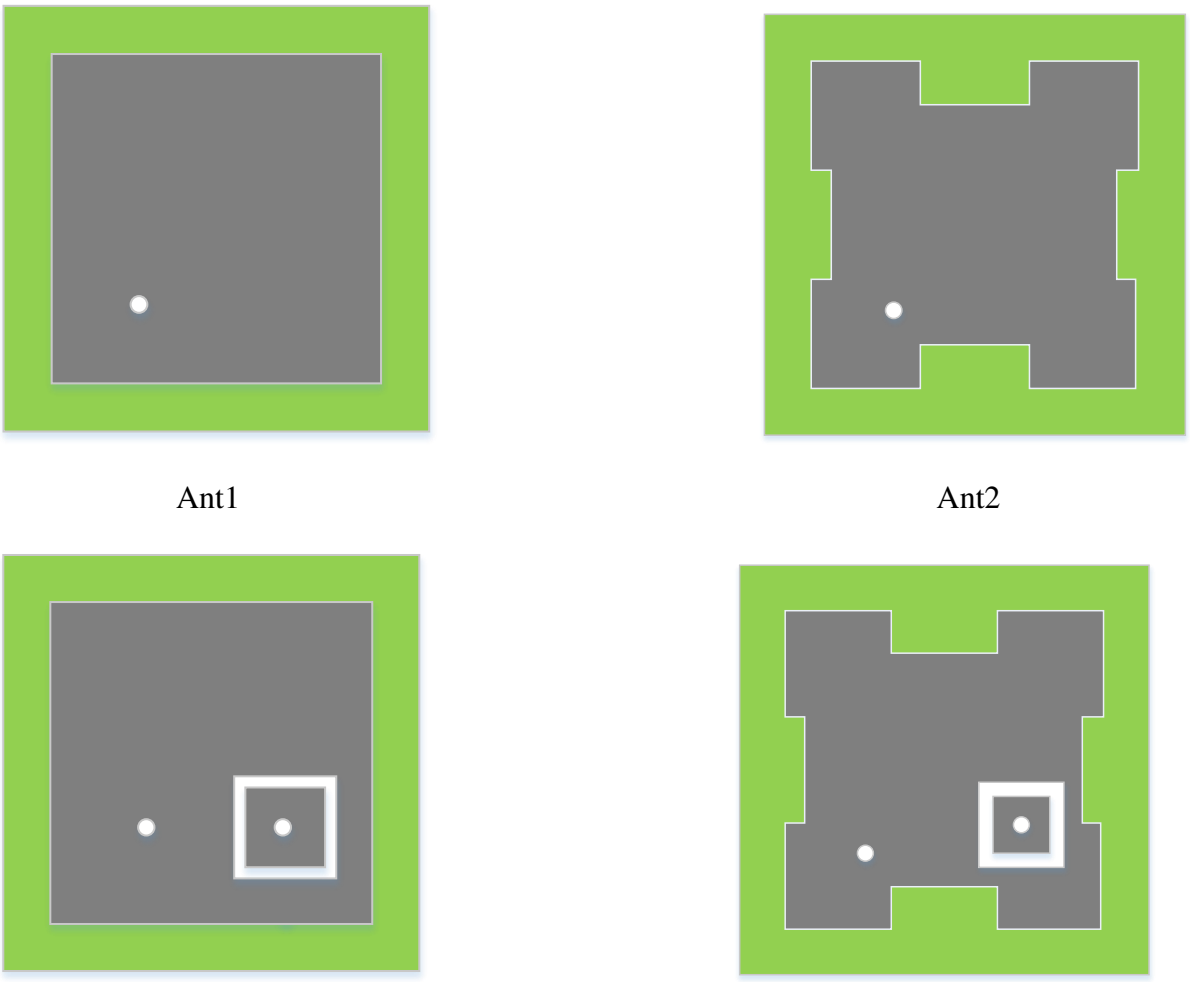

Fig. 3.2 In-between steps in the design

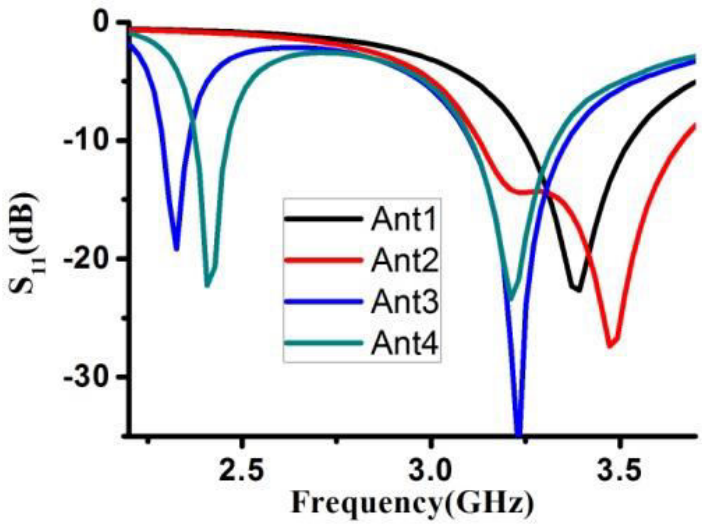

Fig. 3.3 Simulated RL characteristics

Table 3.2: Impedance bandwidth values

S. No	Antenna	Impedance bandwidth (%)		AR bandwidth at patch mode band
		Band1	Band2	
1	Ant1	-----	9.71% (3.31- 3.73 GHz)	-----
2	Ant2	-----	8.21% (3.27- 3.55 GHz)	
3	Ant3	0.79% (2.50- 2.52 GHz)	6.26% (3.09- 3.29 GHz)	
4	Ant4	2.51% (2.36- 2.42 GHz)	6.23% (3.11- 3.31 GHz)	2.77% (3.11- 3.21 GHz)

From the Fig. 3.4, it is observed that, if the dimensions of the square MUC are decreasing, then the left-hand band is moving from left side to right side on the frequency scale. The dimensions of the MUC are optimized (S2= 9.5 mm) to get the left-hand band exactly at 2.4 GHz.

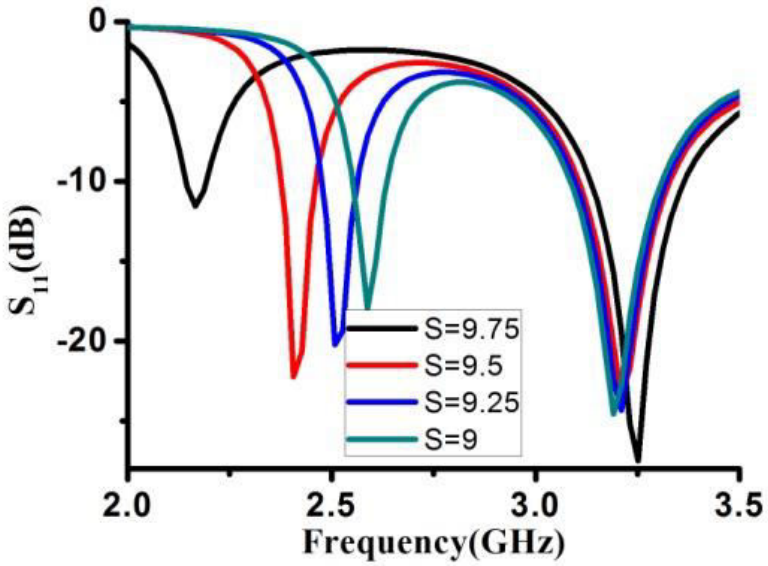

Fig. 3.4 Optimized RL characteristics

To interpret the operational mechanism of the proposed antenna, the HFSS simulated surface current distributions on the patch at each frequency band are shown in the Fig. 3.5. The lower resonating frequency (2.4 GHz) is mainly due to powerful current distribution at MUC. The upper resonating frequency (3.3 GHz) is mainly due to the strong surface current at the edges of the patch.

(a) (b)

Fig. 3.5 Simulated surface current distribution (a) at 2.4 GHz (b) at 3.4 GHz

3.2 MUC based dual band Koch fractal boundary antenna

The geometry of the Koch fractal boundary patch antenna is shown in Fig. 3.6. The antenna is designed on Rogers RT/Duroid substrate with a thickness of 3.175 mm and dielectric constant of 2.2. The radiating patch is slotted at the right bottom corner to load MUC. The dimensions of the slot are 10x10 mm^2. Square MUC having a metallic patch with a side length of 9.5 mm and a VIA with 0.3 mm radius is loaded into the patch. The series capacitance due to the gap between patch and MUC and shunt inductance due to VIA are the main cause for getting zeroth order band (left-hand band). The dimensions of the proposed antenna are shown in Table 3.3.

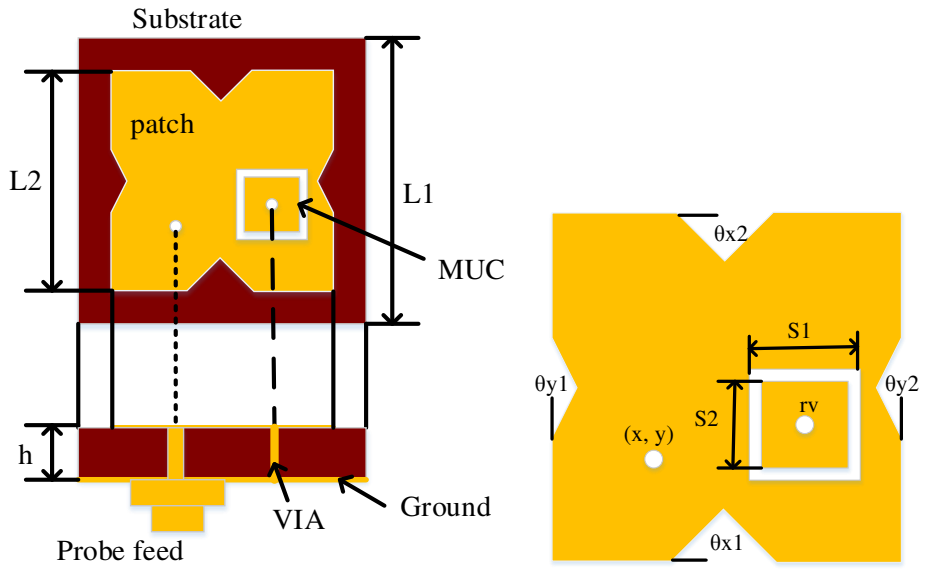

(a) (b)

Fig. 3.6 Geometry of (a) proposed antenna (b) IAs of Koch fractal boundary

Table 3.3: parameter values

Parameter	Value in mm
L_1	37
L_2	27
S_1	10
S_2	9.5
$\theta_{x1}=\theta_{x2}$	60
$\theta_{y1}=\theta_{y2}$	30
H	3.175
r_v	0.3

The evolution of proposed patch antenna design is shown in Fig. 3.7. Initially, the square patch Ant1 is chosen as a reference which is resonating at 3.5 GHz with linear polarization (LP). The CP at this single band can be obtained by replacing edges of the square patch with Minkowski fractal curves which results in Ant2. Ant3 is achieved by inserting MUC along the bottom right corner of Ant1 to produce two bands with LP. Finally, Ant4 can be designed by loading MUC in Ant2 to result in dual-band patch antenna with first band LP and the second band with CP. The optimized feed point location is obtained from the software tool which is 4.5 mm distance away diagonally from the midpoint of the patch. The simulated Return Loss (RL) characteristics of the proposed Koch fractal boundary patch antenna are shown in the Fig. 3.8.

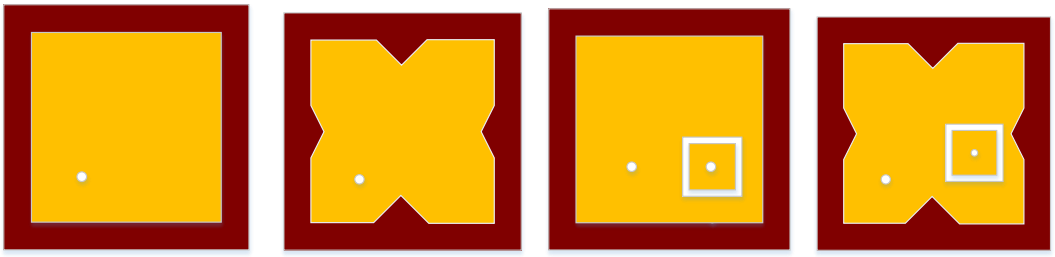

Ant1 Ant2 Ant3 Ant4

Fig. 3.7 In between steps in the design

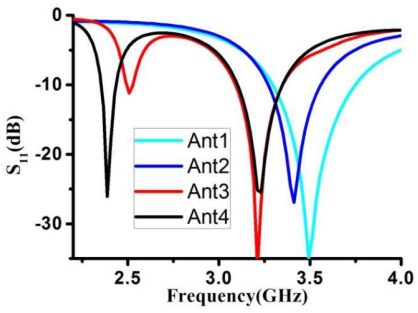

Fig. 3.8 Simulated RL characteristics

Table 3.4: Impedance bandwidth values

S. No	Antenna	Impedance bandwidth (%)		AR bandwidth at patch mode band
		Band1	Band2	
1	Ant1	-----	9.71% (3.31- 3.73 GHz)	-----
2	Ant2	-----	8.21% (3.27- 3.55 GHz)	
3	Ant3	0.79% (2.50- 2.52 GHz)	6.26% (3.09- 3.29 GHz)	
4	Ant4	2.51% (2.36- 2.42 GHz)	6.23% (3.11- 3.31 GHz)	2.77% (3.11- 3.21 GHz)

To understand the operational mechanism of the proposed antenna, the HFSS simulated surface current distributions on the patch at each frequency band are shown in the Fig. 3.9. The lower resonating frequency (2.4 GHz) is mainly due to heavy current distribution at MUC. The upper resonating frequency (3.3 GHz) is mainly due to the well built surface current at the edges of the patch.

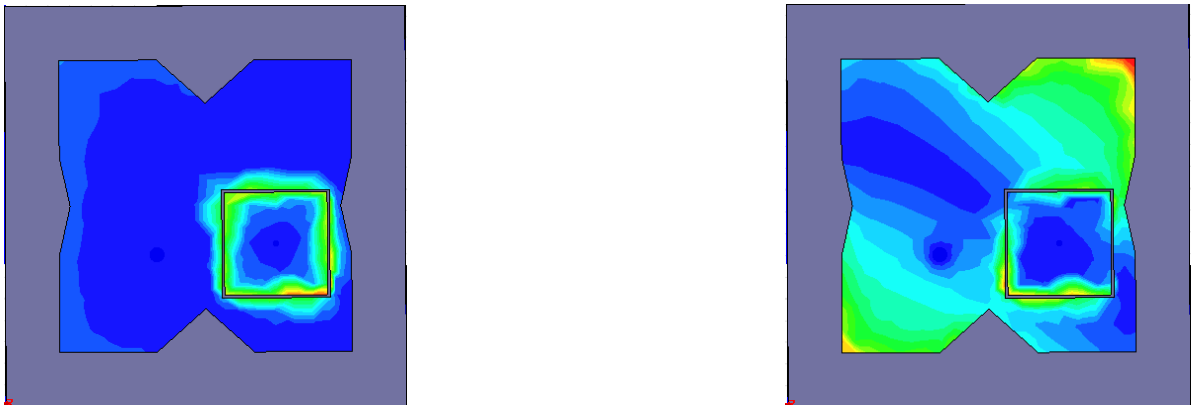

(a) (b)

Fig. 3.9 Simulated surface current distribution (a) at 2.4 GHz (b) at 3.25 GHz

3.3 MUC based dual band Poly fractal boundary antenna

The geometry of the Poly fractal boundary patch antenna is shown in Fig. 3.10. The antenna is designed on Rogers RT/Duroid substrate with a thickness of 3.175 mm and dielectric constant of 2.2. The radiating patch is slotted at the right bottom corner to load MUC. The dimensions of the slot are 10x10 mm^2. Square MUC having a metallic patch with a side length of 9.5 mm and a VIA with 0.3 mm radius is loaded into the patch. The series capacitance due to the gap between patch and MUC and shunt inductance due to VIA are the main cause for getting zeroth order band (left-hand band). The dimensions of the proposed antenna are shown in Table 3.5.

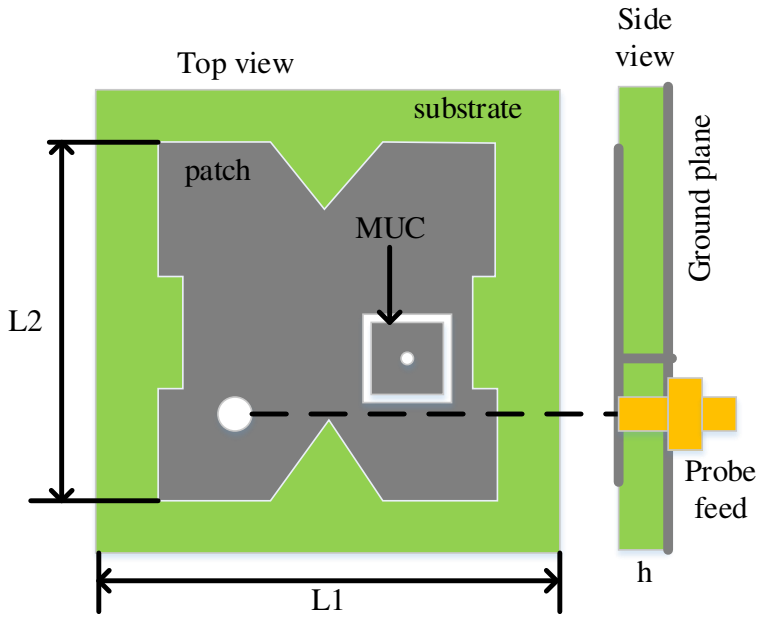

(a)

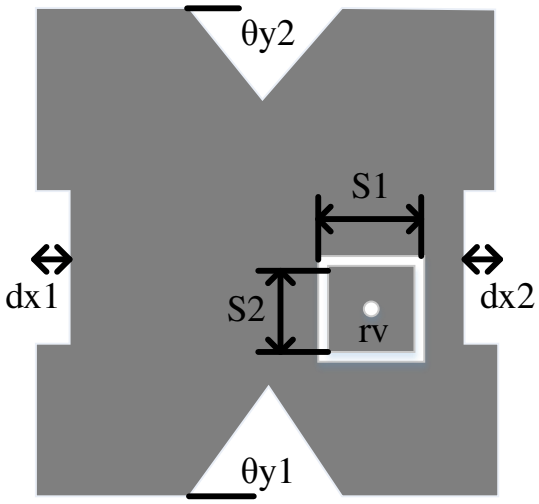

(b)

Fig. 3.10 Geometry of (a) proposed antenna (b) IAs of Poly fractal boundary

Table 3.5: parameter values

Parameter	Value in mm
L_1	37
L_2	27
S_1	10
S_2	9.5
$\theta_{x1}=\theta_{x2}$	60
$\theta_{y1}=\theta_{y2}$	30
H	3.175
r_v	0.3

The development of proposed patch antenna is shown in Fig. 3.11. Initially, the square patch Ant1 is chosen as a reference which is resonating at 3.5 GHz with linear polarization (LP). The CP at this single band can be obtained by replacing edges of the square patch with Minkowski fractal curves which results in Ant2. Ant3 is achieved by inserting MUC along the bottom right corner of Ant1 to produce two bands with LP. Finally, Ant4 can be designed by loading MUC in Ant2 to result in dual-band patch antenna with first band LP and the second band with CP. The optimized feed point location is obtained from the software tool which is 4.5 mm distance away diagonally from the midpoint of the patch. The simulated Return Loss (RL) characteristics of the proposed Poly fractal boundary patch antenna are shown in the Fig. 3.12.

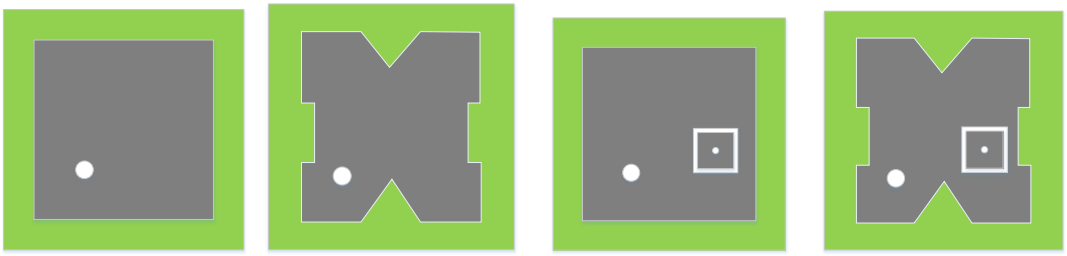

Ant1 Ant2 Ant3 Ant4

Fig. 3.11 In between steps in the design

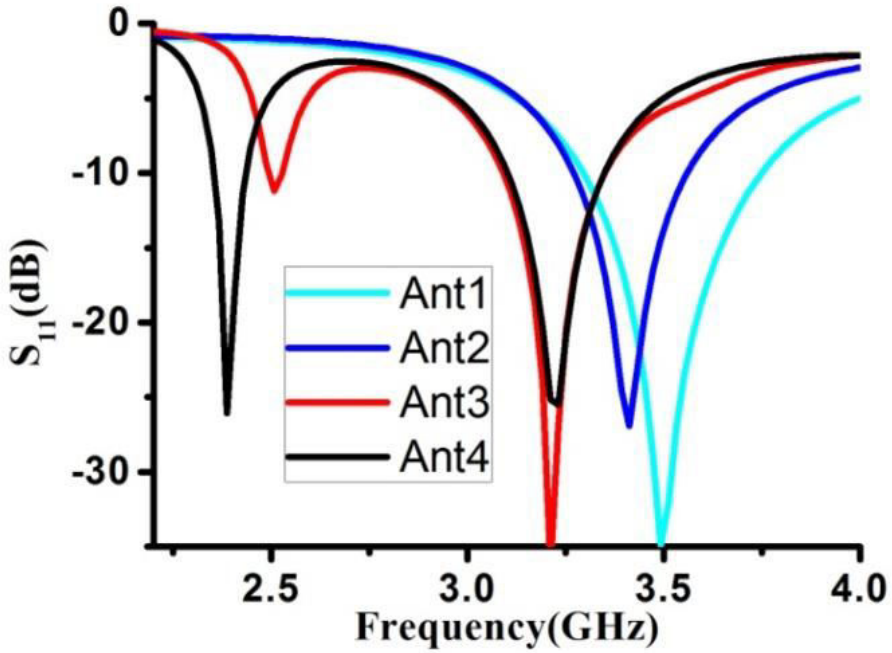

Fig. 3.12 Simulated RL characteristics

Table 3.6: Impedance bandwidth values

S. No	Antenna	Impedance bandwidth (%)		AR bandwidth at patch mode band
		Band1	Band2	
1	Ant1	-----	9.71% (3.31- 3.73 GHz)	-----
2	Ant2	-----	8.21% (3.27- 3.55 GHz)	
3	Ant3	0.79% (2.50- 2.52 GHz)	6.26% (3.09- 3.29 GHz)	----
4	Ant4	2.51% (2.36- 2.42 GHz)	6.23% (3.11- 3.31 GHz)	2.77% (3.11- 3.21 GHz)

To understand the operational mechanism of the proposed antenna, the HFSS simulated surface current distributions on the patch at each frequency band are shown in the Fig. 3.13. The lower resonating frequency (2.4 GHz) is mainly due to strong current distribution at MUC. The upper resonating frequency (3.3 GHz) is mainly due to the strong surface current at the edges of the patch. The simulated radiation efficiency of the proposed antenna is shown in the Fig 3.14. The radiation efficiency of the proposed antenna is 97.5% at lower resonating frequency (2.4 GHz) and is 98.75% at upper resonating frequency (3.4 GHz).

(a) (b)

Fig. 3.13 Simulated surface current distribution (a) at 2.4 GHz (b) at 3.25 GHz

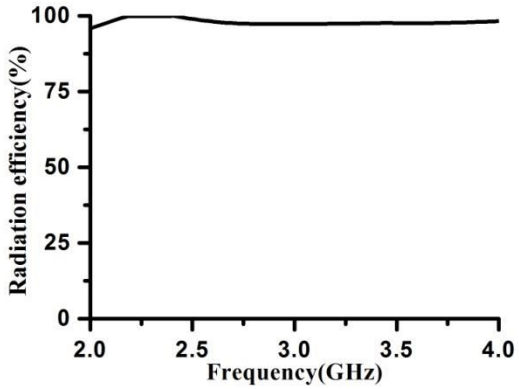

Fig 3.14 Simulated radiation efficiency of the proposed antenna

3.4 Experimental Results

The proposed antenna (Ant4) is fabricated on Rogers RT/Duroid substrate with dimensions 37 x 37 x 3.175 mm^3 as shown in Fig. 3.15. The vertical metallic VIAs (copper wires) are loaded into the patch through ground plane by using through-hole copper technique. Agilent 8719A microwave network analyzer is used to measure the return loss characteristics. Radiation pattern measurements are taken in an anechoic chamber having physical dimensions of 22.5 x 12.5 x 11.5 m^3. The operating frequency range of the anechoic chamber is 400 MHz to 18 GHz.

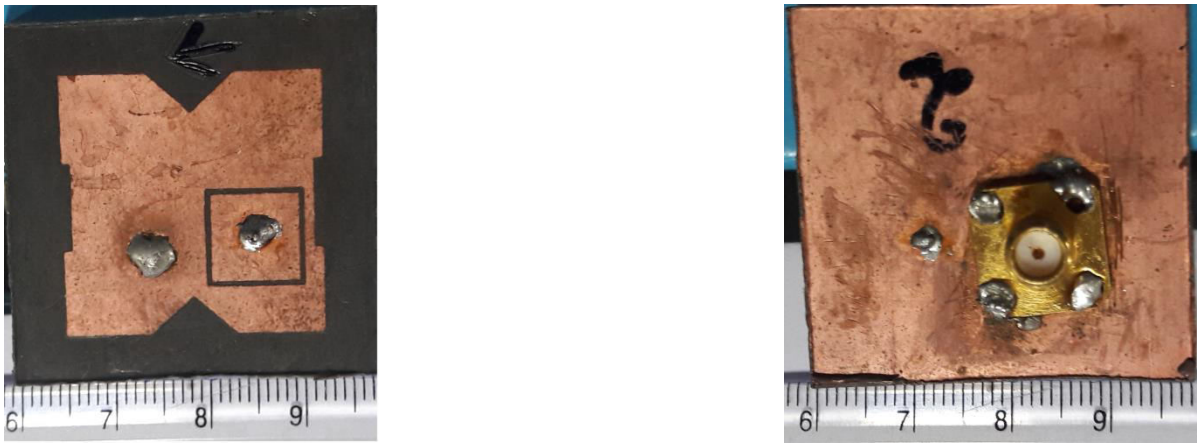

(a) (b)

Fig: 3.15 prototype of Ant4 (a) Top view (b) Bottom view

The measured and simulated return loss characteristics of Ant4 are shown in the Fig. 3.16. Measured results are in close agreement with simulated data. The measured return loss bandwidth of Poly fractal boundary patch antenna is 2.51% at the lower resonating band and 6.23% at upper resonating band respectively. The discontinuity at upper resonating band indicates the possibility of circular polarization radiation. The measured AR characteristics are given in Fig. 3.17. The 3- dB Axial Ratio bandwidth at upper resonating band is 2.35%.

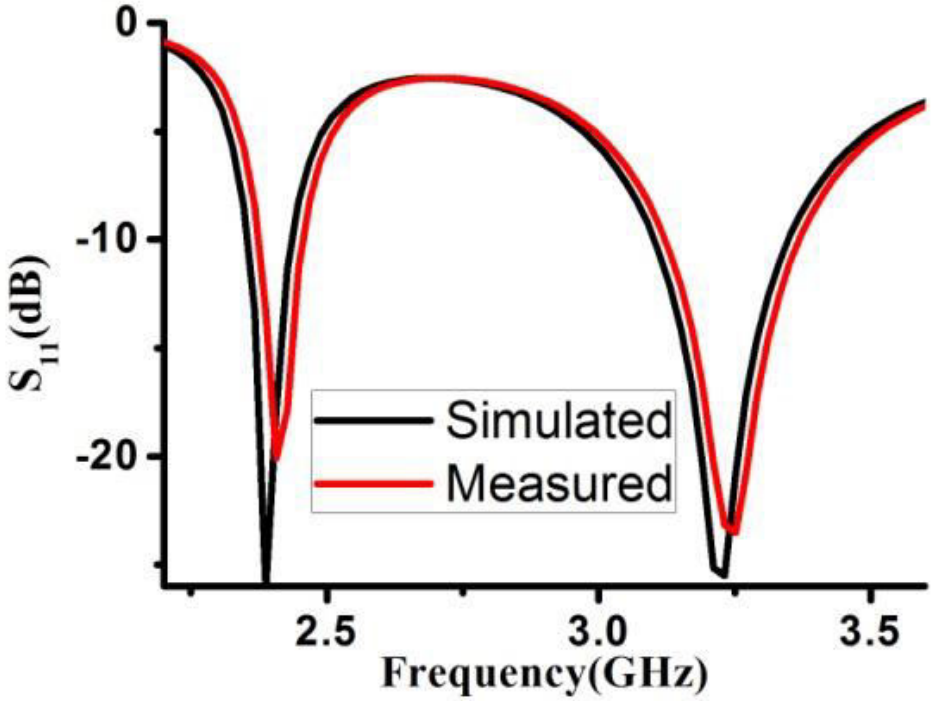

Fig. 3.16 Return loss characteristics of Ant4

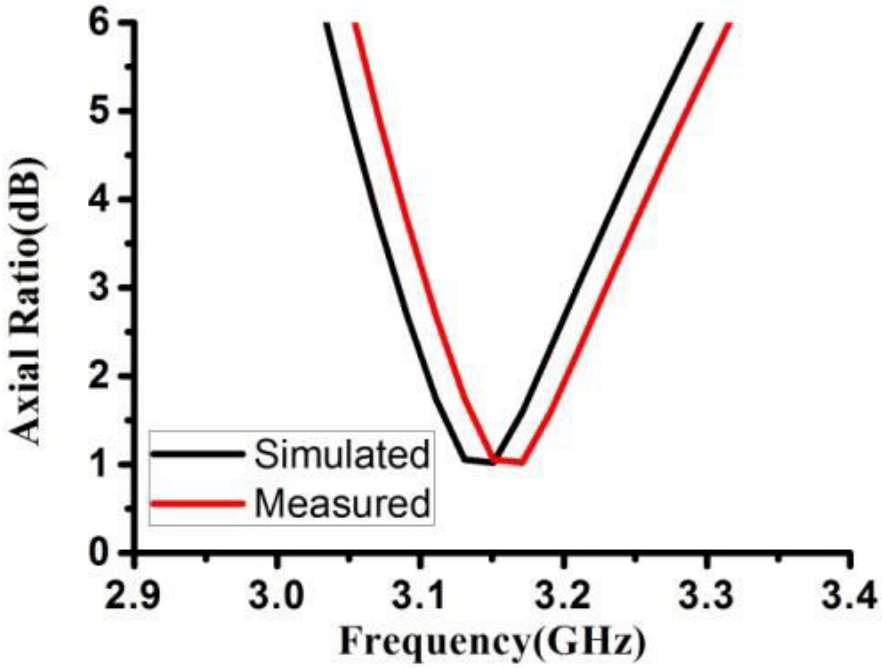

Fig. 3.17 Axial Ratio characteristics of Ant4

The measured radiation patterns are shown in the Figs.3.18 and 3.19. The gain characteristics of the proposed antenna are shown in the Fig. 3.20, which indicates that the gain at left-hand band is moderate where as the gain at patch mode band is high.

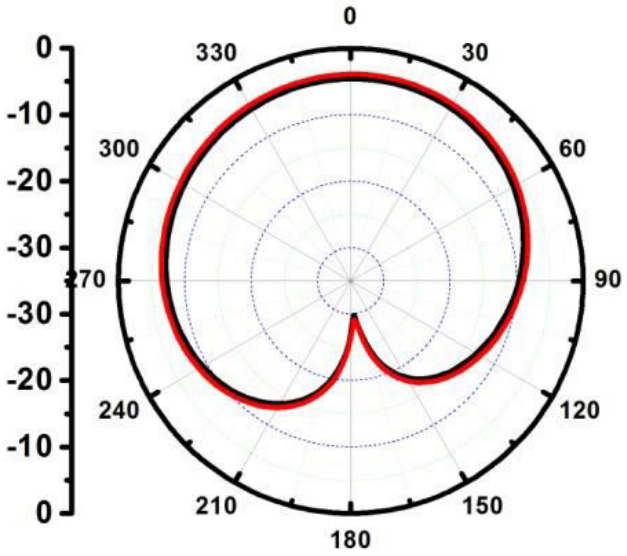

(a)

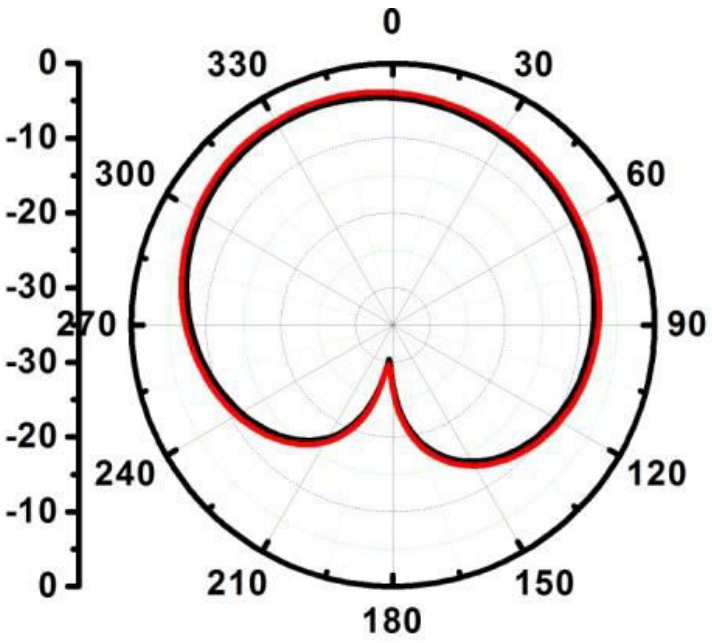

(b)

Simulated
Measured

Fig. 3.18 Radiation patterns of Ant4 at 2.4 GHz (a) E Plane (b) H Plane

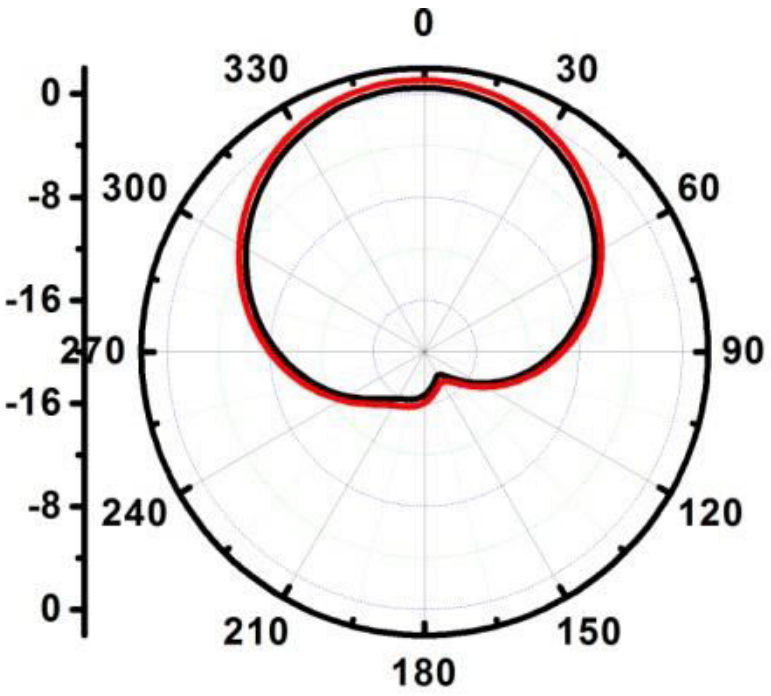

(a)

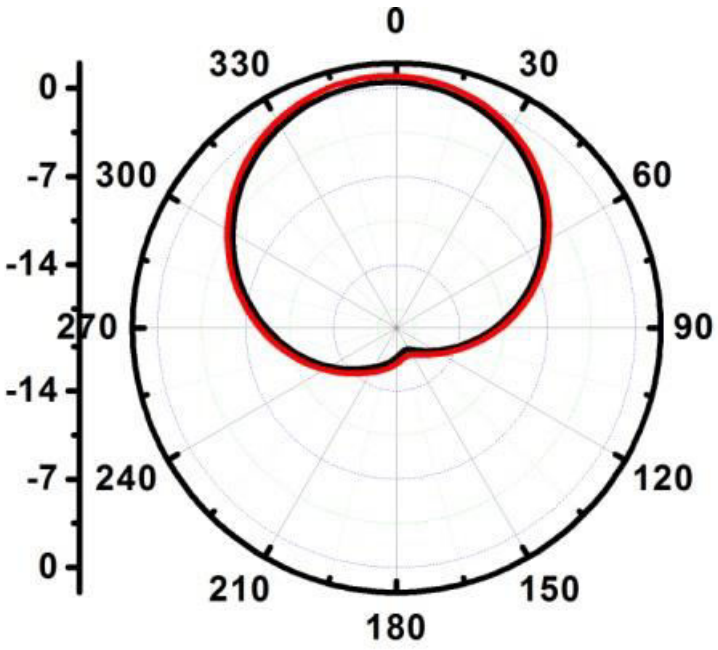

(b)

Simulated

Measured

Fig. 3.19 Radiation patterns of Ant4 at 3.4 GHz (a) E Plane (b) H Plane

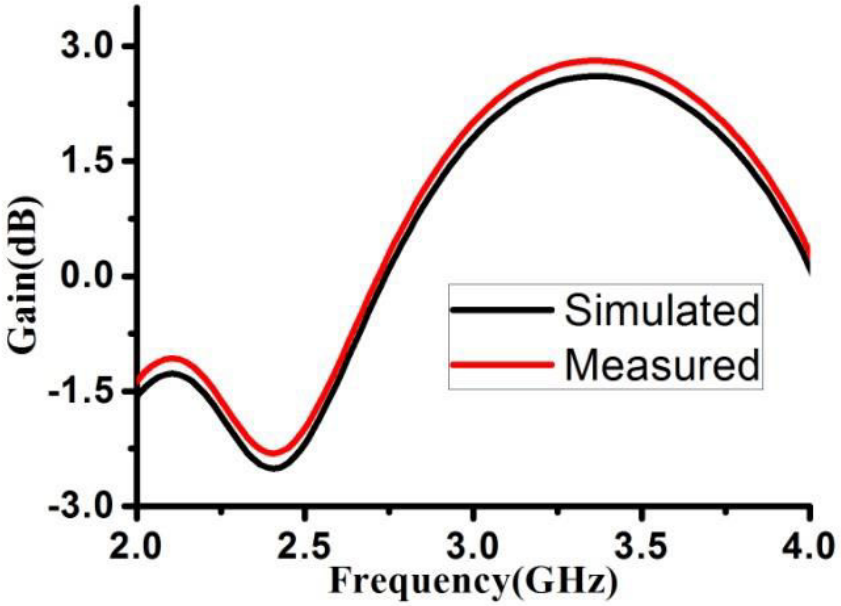

Fig. 3.20 Gain characteristics of the proposed antenna

Comparison between the results of the proposed antenna and the antennas which already exist in the literature are given in the Table 3.7. The proposed antenna is more compact and producing wide bandwidth compared to remaining antennas listed in Table 3.7.

Table 3.7 Comparison between results of proposed antenna with existing literature

Antenna	Patch Size (mmxmm)	Board size (mmxmmxmm)	10- dB return loss bandwidth at corresponding centre frequency	
			At left hand band	At patch mode band
proposed	27x27	37x37x3.175	2.51% (2.36- 2.42 GHz)	6.23% (3.11- 3.31 GHz)
[35]	28.8x28.8	60x60x1.6	3.5% at 2.3 GHz	1.97% at 2.56 GHz
[98]	19x10.5	50x20x6	2.4 – 2.485 GHz	5.15- 5.35 GHz
[37]	16x16	36x36x3	2.76 GHz	5.23 GHz

3. 5. Conclusions

Dual band patch antennas with embedded square Mushroom Unit Cell at right bottom corner are presented. Various fractal antennas using Minkowski, Koch and poly curves are studied for dual band operation. By varying the feed point position dual band antennas which resonate at 2.4 GHz and 3.4 GHz are designed. The 3-dB CP bandwidths obtained at upper

bands are more than 2%. These antennas are useful for systems operating at Wi-Fi and Wi-MAX standards IEEE 802.11 and IEEE 802.16. These antennas are fabricated and performance is measured. A good comparison is obtained.

Here the bandwidth at left hand band is found to be much improved over the case of an antenna with CSRR. However there is a penalty for this i.e. the bandwidth at the patch mode band is reduced to 6%. To overcome this ENG material has been attempted in chapter 4 where impressive bandwidths at both the bands are demonstrated.

Chapter 4

ENGTL metamaterials based Dual Band Microstrip Patch antennas

The ongoing improvements in the field of wireless communications have expanded the requirement for multiband and multifunctional antennas. The essential requirements of present day communication systems have additionally inspired an extended interest for ease and more minimized antennas. The benefit of the multi-band antennas is to have the capacity to coordinate several frequencies on one single antenna, making it helpful for several ranges. In this way, multifunctional antennas are exceptionally appealing in wireless communications. For the purpose of adaptable complementary introduction between the transmitting and receiving antennas circular polarization is also becoming more and more attractive. In perspective of these viewpoints, minimal circularly polarized antennas with multi-band activities will be more helpful in the future wireless communication systems.

The majority of the dual band antennas existing in the literature are utilizing line fed and probe fed ENGTL (Epsilon Negative Transmission Line) metallic VIAs loaded rectangular patch antennas. However, a large portion of these structures are linearly polarized. Some dual band antennas exist in light of multi layer design, yet the 10-dB return loss bandwidth at both the bands and the produced 3-dB CP bandwidths at patch mode band are extremely narrow (<2%), which is not meeting the prerequisites of present day communication systems.

Here, in the present work dual band dual polarized antennas are demonstrated utilizing the VIAs and different fractal curves. By using asymmetrical fractal curves as boundaries of a square patch and embedding metallic vertical VIAs along the circumference of the patch, dual band operation with LP at lower band and CP at upper band is obtained.

In this section three new antennas are studied for dual band operation where lower band is resonating with LP and upper band is resonating with CP with a single probe feed based on vertical metallic VIAs and fractal curves. They are:

(1) ENGTL based dual band Minkowski fractal boundary antenna

(2) ENGTL based dual band Koch fractal boundary antenna

(3) ENGTL based dual band Poly fractal boundary antenna

4.1 ENGTL based dual band Minkowski fractal boundary antenna

For detailed analysis of metamaterials another dual band antenna operating at same frequencies (Wi-Fi and WiMAX bands) is designed based on ENGTL theory, which is shown in Fig. 4.1. The antenna is designed on Rogers RT/Duroid substrate with a thickness of 3.175 mm and dielectric constant of 2.2. Four vertical VIAs with radius of 0.3 mm and height of 3.175mm are inserted in between patch and ground plane. These VIAs provide shunt inductance which is main reason for getting zeroth order band (left hand band). The optimized dimensions of the proposed antenna are shown in the Table 3.

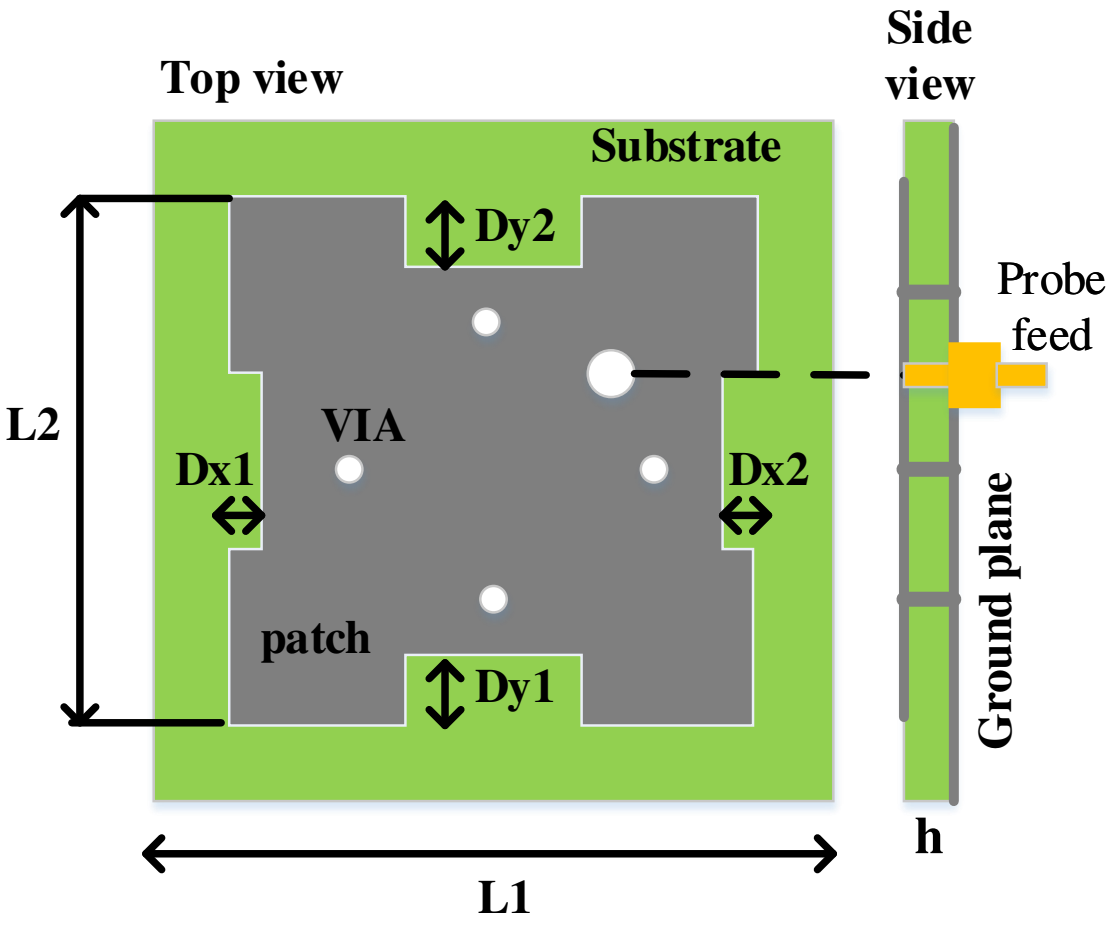

Fig. 4.1 Geometry of the ENGTL based Minkowski fractal boundary patch antenna

Table 4.1: parameter values

parameter	Value in mm
L_1	46
L_2	30
Dx1=Dx2	1
Dy1=Dy2	3
h	3.175
r_v	0.3

The design of the proposed antenna can easily be understood by considering an evolution of patch antenna design shown in Fig. 4.2. Initially the square patch Ant5 is chosen as reference which is resonating at 3.05 GHz with linear polarization (LP). The CP at this single band can be obtained by replacing edges of the square patch with Minkowski fractal curves which is the main cause for Ant6. Ant7 is achieved by inserting the metallic VIAs along the circumference of Ant1, in which this antenna produces two bands with linear polarization. Finally, Ant8 can be designed by inserting VIAs in Ant6 to result in dual band patch antenna with one band LP and another band with CP. The simulated return loss characteristics of the proposed Minkowski fractal boundary patch antenna are shown in the Fig. 4.3. The impedance bandwidth values are listed in the Table 4.2.

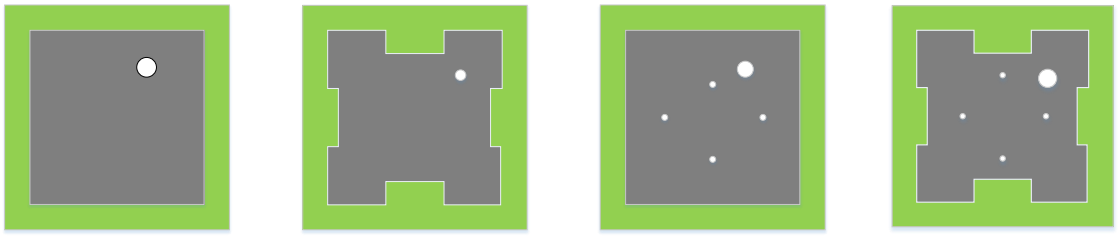

Ant5 Ant6 Ant7 Ant8

Fig. 4.2 In between steps in the design of ENGTL based patch antenna

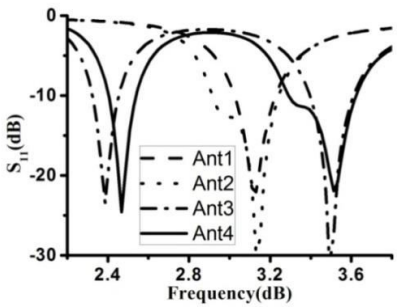

Fig. 4.3 Simulated RL characteristics of the proposed antennas

Table 4.2: Impedance bandwidth values

S. No	Antenna	Impedance bandwidth (%)		3- dB AR bandwidth (%)
		Band1	Band2	At band2
1	Ant1	-----	5.76% (3.03- 3.21 GHz)	----
2	Ant2	-----	10.26% (2.92- 3.23 GHz)	----
3	Ant3	5.04% (2.32- 2.44 GHz)	5.14% (3.41- 3.59 GHz)	----
4	Ant4	4.83% (2.42- 2.54 GHz)	9.22% (3.31- 3.63 GHz)	2.37% (3.33- 3.41 GHz)

To understand the operational mechanism of the proposed antenna, the HFSS simulated surface current distributions on the patch at each frequency band are shown in the Fig. 4.4. The lower resonating frequency (2.4 GHz) is mainly due to strong current distribution at VIAs. The upper resonating frequency (3.4 GHz) is mainly due to strong surface current at the edges of the patch.

(a) (b)

Fig. 4.4 Simulated surface current distribution (a) at 2.4 GHz (b) at 3.4 GHz

4.2 ENGTL based dual band Koch fractal boundary antenna

The geometry of the Koch fractal boundary patch antenna is shown in Fig. 4.5. The antenna is designed on Rogers RT/Duroid substrate with thickness of 3.175 mm and dielectric constant of 2.2. Four vertical VIAs with radius of 0.3 mm and height of 3.175mm are inserted in between patch and ground plane. These VIAs provide shunt inductance which is main cause for getting zeroth order band (left hand band). The dimensions of the proposed antenna are shown in the Table 4.3.

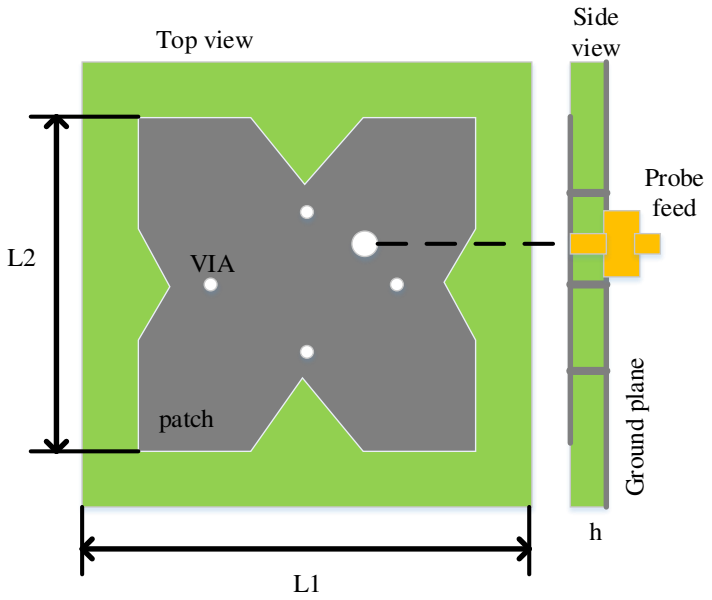

Fig. 4.5 Geometry of the Koch fractal boundary patch antenna

Table 4.3: parameter values

parameter	Value in mm
L1	46
L2	30
Dx1=Dx2	3
Dy1=Dy2	1
θx1=θx2	60
θy1=θy2	30
h	3.175
rv	0.3

Simulated results

The design of the proposed antenna can easily be understood by considering an evolution of patch antenna design shown in Fig. 4.6. Initially the square patch Ant1 is chosen as reference which is resonating at 3.05 GHz with linear polarization (LP). The CP at this single band can be obtained by replacing edges of the square patch with Koch fractal curves. Ant3 is achieved by inserting the metallic VIAs along the circumference of Ant1, in which this antenna produces two bands with linear polarization. Finally the dual band dual polarized antenna (one band LP and another band with CP) Ant4 can be designed by inserting VIAs in Ant2. The simulated return loss characteristics of the Koch fractal boundary patch antenna are shown in the Fig. 4.7. The impedance bandwidth values are listed in the Table 4.4.

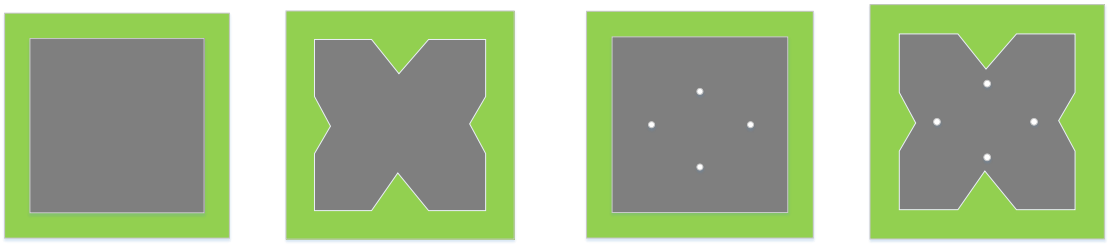

Ant1 Ant2 Ant3 Ant4

Fig. 4.6 In between the steps in the design

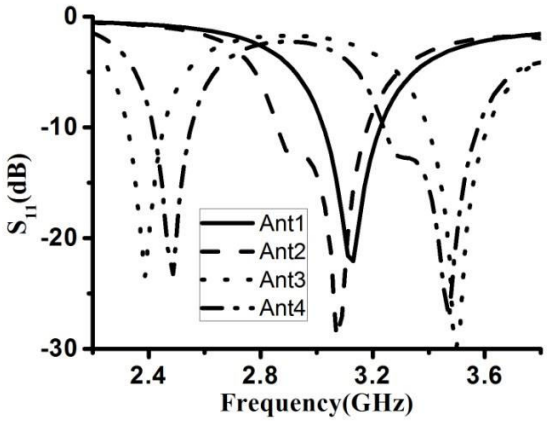

Fig. 4.7 Simulated RL characteristics of the proposed antennas

Table 4.4: Return loss characteristics

S. No	Antenna	10- dB RL bandwidth (%)		3- dB AR bandwidth (%)
		Band1	Band2	At band2
1	Ant1	-----	5.76% (3.03- 3.21 GHz)	----
2	Ant2	-----	10.29% (2.86- 3.17 GHz)	----
3	Ant3	5.04% (2.32- 2.44 GHz)	5.14% (3.41- 3.59 GHz)	----
4	Ant4	4.83% (2.42- 2.54 GHz)	9.38% (3.25- 3.57 GHz)	2.41% (3.27- 3.35 GHz)

To understand the operational mechanism of the proposed antennas, the HFSS simulated surface current distribution on the patches at each frequency band is shown in the Fig. 4.8. The lower resonating frequency (2.4 GHz) is mainly due to strong current distribution at VIAs. The upper resonating frequency (3.4 GHz) is mainly due to strong surface current at the edges of the patch.

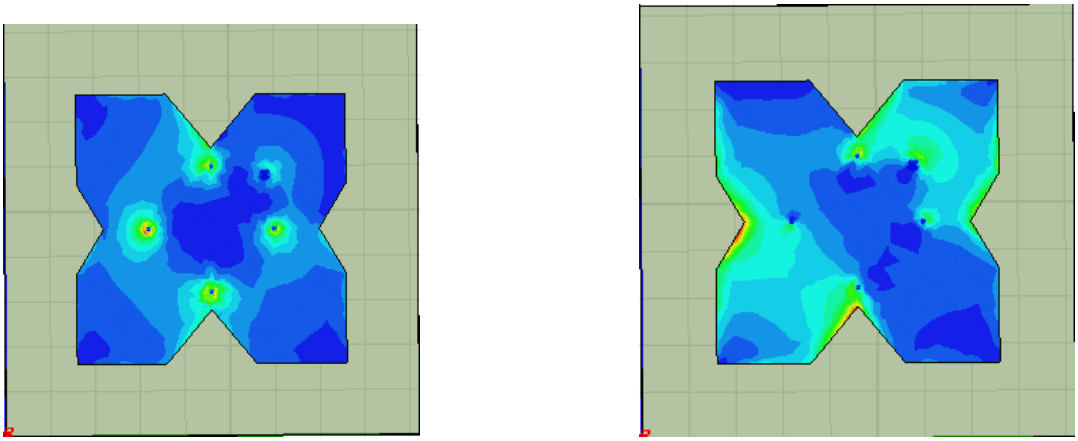

(a) (b)

Fig. 4.8 Simulated surface current distribution (a) at 2.4 GHz (b) at 3.4 GHz

4.3 ENGTL based dual band Poly fractal boundary antenna

The geometry of the poly fractal boundary patch antenna is shown in Fig. 4.9. The antenna is designed on Rogers RT/Duroid substrate with thickness of 3.175 mm and dielectric constant of 2.2. Four vertical VIAs with radius of 0.3 mm and height of 3.175mm are inserted in between patch and ground plane. These VIAs provide shunt inductance which is the main cause for getting zeroth order band (left hand band). The dimensions of the proposed antenna are shown in the Table 4.5.

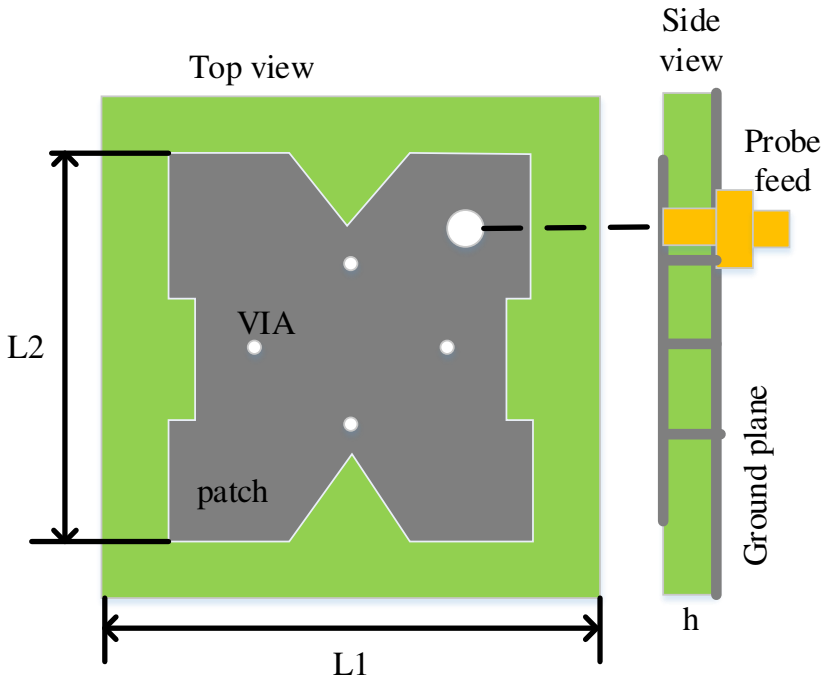

Fig. 4.9 Geometry of the poly fractal boundary patch antenna

Table 4.5 parameter values in mm

parameter	Value in mm
L1	46
L2	30
Dx1=Dx2	3
Dy1=Dy2	1
θx1=θx2	60
θy1=θy2	30
h	3.175
rv	0.3

Simulated results

The design of the proposed antenna can be easily understood by considering an evolution of patch antenna design shown in Fig. 4.10. Initially the square patch Ant1 is chosen as reference which is resonating at 3.05 GHz with linear polarization (LP). The CP at this single band can be obtained by replacing edges of the square patch with poly fractal curves. Ant3 is achieved by inserting the metallic VIAs along the circumference of Ant1, in which this antenna produce two bands with linear polarization. Finally, Ant4 can be designed by inserting VIAs in Ant2 which results in dual band patch antenna with one band LP and another band with CP. The simulated return loss characteristics of the proposed poly fractal boundary patch antenna are shown in the Fig. 4.6. The impedance bandwidth values are listed in the Table 4.6.

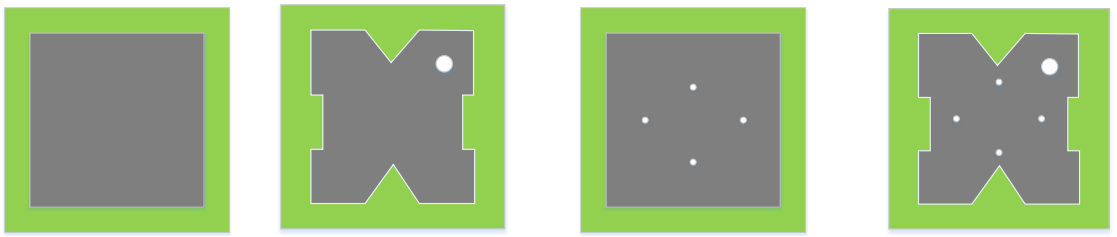

Ant1 Ant2 Ant3 Ant4

Fig. 4.10 In between the steps in the design

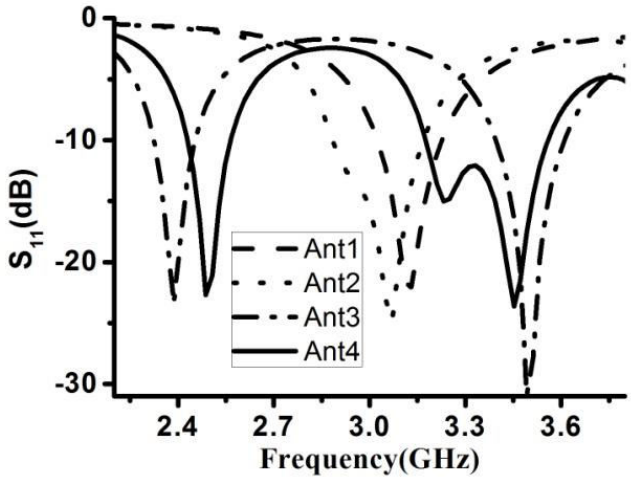

Fig.4.11 Simulated RL characteristics of the proposed antennas

Table 4.6: Impedance bandwidth values of Ant5 and Ant6

S. No	Antenna	10- dB RL bandwidth (%)		3- dB AR bandwidth (%)
		Band1	Band2	At band2
1	Ant1	-----	5.76% (3.03- 3.21 GHz)	----
2	Ant2	-----	8.97% (2.88- 3.15 GHz)	----
3	Ant3	5.04% (2.32- 2.44 GHz)	5.14% (3.41- 3.59 GHz)	----
4	Ant4	4.01% (2.44- 2.54 GHz)	10.6% (3.19- 3.55 GHz)	2.43% (3.25- 3.33 GHz)

To understand the operational mechanism of the proposed antenna, the HFSS simulated surface current distribution on the patch at each frequency band is shown in the Fig. 4.12. The lower resonating frequency (2.4 GHz) is mainly due to strong current distribution at VIAs. The upper resonating frequency (3.4 GHz) is mainly due to strong surface current at the edges of the patch.

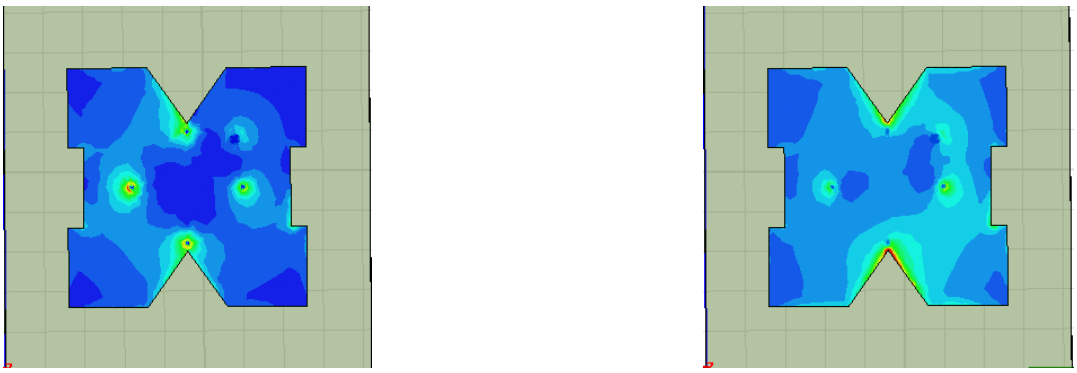

(a) (b)

Fig. 4.12 Simulated surface current distribution (a) at 2.4 GHz (b) at 3.4 GHz

The simulated radiation efficiency of the proposed antenna is shown in the Fig 4.13. The radiation efficiency of the proposed antenna is 98.5% at lower resonating frequency (2.4 GHz) and is 97.5% at upper resonating frequency (3.4 GHz).

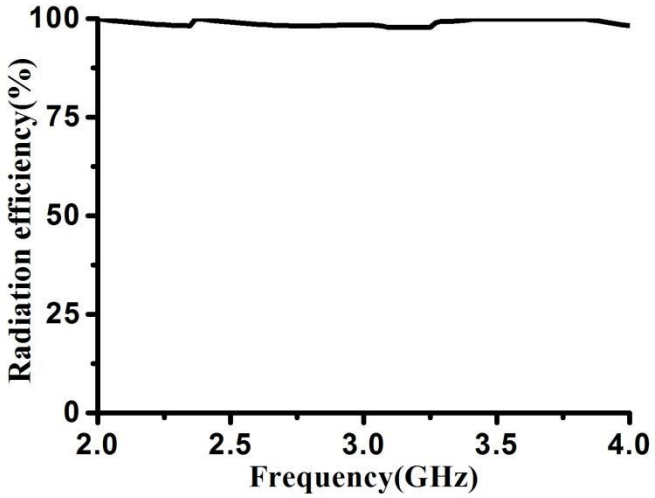

Fig 4.13 Simulated radiation efficiency of the proposed antenna

4.4 Experimental results

The proposed antenna (Ant6) is fabricated on Rogers RT/Duroid substrate with dimensions 46 x 46 x 3.175 mm^3 and is shown in Fig. 4.14. The vertical metallic VIAs (copper wires) are inserted between the patch and ground plane. Agilent 8719A microwave network analyzer is used to measure the return loss characteristics. Radiation pattern measurements are taken in an anechoic chamber having physical dimensions of 22.5 x 12.5 x 11.5 m^3. The operating frequency range of the anechoic chamber is 400 MHz to 18 GHz.

(a) (b)

Fig. 4.14 Fabricated prototype of Ant6 a Top view b Bottom view

The measured return loss characteristics of Ant6 shown in the Fig. 4.15. Measured results are in close agreement with simulated results. The kink at upper resonating band indicates that possibility of circular polarization radiation. The measured 10-dB return loss bandwidth of Poly fractal boundary patch antenna is 4.01% at lower resonating band and 10.68% at upper resonating band respectively. The measured AR characteristics are given in Fig. 4.16. The 3- dB Axial Ratio bandwidth at upper resonating band is 2.43%.

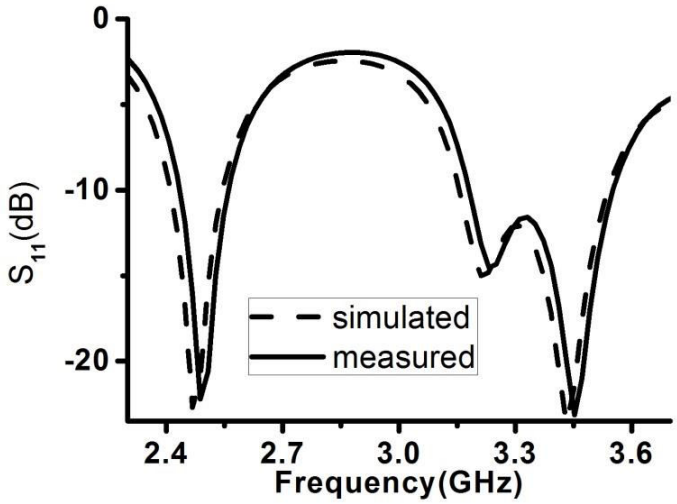

Fig. 4.15 Measured Return loss characteristics of Ant6

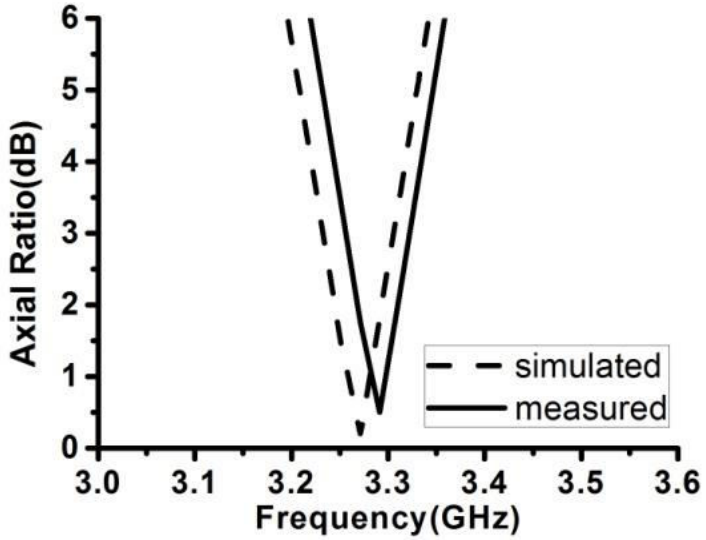

Fig. 4.16 Measured Axial Ratio characteristics of Ant6

The measured radiation patterns are shown in the Figs. 4.17 and 4.18. The pattern at 2.4 GHz is like doughnut type pattern which is due to presence of VIAs, where as the pattern at 3.4 GHz is like uni directional which is due to fractal boundary patch. The gain

characteristics of the proposed antenna are shown in the Fig. 4.19 which indicates that the gain at left hand band is moderate where as the gain at patch mode band is high.

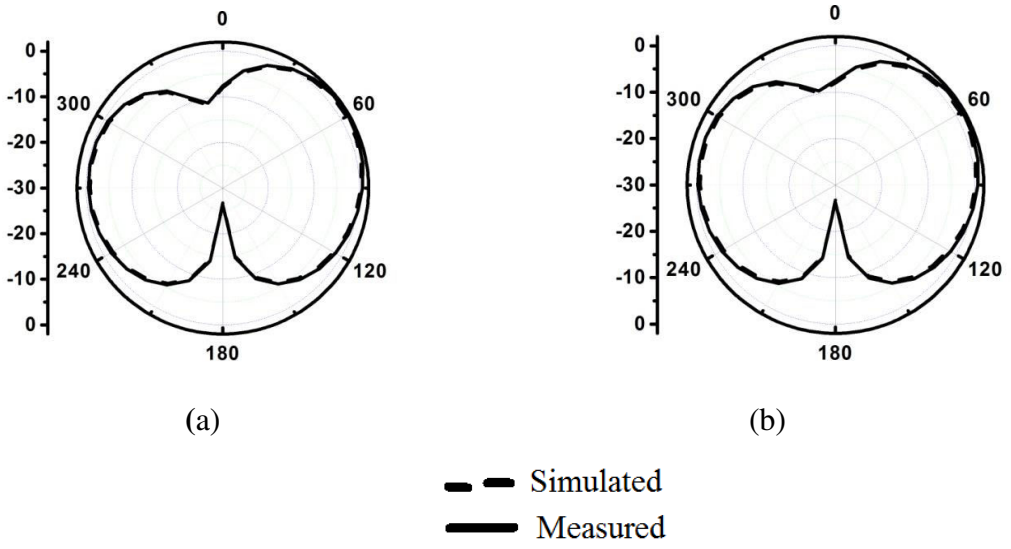

Fig. 4.17 Radiation patterns of Ant6 at 2.4 GHz (a) E Plane (b) H Plane

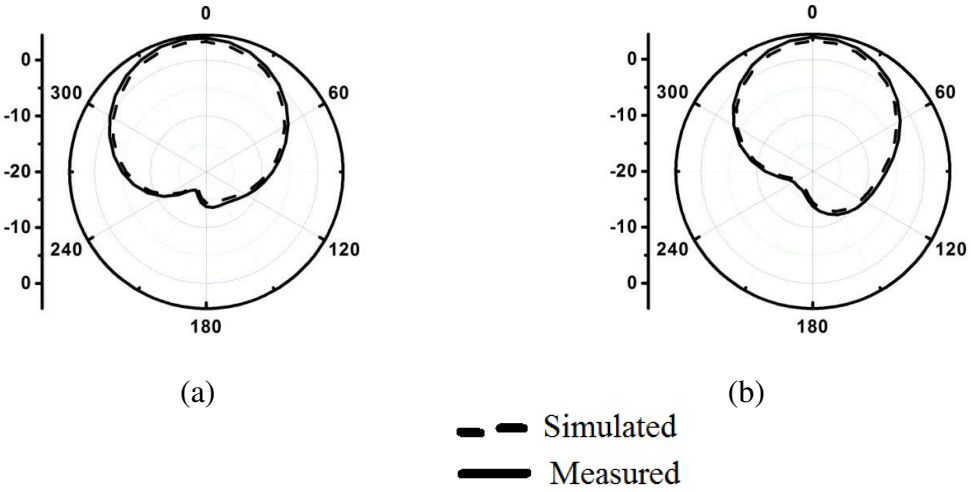

Fig. 4.18 Radiation patterns of Ant6 at 3.4 GHz (a) E Plane (b) H Plane

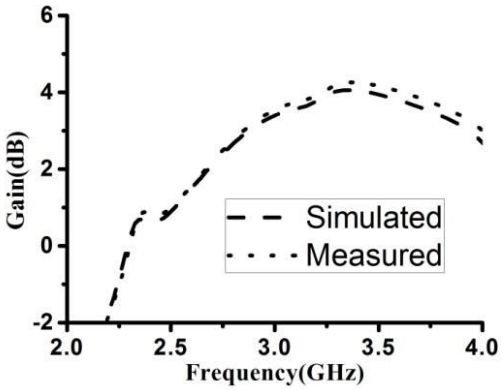

Fig. 4.19 Gain characteristics of the proposed antenna

Comparison between the results of the proposed antenna and the antennas which already exist in the literature are given in the Table 4.7. The proposed antenna is more compact and producing wide bandwidth compared to remaining antennas listed in Table 4.7.

Table 4.7 Comparison between the proposed antenna and existing literature

Antenna	Patch Size (mmxmm)	Board size (mmxmmxmm)	10- dB return loss bandwidth at corresponding centre frequency	
			At ZOR	At patch mode
proposed	30x30	46x46x3.175	4.01% at 2.4 GHz	10.6% at 3.4 GHz
[41]	3.5x10.5	-----	Resonance at 10 GHz only	
[43]	26x26	50x50x1.5	5.25 GHz	8.325 GHz
[46]	24.4x12.2	50x50x1.524	2.5 GHz	3.74 GHz
[47]	46.8x46.8	76.8x76.8x3.175	2 GHz	2.4 GHz

4. 5 Conclusions

Dual band patch antennas with embedded metallic VIAs around the circumference are presented. Various fractal antennas using Minkowski, Koch and poly curves are studied for dual band operation. By varying the feed point position dual band antennas which resonate at 2.4 GHz and 3.4 GHz are designed. The 3-dB CP bandwidths obtained at upper bands are more than 2%. These antennas are useful for systems operating at Wi-Fi and Wi-MAX standards IEEE 802.11 and IEEE 802.16. These antennas are fabricated and performance is measured. A good comparison is obtained.

But the size of the patch required for this operation is found to be 30x30x3.2 mm^3. To further minimize the size without reducing bandwidths, another approach is to use RIS. This is presented in the following chapter.

Chapter 5

RIS based dual band Microstrip patch Antenna

The present-day handheld devices are required to operate with various standards thus forcing them to operate at different frequency bands. Instead of using multiple antennas, a single Microstrip Patch Antenna (MPA) which operates for WLAN, Wi-Fi and WiMAX applications with less size and wider bandwidth at each operating frequency is highly desirable for daily life wireless portable devices. In a conventional dual-band or multi-band, MPAs the dimensions of the radiating patch are taken with reference to the lowest frequency band which requires more size. Then the current on the patch is perturbed to obtain resonance at higher frequency band. Moreover, they offer only linear polarization at both the bands with narrow bandwidth. But modern devices need to provide circular polarization at WiMAX band to avoid orientation problems.

The majority of the dual band antennas existing in the literature are utilizing line fed and probe fed RIS (Reactive Impedance Surface) based rectangular patch antennas. However, a large portion of these structures are linearly polarized. Some dual band antennas exist in light of multi layer design, yet the produced 10-dB return loss bandwidth at both the bands and 3-dB CP bandwidth at patch mode band are extremely narrow (<1%), which is not meeting the prerequisites of present day communication systems.

Here, in the present work dual band dual polarized antennas are demonstrated utilizing the RIS, MUC and different fractal curves. By using asymmetrical fractal curves as boundaries of a square patch and implementing the patch over RIS, dual band operation with LP at lower band and CP at upper band is obtained.

In this section four new antennas are studied for dual band operation where lower band is resonating with LP and upper band is resonating with CP with a single probe feed based on Reactive Impedance Surface, Mushroom Unit cell and fractal curves. They are:

(1) RIS based dual band Minkowski fractal boundary patch antenna
(2) RIS based dual band Poly fractal boundary patch antenna

(3) RIS based dual band Semi circular fractal boundary patch antenna

5.1 RIS based dual band Minkowski fractal boundary patch antenna

The structure of the proposed antenna is shown in the Fig. 5.1. It is fed by single coaxial probe feed. It is a three layer structure where the top and bottom dielectric substrates are "FR4 EPOXY" with a dielectric constant of 4.4. The RIS is sandwiched between them which is composed of 4 by 4 periodic planar array of metallic Minkowski fractal patches. The optimized dimensions of the suggested antenna are listed in Table 5.1.

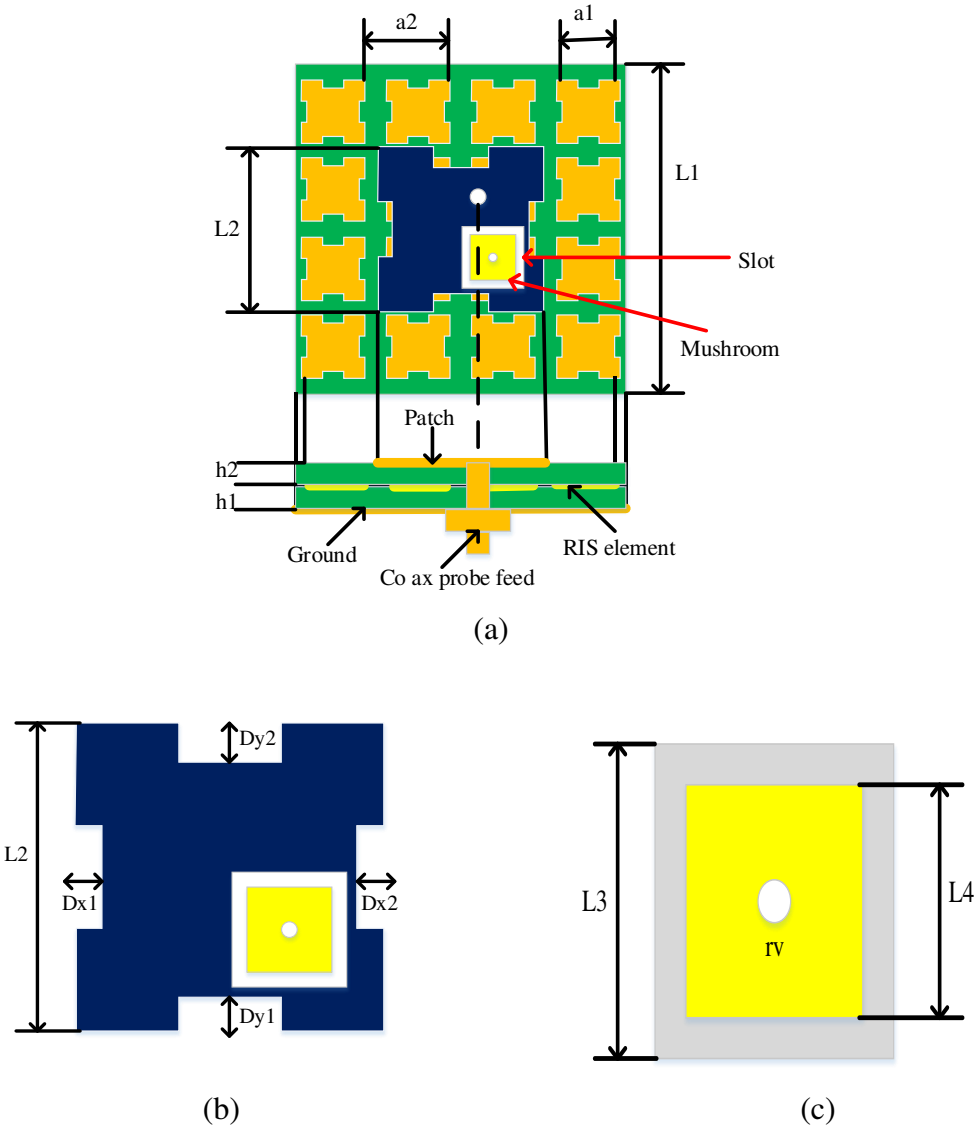

Fig. 5.1 structure of (a) RIS based CP Patch antenna (b) patch antenna with slot and mushroom unit cell (c) slot with mushroom unit cell

Table 5.1: Optimized Parameter Values

parameter	Value (in mm)
L1	35
L2	18
h1	2.6
h2	0.4
a1	6
a2	9
L3	6
L4	5
rv	0.5
Dx1	1
Dx2	1
Dy1	3
Dy2	3

Fractals are analyzed and characterized by two important factors: iteration order (IO) and indentation factor (IF). For Minkowski fractal curves the indentation factor is indentation depth (ID). The proposed square patch length is L2 and Dx and Dy are IDs along the x- and y-axes. The CP operation is accomplished by deploying the Minkowski fractal curves. The four sides of the square patch antenna are etched with fractal curve of different IDs. Two orthogonal modes with 90^0 phase shift are introduced for CP radiation with the use of Minkowski fractal curves along the sides of the square patch antenna.

Single square Mushroom unit cell is inserted into the Minkowski fractal patch antenna to get the double band. To separate the RIS from VIA and feed, two separate holes are etched from the RIS so that VIA and feed do not touch the RIS. Good CP can be obtained by adjusting the slot position on the patch and mushroom position. The patch and mushroom unit cell are capacitively coupled by a small gap. Because of mushroom unit structure a lower resonance frequency band is present.

SIMULATION RESULTS

Operation of the proposed design can be understood by considering an evolution of patch antenna design shown in Fig. 5.2. Initially a square patch with 18x18 mm^2 is chosen as reference which is implemented on different types of RIS for single band operation. The RIS of Ant1 is composed of 4 by 4 planar array of square elements with each element size as 6 mm. Ant2 is obtained from Ant1 by applying Minkowski fractal curves to square patch of Ant1. Ant3 is obtained from Ant1 by making RIS square elements as fractal elements. Ant4 is designed from Ant3 by making square patch into fractal patch. The Simulated return loss characteristics of single band antennas from Ant1 to Ant4 are shown in Fig. 5.3 and the 10-dB return loss bandwidths of each antenna are listed in Table 5.2.

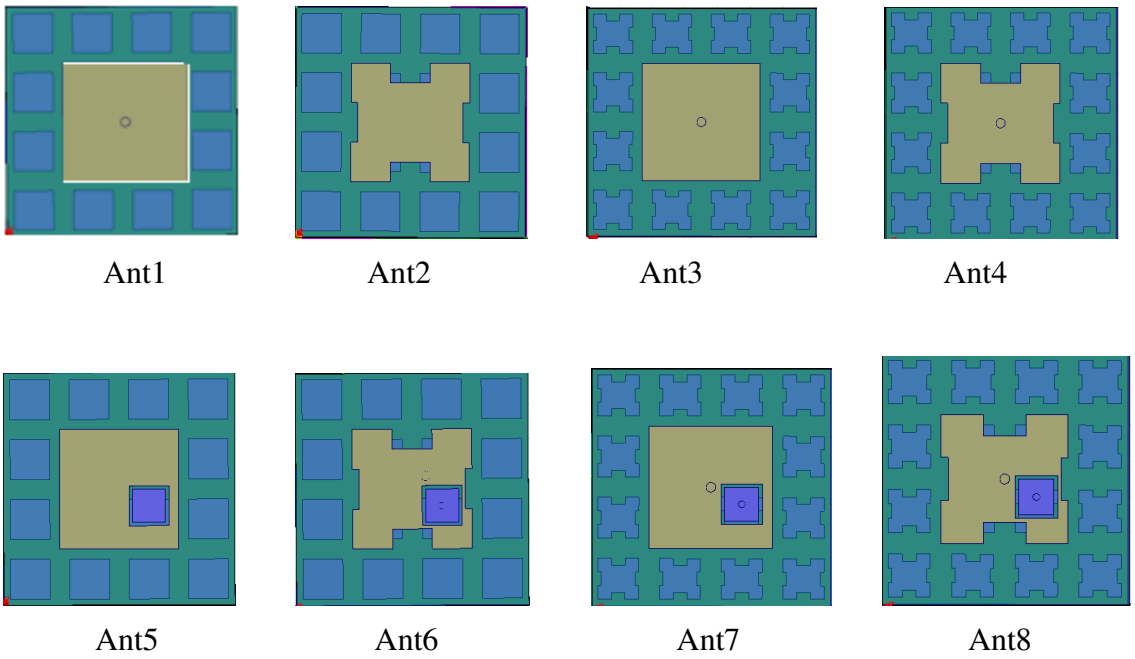

Fig. 5.2 proposed antenna structures

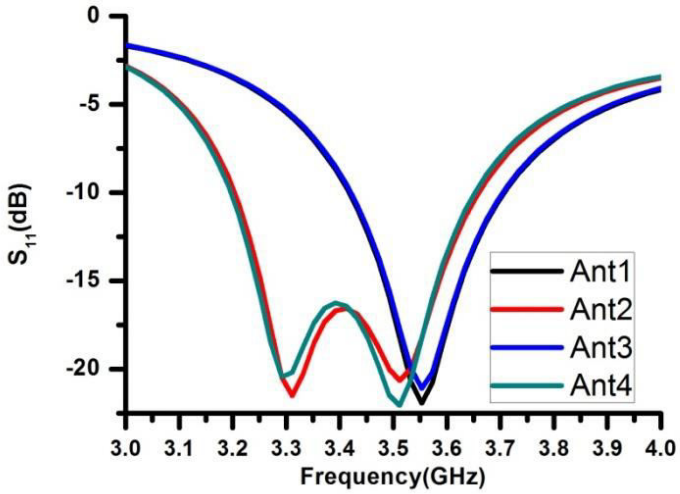

Fig. 5.3 Simulated return loss characteristics of single band antennas Ant1- Ant4

Table 5.2 Simulated impedance bandwidth values of single band antennas

Antenna	10-dB return loss bandwidth	
	Lower frequency band	Upper frequency band
Ant1	----	(3.43- 3.69 GHz) 7.30%
Ant2	----	(3.21- 3.65 GHz) 12.82%
Ant3	----	(3.43- 3.69 GHz) 7.30%
Ant4	----	(3.21- 3.63 GHz) 12.28%

Antennas from Ant5 to Ant8 are designed by loading Mushroom unit cell into every square patch of antennas from Ant1 to Ant4 respectively for dual band operation with dual polarization. From the above four antennas Ant8 is selected as proposed antenna because of its resonance close to WLAN and WiMAX bands. The simulated return loss characteristics of all dual band dual polarized antennas from Ant5 to Ant8 are shown in Fig. 5.4 and the impedance bandwidth at two resonating bands of each antenna is listed in Table 5.3.

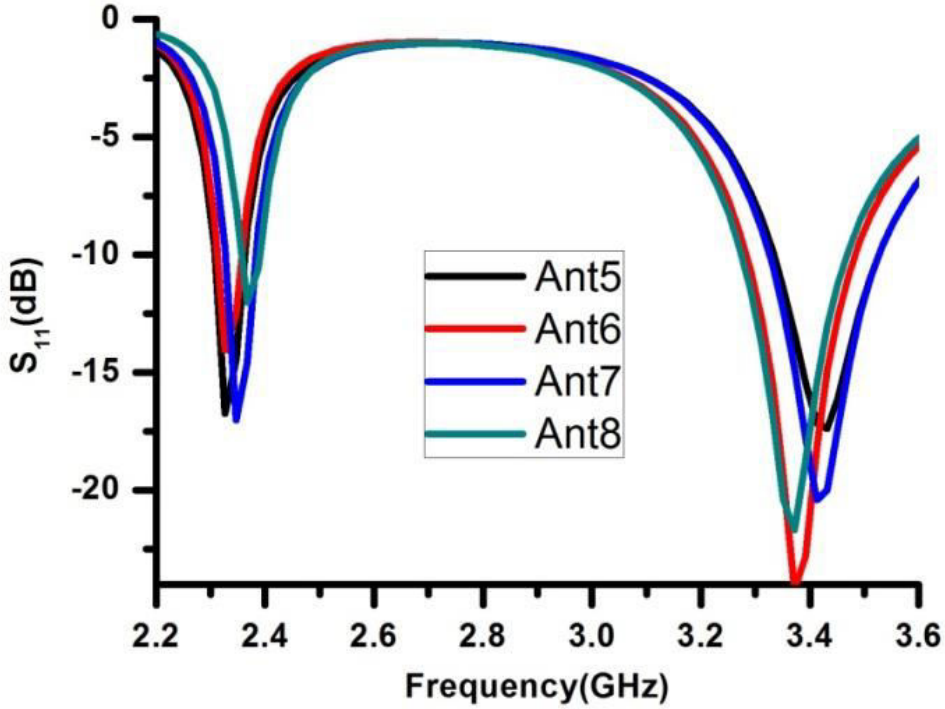

Fig. 5.4 Simulated return loss characteristics of single band antennas Ant5- Ant8

Table 5.3 Simulated Impedance Bandwidth values

Ant	10-dB return loss bandwidth	
	Lower frequency band	Upper frequency band
Ant 5	(2.30- 2.34 GHz) 1.72%	(3.35- 3.59 GHz) 6.91%
Ant 6	(2.32- 2.34 GHz) 0.86%	(3.29- 3.47 GHz) 5.32%
Ant 7	(2.34- 2.36 GHz) 0.85%	(3.33- 3.51 GHz) 5.26%
Ant 8	(2.36- 2.38 GHz) 0.84%	(3.29- 3.45 GHz) 4.74%

The simulated results such as Axial Ratio plot, gain plot and radiation plots of the proposed antenna are shown in Fig. 5.5.

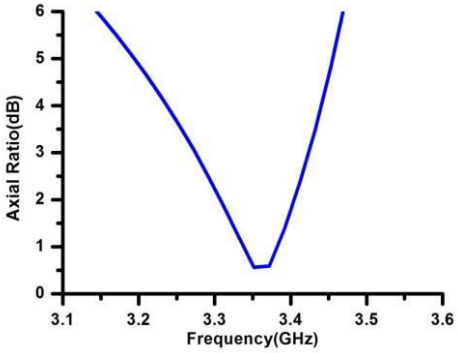

(a)

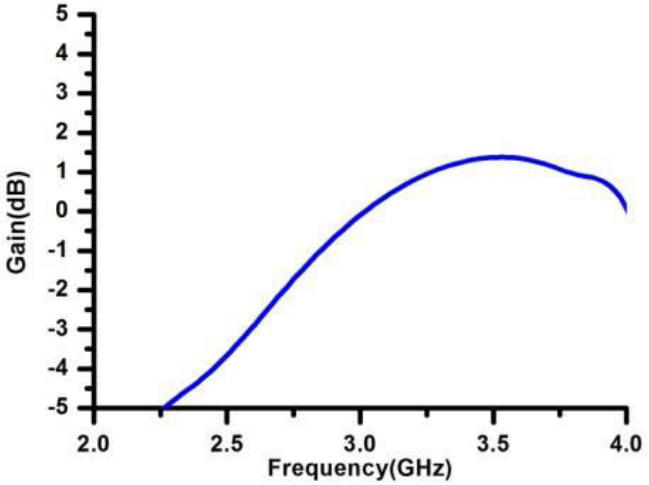

(b)

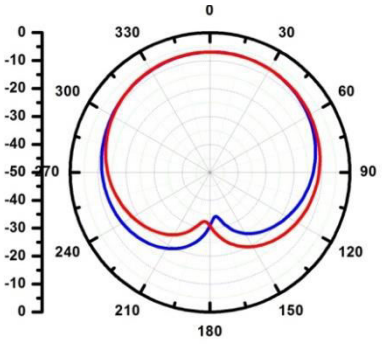

(c)

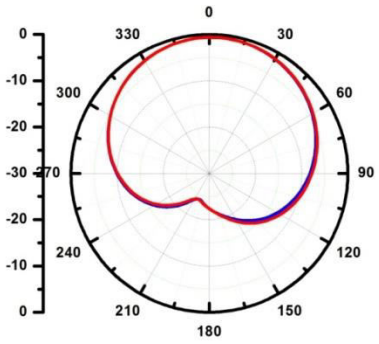

(d)

Fig. 5.5 Simulated characteristics of the proposed antenna (a) Axial Ratio characteristics (b) Gain (c) Radiation patters at 2.38 GHz (both E and H planes) (d) Radiation patters at 3.37 GHz (both E and H planes).

5.2 RIS based dual band poly fractal boundary patch antenna

The geometry of the proposed antenna is shown in the Fig.5.6. It consists of two FR4 epoxy substrates (ε_r= 4.4), where the RIS is composed of a 4 by 4 array of metallic fractal patches implemented on bottom grounded dielectric substrate with thickness 2.4 mm. The radiating patch is designed on top surface of a ground free substrate with thickness 0.5 mm. A coaxial probe feeding is utilized. MUC is loaded into the radiating patch to get dual band operation. The dimensions of the proposed antenna are listed in Table 5.4.

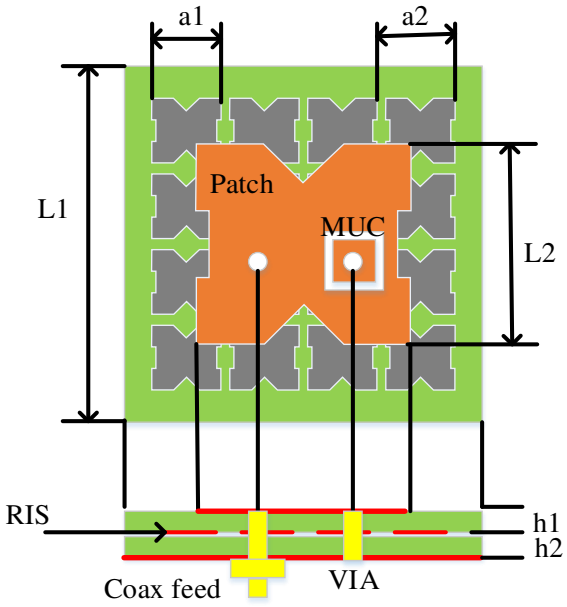

Fig. 5.6 Geometry of the proposed RIS based Poly fractal boundary patch antenna

Table 5.4: Parameter values in mm

parameter	Value in mm
L1	30
L2	18
h1	2.4
h2	0.5
a1	6
a2	7.8
s1	4
s2	3
rv	0.3
Rx1=Rx2	2.5
Ry1=Ry2	1

Simulation Results

The evolution of the proposed design can be understood by considering an evolution of patch antenna design shown in Fig. 5.7.

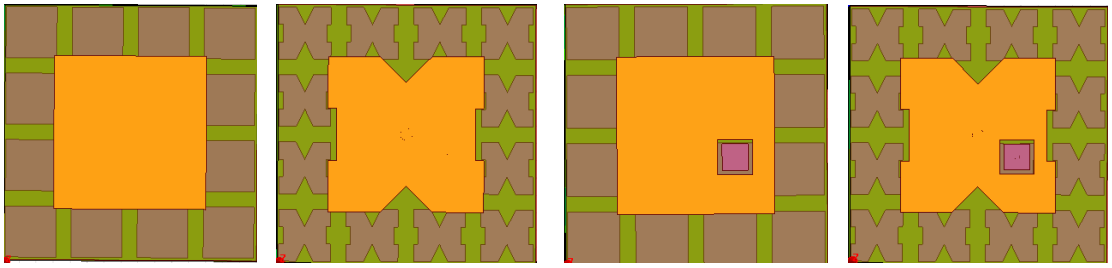

Ant1 Ant2 Ant3 Ant4

Fig. 5.7 Evolution of the proposed antenna

Initially, the square patch on square RIS Ant1 is chosen as a reference which is resonating at 3.4 GHz with linear polarization. Poly fractal curves are introduced into Ant1 to get Ant2 which results in CP. Ant3 can be obtained by introducing Mushroom Unit Cell into the radiating patch of Ant1 which results in double band operation with Linear Polarization. Ant4 can be obtained by loading MUC into radiating patch of Ant2 which causes the dual band operation in which lower band is with LP and upper band is with CP.

The simulated return loss characteristics of all proposed antennas are shown in the Fig. 5.8. By loading MUC into the radiating patch, the dual band operation is obtained. The 10-dB return loss bandwidth of all resonating frequencies is listed in Table 5.5. The circular polarization bandwidth at patch mode can be achieved by inserting poly fractal curves along the edges of the patch. The simulated axial ratio characteristics are shown in the Fig. 5.9. The 3- dB axial ratio bandwidth at patch mode band is given by 4.29% (3.19- 3.33 GHz).

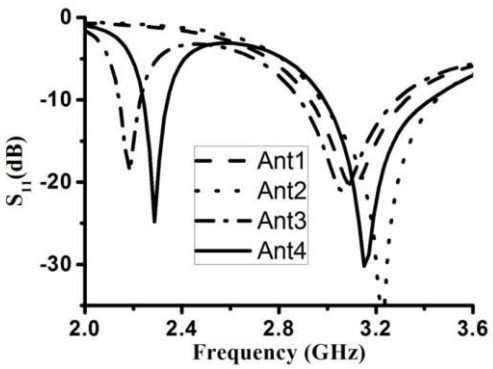

Fig. 5.8 Return loss characteristics of the proposed antennas

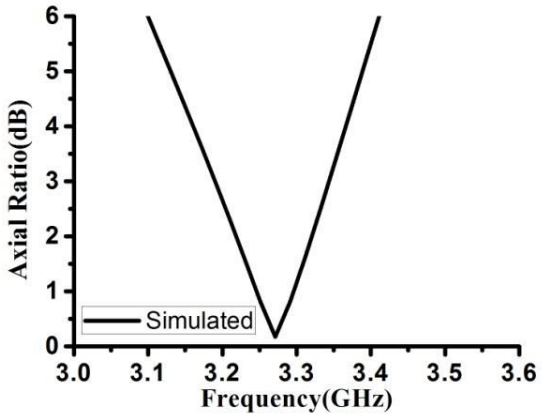

Fig. 5.9 Axial Ratio characteristics of the proposed antennas

Table 5.5: Impedance bandwidth of the simulated antennas

Antenna	10-dB return loss bandwidth	
	at left hand band	at patch mode band
Ant1	---	11.84% (2.94- 3.31 GHz)
Ant2	---	11.94% (3.01- 3.39 GHz)
Ant3	3.66% (2.14- 2.22 GHz)	12.75% (2.88- 3.27 GHz)
Ant4	3.35% (2.20- 2.28 GHz)	13.47% (2.98- 3.43 GHz)

To understand the operational mechanism of the proposed antenna, the HFSS simulated current distribution on patch Ant4 at each frequency band is shown in the Fig. 5.10.

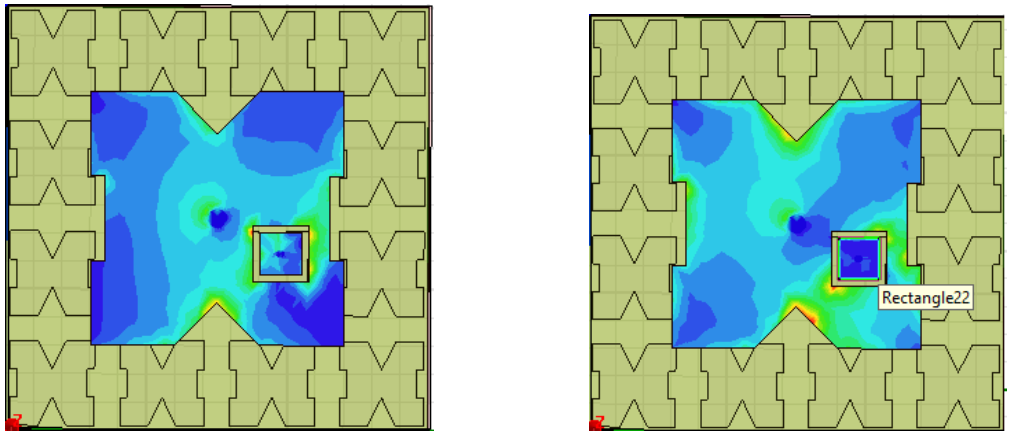

(a) (b)

Fig. 5.10 Simulated Surface current distribution at (a) 2.4 GHz (b) 3.3 GHz

The lower resonating frequency (2.4 GHz) is mainly due to strong surface current distribution at MUC where as the upper resonating frequency (3.3 GHz) is due to current at fractal edges of the patch. The radiation patterns of the proposed antenna are shown in Fig. 5.11.

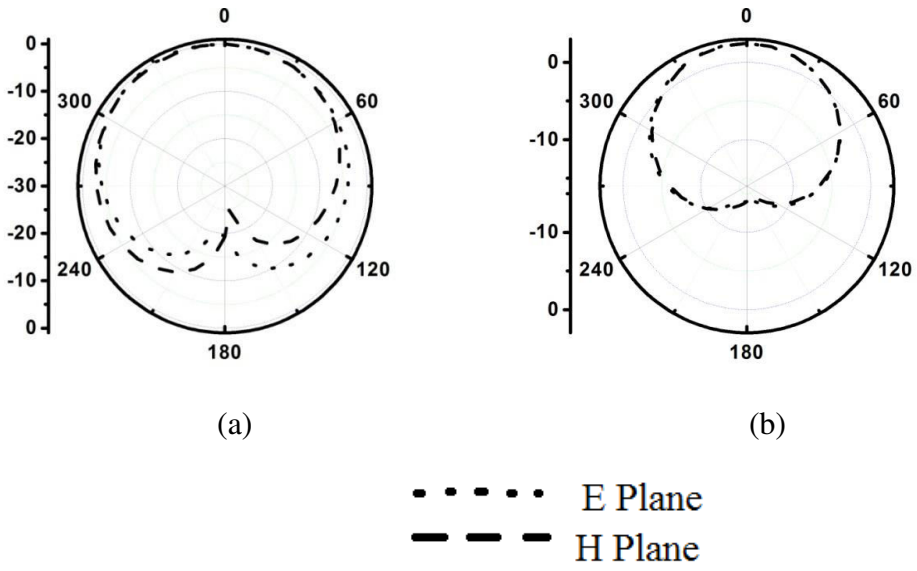

Fig. 5.11 Simulated Radiation patterns at (a) 2.4 GHz (b) 3.4 GHz

5.3 RIS based dual band Semi circular fractal boundary patch antenna

The structure of the proposed antenna which is fed by single coaxial probe feed is shown in the Fig. 5.12. It is a three layer structure where the top and bottom dielectric substrates are "FR4 EPOXY" with a dielectric constant of 4.4. The RIS is sandwiched between these dielectric materials and is composed of 4 by 4 periodic planar array of metallic asymmetrical fractal patches. The optimized dimensions of the suggested antenna are listed in Table 5.6.

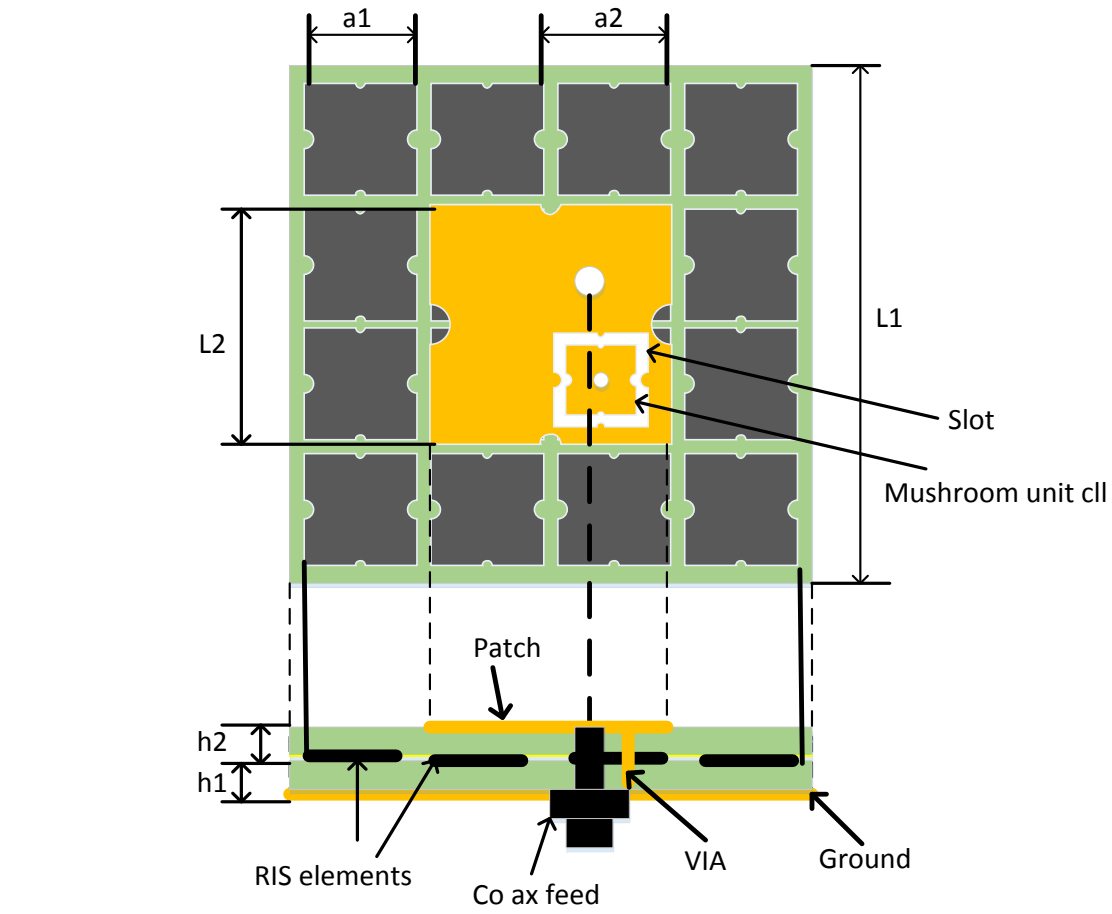

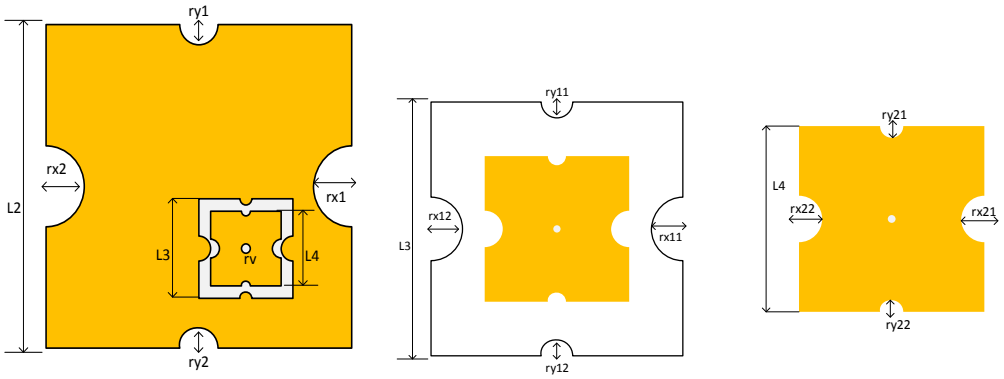

(a) (b) (c)

Fig. 5.12 structure of the CP Patch antenna (a) patch antenna with slot and mushroom unit cell (b) slot with mushroom unit cell (c) mushroom unit cell

Table 5.6 Optimized Parameter Values

parameter	Value(in mm)
L1	35
L2	18
h1	2.6
h2	0.4
a1	7
a2	9
L3	7
L4	6
rv	0.5
rx1	1
rx2	1
ry1	0.5
ry2	0.5

Fractals are analyzed by two important factors: iteration order (IO) and indentation factor (IF). For semi circle fractal curves the indentation factor is indentation radius (IR). The proposed square patch length is L2 and rx and ry are IRs along the x- and y-axes. The CP operation is accomplished by deploying the fractal semi circled curves. The four sides of the square patch antenna are etched with fractal curves of different IRs. Two orthogonal modes with 90^0 phase shift are introduced for CP radiation with the use of asymmetrical fractal curves along the sides of the square patch antenna.

Single fractal Mushroom unit cell is inserted into the fractal patch antenna to get the double band. To separate the RIS from VIA and feed, two separate holes are etched from the RIS so that VIA and feed do not touch the RIS. Desirable CP bandwidth can be obtained by adjusting the slot position on the patch and mushroom position. The patch and mushroom unit cell are capacitively coupled by a small gap. Because of mushroom unit structure a lower resonance frequency band is observed.

Half circled or Semi circled fractal curves are characterized by two parameters: Iteration Order (IO) and Indentation Radius (IR). Equal Indentation Radius (Rx1=Rx2=Ry1=Ry2) along four sides of the square patch antenna results in linear polarization at upper frequency band. Circular polarization radiation can be obtained by loading different Indentation Radii

along each side of the patch (Rx1≠ Rx2≠ Ry1≠ Ry2) or (Rx1= Rx2= Rx ≠ Ry1= Ry2 =Ry). High bandwidth can be obtained when Indentation Radii along same axis are equal and are not equal along the perpendicular axis (Rx1= Rx2= Rx ≠ Ry1= Ry2 =Ry).

Operation of the proposed design can be understood by considering an evolution of patch antenna design shown in Fig. 5.13. Initially a square patch with 18x18 mm^2 is chosen as reference which is implemented on different types of RIS for single band operation. The RIS of Ant1 is composed of 5 by 5 planar array of square elements with each element size is 5 mm. Ant2 has 5 by 5 planar array of each element size is 6 mm. Ant3 has planar array of each element size is 7 mm. Ant4 has planar array of each element size is 8 mm. From the above four antennas Ant3 is selected for dual band operation because of its high impedance bandwidth. Ant5 is designed with square RIS (all elements are square) and fractal Mushroom unit cell loaded square patch for dual band dual polarization operation. Ant6 is designed by introducing asymmetrical fractal curves to patch in Ant5. Ant7 is obtained from Ant5 by introducing fractal curves to each element of RIS. Ant8 is designed by introducing fractal curves to all elements of RIS and radiating patch. Finally Ant8 is the proposed antenna with dual band dual polarization.

The simulated return loss characteristics of single band antennas from Ant1 to Ant4 are shown in Fig. 5.14 and the 10-dB return loss bandwidth of each antenna is listed in Table 5.7.

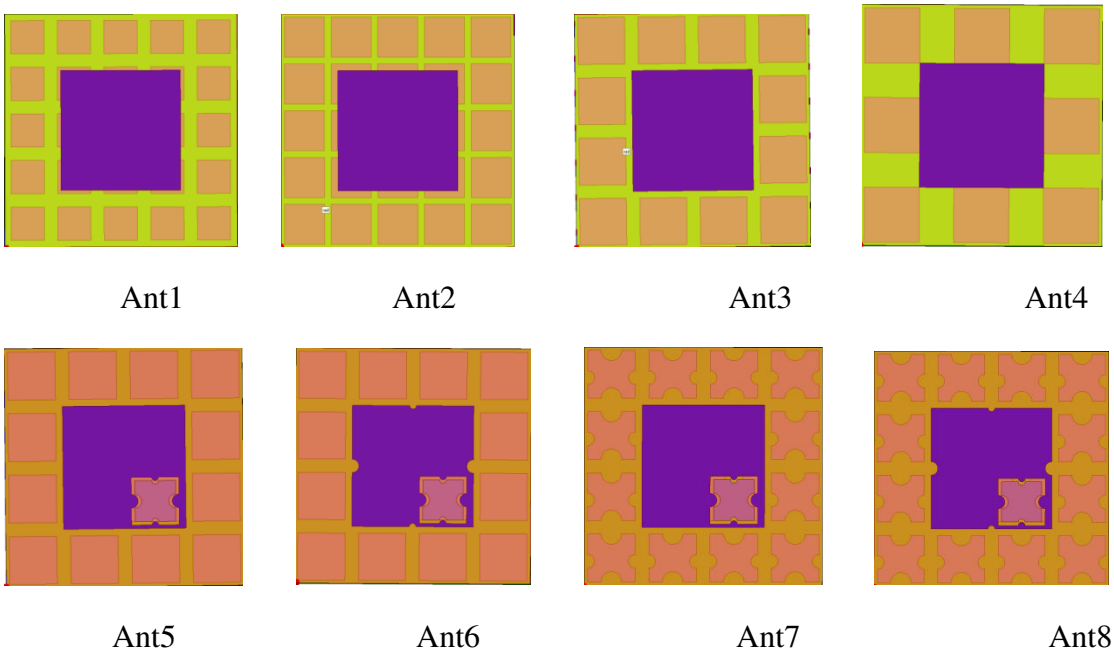

Fig. 5.13 proposed antenna structures

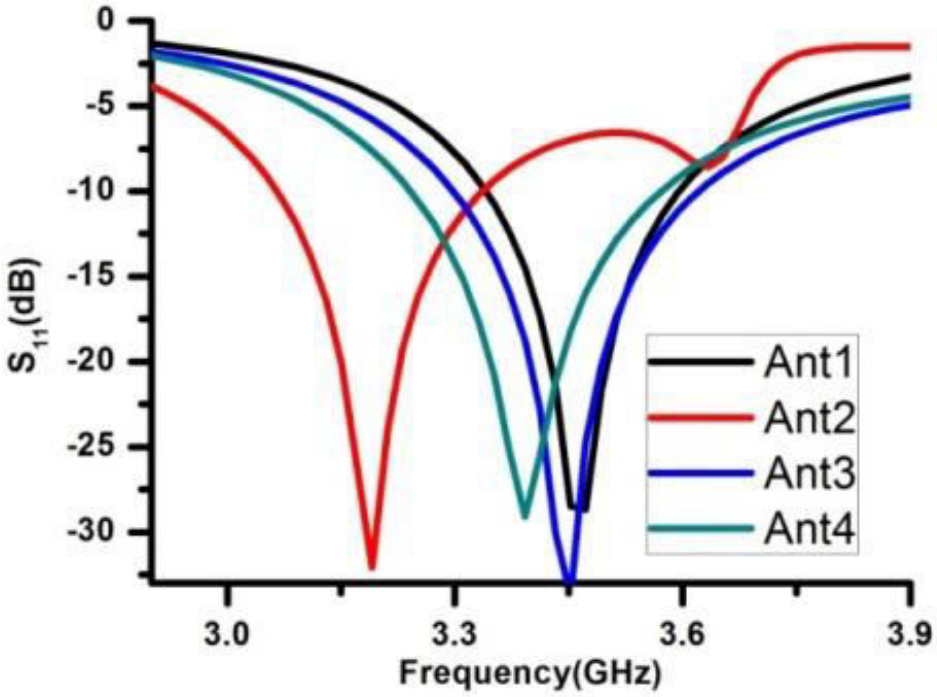

Fig. 5.14 Simulated return loss characteristics of single band antennas Ant1- Ant4

Table 5.7 Simulated Impedance Bandwidth Of Single Band Antennas

Antenna	No. of RIS elements	Size of a1 and a2 in mm	10-dB return loss bandwidth (%)
Ant1	25	a1=5 and a2=7	6.91 (3.35- 3.59 GHz)
Ant2	25	a1=6 and a2=7	8.12 (3.07- 3.33 GHz)
Ant3	16	a1=7 and a2=9	8.82 (3.31- 3.61 GHz)
Ant4	9	a1=8 and a2=13	8.80 (3.25- 3.55 GHz)

The simulated return loss characteristics of all dual band dual polarized antennas from Ant5 to Ant8 are shown in Fig. 5.15 and the impedance bandwidth at two resonating bands of each antenna is listed in Table 5.8. The simulated radiation efficiency of the proposed antenna is shown in the Fig 5.16. The radiation efficiency of the proposed antenna is 70.5% at lower resonating frequency (2.4 GHz) and is 90.75% at upper resonating frequency (3.4 GHz).

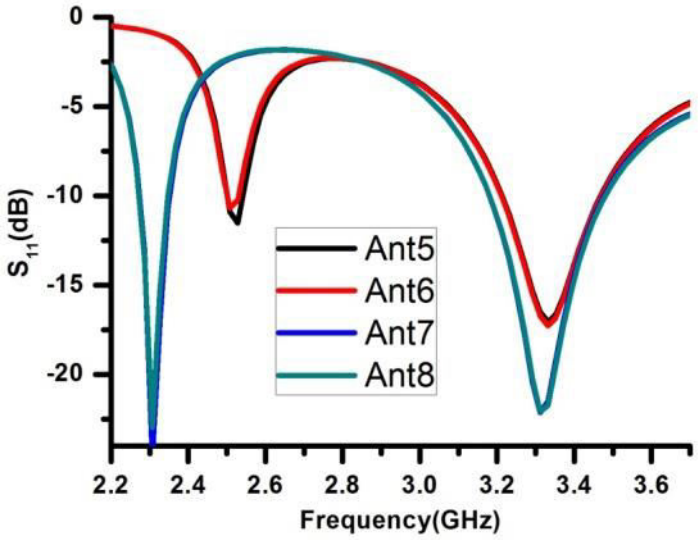

Fig. 5.15 Simulated return loss characteristics of dual band antennas Ant5- Ant8

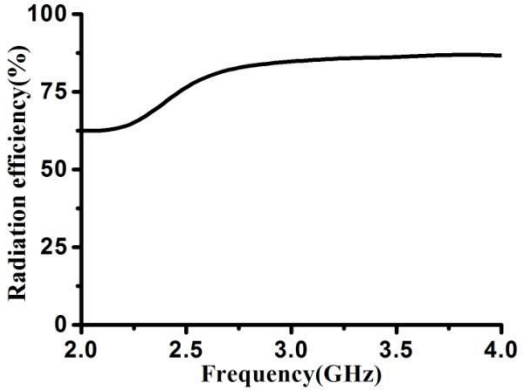

Fig 5.16 Simulated radiation efficiency of the proposed antenna

Table 5.8 Impedance Bandwidth of Dual Band Antennas

Antenna	RIS	patch	10- dB return loss bandwidth	
			at lower frequency	at upper frequency
Ant5	Square	Square	0.79% (2.50- 2.52 GHz)	6.58% (3.23- 3.45 GHz)
Ant6	square	Fractal	0.79% (2.50- 2.52 GHz)	7.20% (3.21- 3.45 GHz)
Ant7	fractal	Square	2.59% (2.28- 2.34 GHz)	7.78% (3.21- 3.47 GHz)
Ant8 (proposed)	fractal	fractal	2.59% (2.28- 2.34 GHz)	8.40% (3.19- 3.47 GHz)

5. 4 MEASURED RESULTS AND DISCUSSIONS

The proposed antenna (Ant8) is printed on FR4 epoxy material and is shown in the Fig. 5.17. The experimental results of the fabricated CP patch antenna are compared with the simulated results. The return loss characteristics are shown in the Fig. 5.18. The upper resonance frequency band occurred due to RIS and fractal patch results in wide impedance bandwidth that covers 10-dB return loss bandwidth of 8.48% (3.21- 3.49 GHz). The lower resonance frequency band is achieved due to mushroom unit cell which results in 10-dB return loss bandwidth of 2.59% (2.30- 2.36 GHz).

(a) (b)

Fig. 5.17 photograph of the fabricated patch antenna (a) front view (b) back view

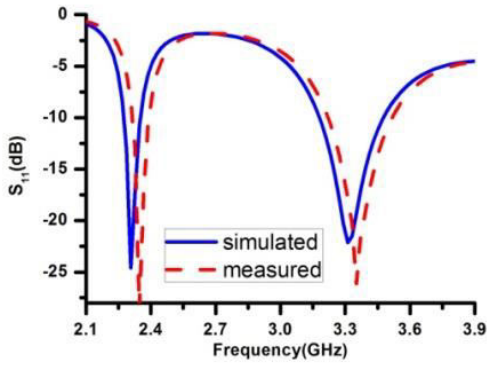

Fig. 5.18 Return loss characteristics of the fabricated antenna

The axial ratio characteristics are shown in the Fig. 5.19. The measured 3-dB axial ratio bandwidth at upper operating frequency band is 4.26% (3.21- 3.35 GHz).

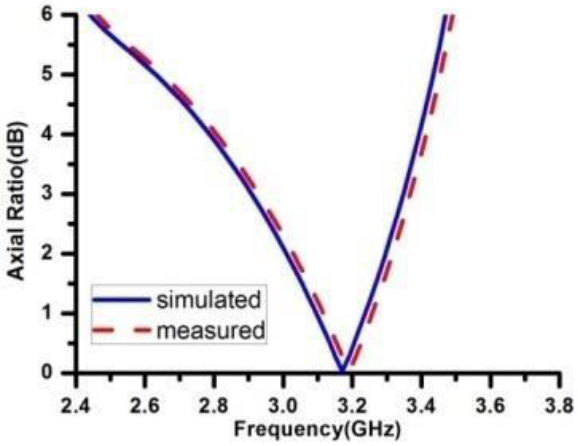

Fig. 5.19 Axial Ratio characteristics of the fabricated patch antenna

The measured and simulated radiation patterns of the proposed antenna at lower resonating band are shown in the Fig. 5.20. The measured and simulated radiation patterns of the proposed antenna at upper resonating band are shown in the Fig. 5.21. The measured and simulated gain of the antenna is given in Fig. 5.22.

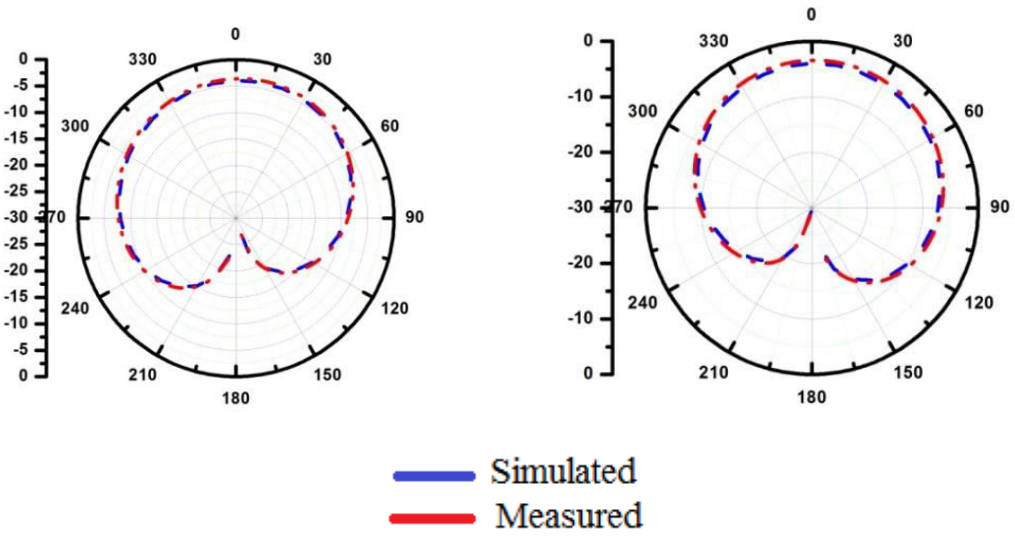

(a) (b)

Fig. 5.20 Radiation patterns at 2.32 GHz, (a) E plane pattern, (b) H plane pattern

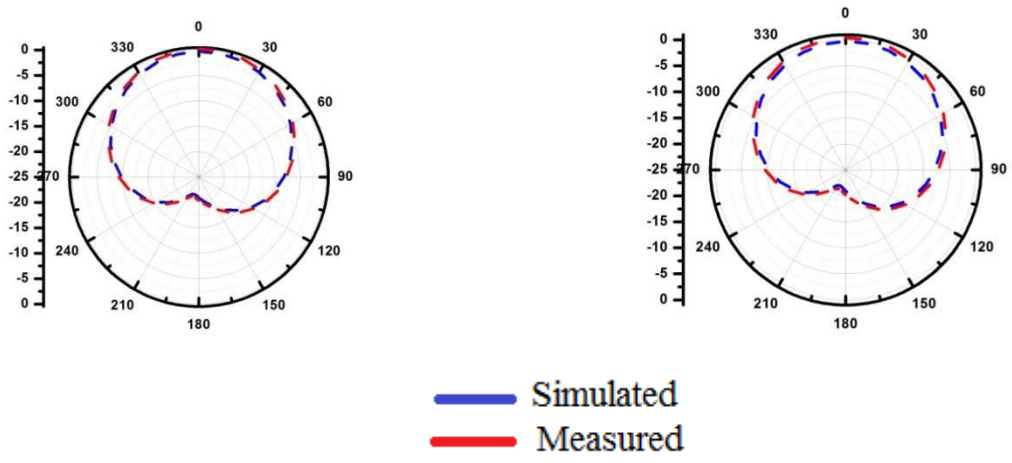

(a) (b)

Fig. 5.21 Radiation patterns at 3.35 GHz, (a) E plane pattern, (b) H plane pattern

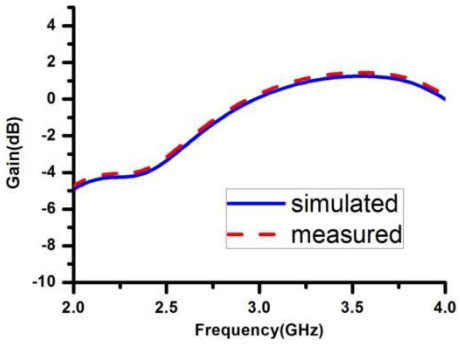

Fig. 5.22 Gain characteristics of the proposed antenna

Comparison between the results of the proposed antenna and the antennas which already exist in the literature are given in the Table 5.9. The proposed antenna is more compact and producing wide bandwidth compared to remaining antennas listed in Table 5.9.

Table 5.9 Comparison between the proposed antenna and the existing literature

Antenna	Patch Size (mmxmm)	Board size (mmxmmxmm)	10- dB return loss bandwidth at corresponding centre frequency	
			At ZOR	At patch mode
proposed	18x18	30x30x2.4 30x30x0.6	2.4 GHz	3.4 GHz
[62]	16.5x23.5	30x30x2.6 30x30x0.4	2.4 GHz	2.9 GHz
[70]	21.5x21.5	40x45x2.5	3.5 GHz (132 MHz) 3.77% at patch mode	
[71]	20x20	30x30x2.4 30x30x0.8	3.29 GHz, 5.11 GHz, 5.4 GHz 5.9 GHz, 6.62 GHz, 8.1 GHz	

5. 5 Conclusions

Dual band patch antennas loaded with MUC is implemented over RIS are presented. Various fractal antennas using Minkowski, poly and Half Circled curves are studied for dual band operation. By varying the feed point position dual band antennas which resonate at 2.4 GHz and 3.4 GHz are designed. The 3-dB CP bandwidths obtained at upper bands are more than 2%. These antennas are useful for systems operating at Wi-Fi and Wi-MAX standards IEEE 802.11 and IEEE 802.16. These antennas are fabricated and performance is measured. A good comparison is obtained.

Here it can be seen that the bandwidths are slightly less at both the bands compared to the antenna presented in chapter 4, but good amount of compactness is achieved. So, the user can exercise his choice between bandwidth and size with all these proposals. However there are instances in the recent times where large bandwidth of the order of 15% is required with a compact antenna for Wi-Fi routers to operate high data rates with multiple tethered devices. To realize this HIS is attempted in the next chapter.

Chapter 6

HIS based wideband Microstrip patch Antennas

The recent improvements in the area of wireless communications have expanded the requirement for wide band antennas. Essential requirements of present day communication systems have also provoked an increased demand for low cost and miniaturized antennas. For proper wave propagation between the transmitting and receiving antennas circular polarization is also becoming more and more attractive. In view of these perspectives, compact circular polarized antennas with wide impedance bandwidth and good CP bandwidth are useful in the future wireless systems.

Most of the wide band structures existing in the literature are using coplanar wave guide fed slot antennas, probe fed antennas and stacked patch techniques. However, most of these antennas are linearly polarized. Some multiband CP antennas exist based on multi layer configuration, but the generated 3-dB CP bandwidth is very narrow (<2%), which is not meeting the requirements of present day communication systems. Here, in the present work wide band CP antennas are designed using the HIS (High Impedance Surface) and asymmetrical fractal boundary curves.

In this section four new antennas are studied for wideband operation with good Circular Polarization based on HIS. Those are:

(1) HIS based Wideband Minkowski fractal boundary antenna
(2) HIS based Wideband Koch fractal boundary antenna
(3) HIS based Wideband Poly fractal boundary antenna
(4) HIS based Wideband Semi circular fractal boundary antenna

6.1 HIS based Wideband Minkowski fractal boundary antenna

The Minkowski fractal boundary patch antenna geometry is shown in the Fig.6.1 which is also printed on Rogers RT/Duroid with dielectric constant 2.2. The presented antenna has two substrates (bottom and top): on the top substrate the recommended antenna is designed and

on the bottom substrate the HIS with a planar array of 3x3 fractal mushroom unit cells is printed. The circular polarization (CP) operation can be obtained by inserting Minkowski fractal curves with IF's Dx and Dy along x and y- axes respectively. The 10- dB return loss bandwidth and axial ratio bandwidth can be improved by optimizing IF along each edge of the antenna. The optimized dimensions of the proposed antenna are given in Table 6.1.

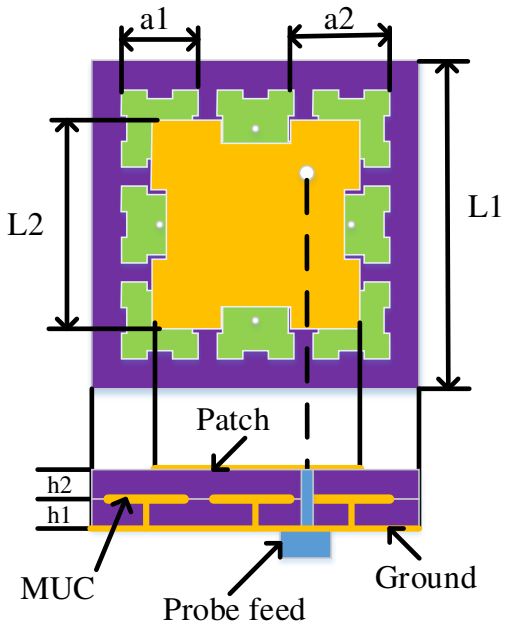

Fig. 6.1 Geometry of HIS based Minkowski fractal patch antenna

Table 6.1 Dimensions of the proposed patch antenna

parameter	Value in mm
L1	38
L2	30
a1	8
a2	13
h1	1.6
h2	1.6
Dx1=Dx2=Dx	2
Dy1=Dy2=Dy	5

Operation of the proposed antenna can be understood by considering an evolution of patch antenna design shown in Fig. 6.2. Initially the square patch Ant1 on single substrate is chosen

as reference which is resonating at 3.05 GHz with linear polarization. The edges of the square patch are replaced with Minkowski fractal curves for Circular polarization in Ant2. Ant1 is implemented over square HIS for bandwidth improvement in Ant3. Ant4 can be obtained by implementing Ant2 on Minkowski curves loaded fractal HIS for good impedance bandwidth and Circular polarization bandwidth. The simulated return loss characteristics are shown in the Fig. 6.3 and the values are listed in Table 6.2.

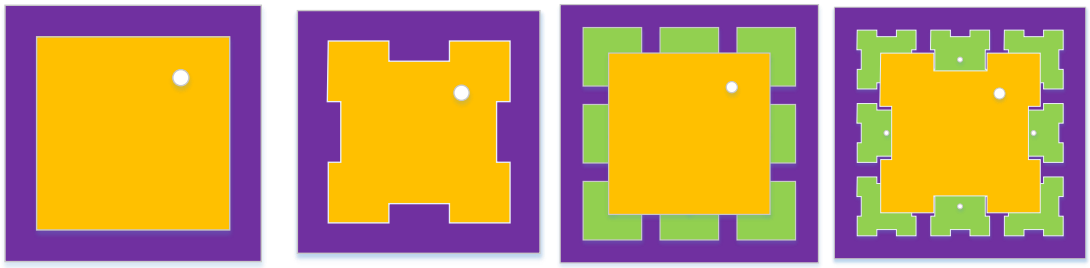

Ant1 Ant2 Ant3 Ant4

Fig. 6.2 Evaluation of patch antennas

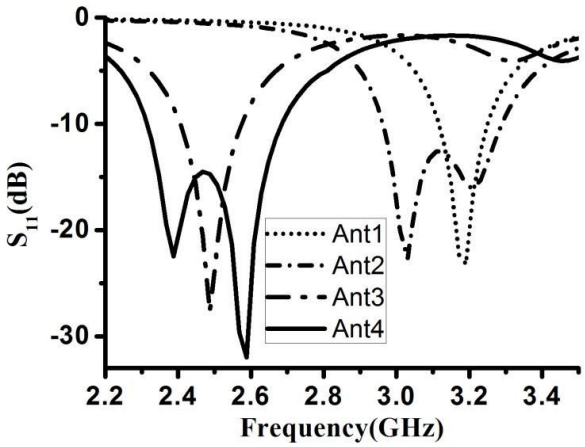

Fig. 6.3 Simulated return loss characteristics

Table 6.2: Simulated return loss bandwidth values

S. No	Antenna	Impedance Bandwidth
1	Ant1	(3.13- 3.23) 3.14%
2	Ant2	(2.96- 3.27) 9.96%
3	Ant3	(2.40- 2.56) 6.45%
4	Ant4	(2.32- 2.66) 13.65%

6.2 HIS based Wideband Koch fractal boundary antenna

The Koch fractal boundary patch antenna geometry is shown in the Fig.6.4 which is also printed on Rogers RT/Duroid with dielectric constant 2.2. The presented antenna has two substrates (bottom and top), on the top substrate the recommended antenna is designed and on the bottom substrate the HIS with a planar array of 3x3 fractal mushroom unit cells is printed. The circular polarization (CP) operation can be obtained by inserting semi circle curves with IF's θx and θy along x and y- axes respectively. The 10- dB return loss bandwidth and axial ratio bandwidth can be improved by optimizing IF along each edge of the antenna. The optimized dimensions of the proposed antenna are given in Table 6.3.

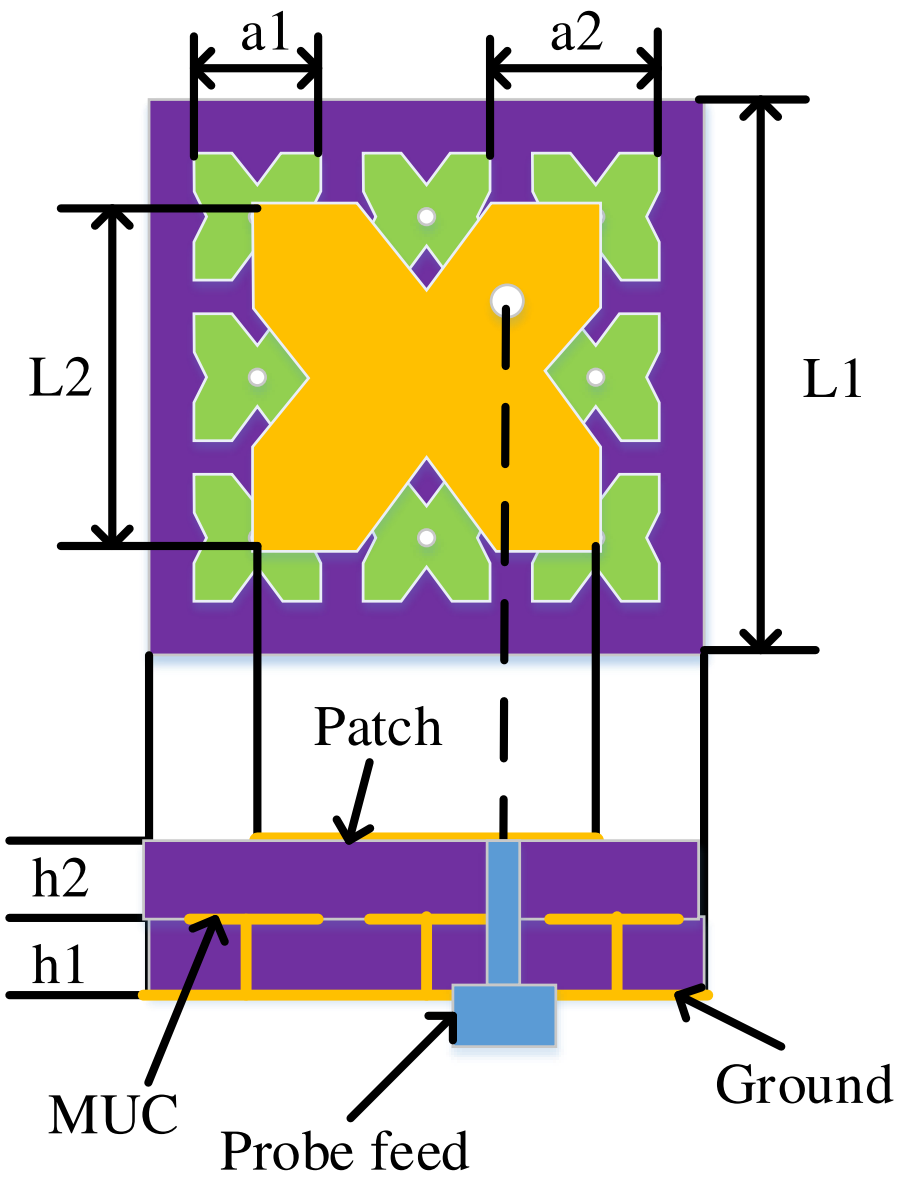

Fig. 6. 4 Geometry of the HIS based Koch fractal boundary patch antenna

Table 6.3 Dimensions of the proposed patch antenna

parameter	Value in mm
L1	38
L2	30
a1	8
a2	13
h1	1.6
h2	1.6
θx1=θx2=θx	30
θy1=θy2=θy	60

Operation of the proposed antenna can be understood by considering an evolution of patch antenna design shown in Fig. 6.5. Initially the square patch Ant1 on single substrate is chosen as reference which is resonating at 3.05 GHz with linear polarization. The edges of the square patch are replaced with Koch fractal curves for Circular polarization in Ant2. Ant1 is implemented over square HIS for bandwidth improvement in Ant3. Ant4 can be obtained by implementing Ant2 on Koch curves loaded fractal HIS for good impedance bandwidth and Circular polarization bandwidth. The simulated return loss characteristics are shown in the Fig. 6.6 and the values are listed in Table 6.4.

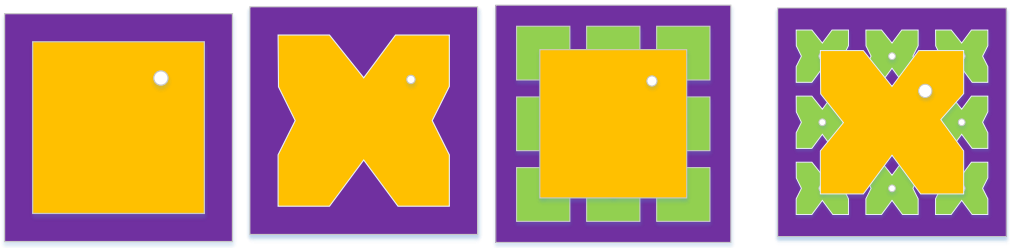

Ant1 Ant2 Ant3 Ant4

Fig. 6.5 Evaluation of proposed antenna

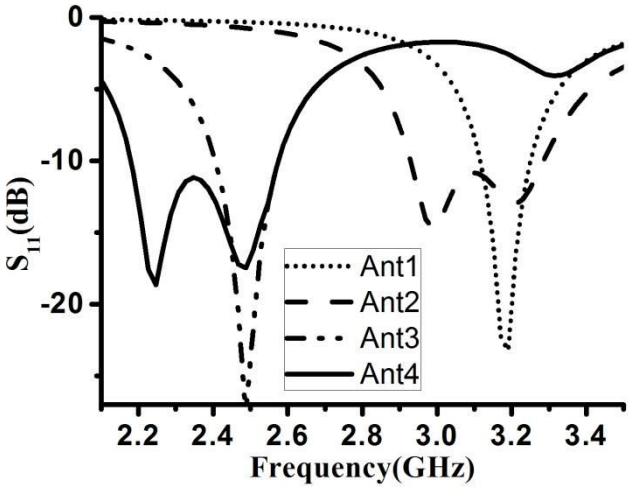

Fig.6. 6 Simulated return loss characteristics

Table 6.4: Impedance bandwidth

S. No	Antenna	Impedance Bandwidth
1	Ant1	(3.13- 3.23) 3.14%
2	Ant2	(2.92- 3.27) 11.32%
3	Ant3	(2.40- 2.56) 6.45%
4	Ant4	(2.18- 2.56) 16.03%

6.3 HIS based Wideband Poly fractal boundary antenna

The Poly fractal boundary patch antenna geometry is shown in the Fig.6.7 which is also printed on Rogers RT/Duroid with dielectric constant 2.2. The presented antenna has two substrates (bottom and top), on the top substrate the recommended antenna is designed and on the bottom substrate the HIS with a planar array of 3x3 fractal mushroom unit cells is printed. The circular polarization (CP) operation can be obtained by inserting Poly fractal curves with IF's θx and Dy along x and y- axes respectively. The 10- dB return loss bandwidth and axial ratio bandwidth can be improved by optimizing IF along each edge of the antenna. The optimized dimensions of the proposed antenna are given in Table 6.5.

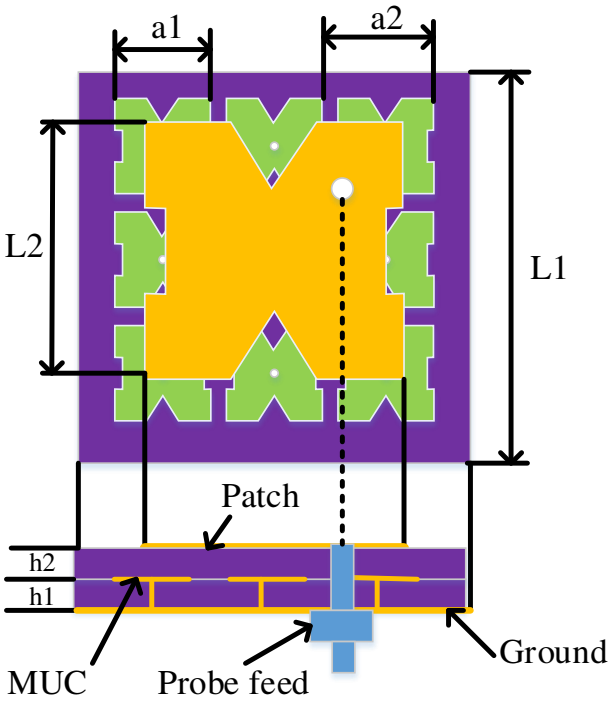

Fig.6. 7 Geometry of HIS based poly fractal patch antenna

Table 6.5: Parameter values

parameter	Value in mm
L1	38
L2	30
a1	8
a2	13
h1	1.6
h2	1.6
θx1=θx2=θx	30
θy1=θy2=θy	60

Operation of the proposed antenna can be understood by considering an evolution of patch antenna design shown in Fig. 6.8. Initially the square patch Ant1 on single substrate is chosen as reference which is resonating at 3.05 GHz with linear polarization. The edges of the square patch are replaced with Minkowski fractal curves for Circular polarization in Ant2. Ant1 is implemented over HIS for bandwidth improvement in Ant3. Ant4 can be obtained by

implementing Ant2 on HIS for good impedance bandwidth and Circular polarization bandwidth. The simulated return loss characteristics are shown in the Fig. 6.9 and the values are listed in Table 6.6.

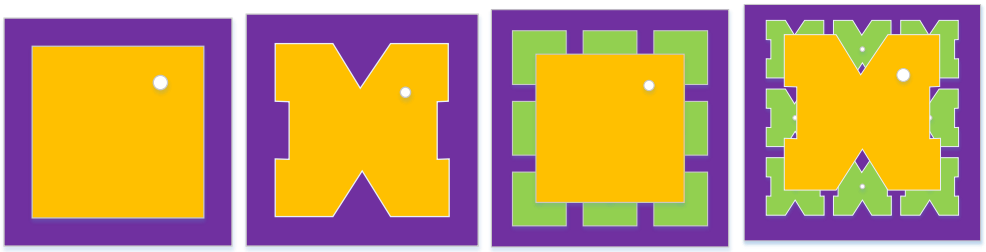

Ant1 Ant2 Ant3 Ant4

Fig. 6.8 Evaluation of proposed antenna

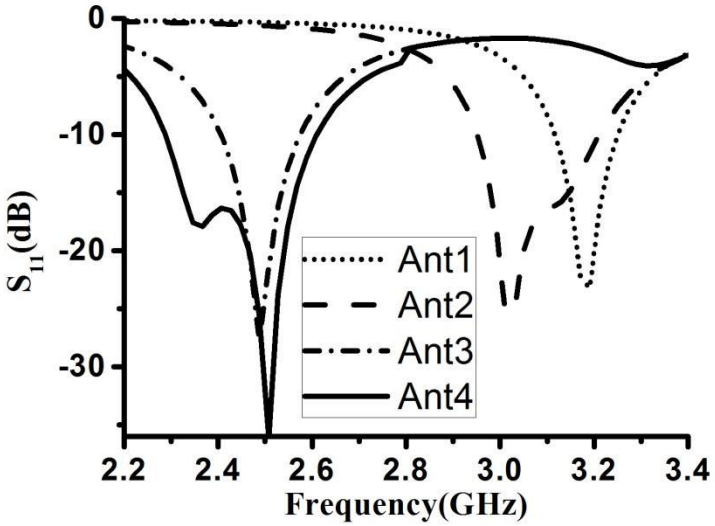

Fig. 6.9 Simulated return loss characteristics

Table 6.6: impedance bandwidth values

S. No	Antenna	Impedance Bandwidth
1	Ant1	(3.13- 3.23) 3.14%
2	Ant2	(2.92- 3.27) 11.32%
3	Ant3	(2.40- 2.56) 6.45%
4	Ant4	(2.18- 2.56) 16.03%

6.4 HIS based Wideband Semi circular fractal boundary antenna

The Semi circle fractal boundary patch antenna geometry is shown in the Fig.6.10 which is also printed on Rogers RT/Duroid with dielectric constant 2.2. The presented antenna has two substrates (bottom and top), on the top substrate the recommended antenna is designed and on the bottom substrate the HIS with a planar array of 3x3 fractal mushroom unit cells is printed. The circular polarization (CP) operation can be obtained by inserting semi circle curves with IF's Rx and Ry along x and y- axes respectively. The 10- dB return loss bandwidth and axial ratio bandwidth can be improved by optimizing IF along each edge of the antenna. The optimized dimensions of the proposed antenna are given in Table 6.8.

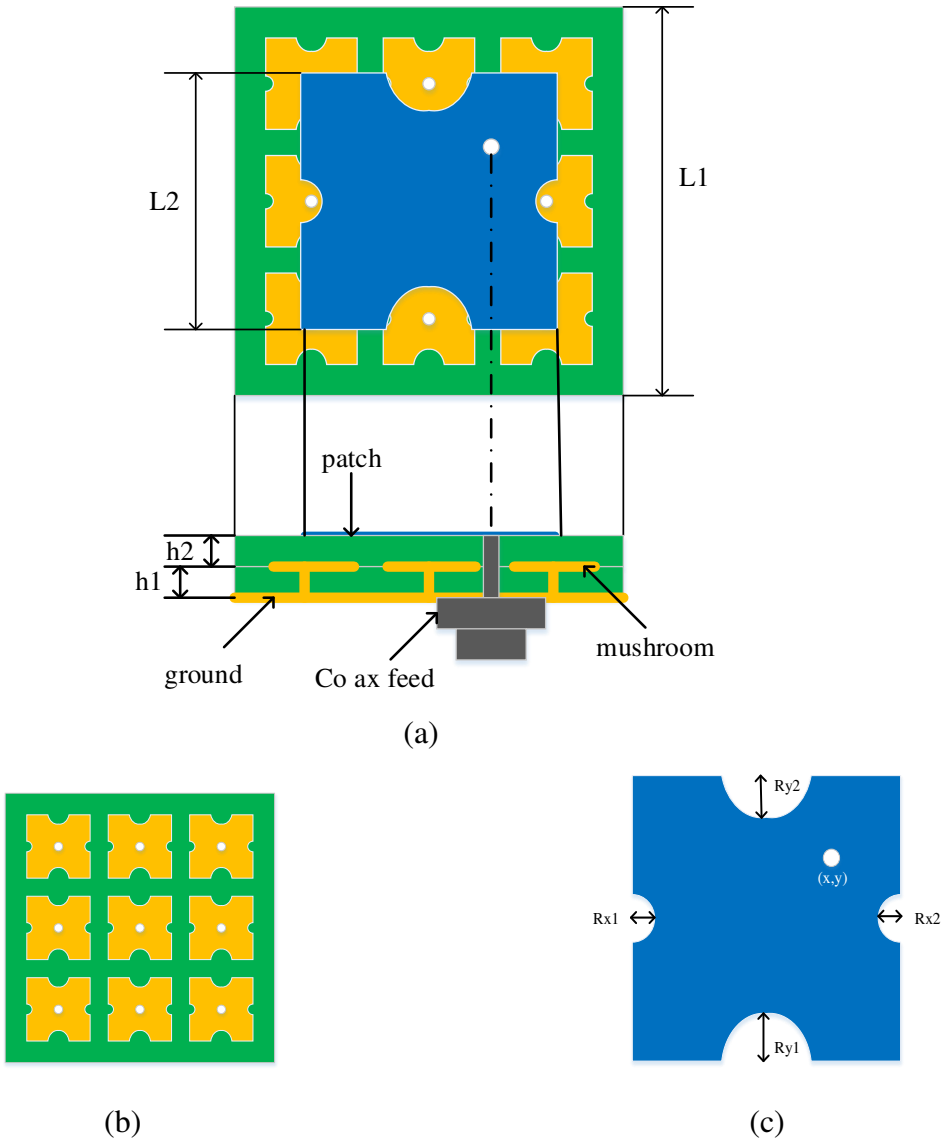

Fig. 6.10 (a) Geometry of the proposed Semi circular fractal boundary patch antenna (b) top view of the HIS (c) top view of the patch

Table 6.7: Parameter Values

parameter	Value in mm
L1	38
L2	30
a1	8
a2	13
h1	1.6
h2	1.6
Rx1=Rx2=Rx	2
Ry1=Ry2=Ry	5

The evolution of the proposed antenna is shown in Fig. 6.11. Initially the square patch ant1 on single substrate is chosen as reference which is resonating at 3.05 GHz with linear polarization. The semi circle fractal curves with different Indentation Radii are inserted into Ant1 to get remaining antennas (Ant2 to Ant11), which results in single band of operation with less 10-dB return loss bandwidth and axial ratio bandwidth. The 10-dB return loss characteristics of all simulated antennas on single substrate are shown in the Fig. 6.12. The impedance bandwidth of each antenna is listed in Table 6.9.

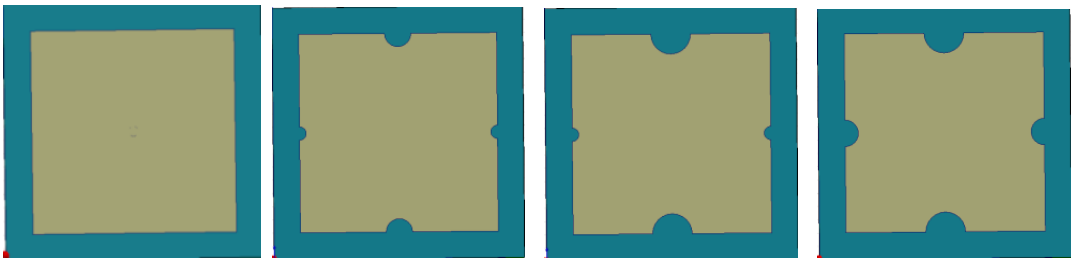

Ant1 Ant2 Ant3 Ant4

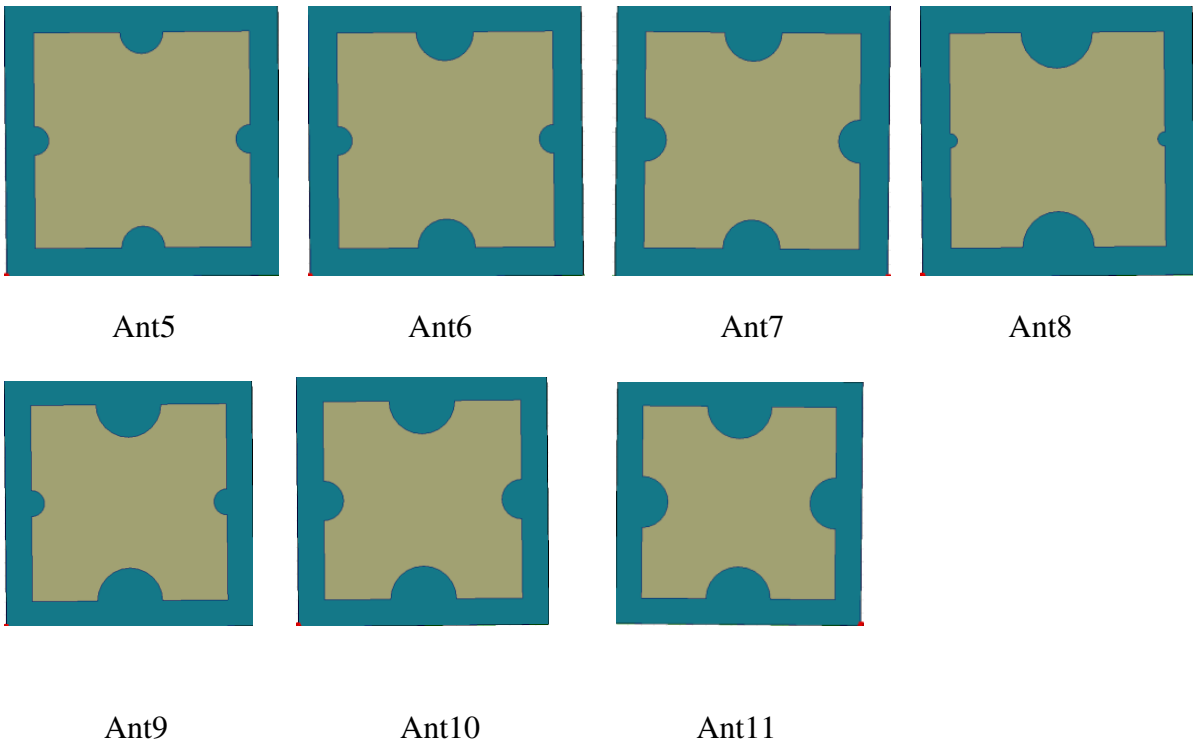

Fig.6.11 Evaluation of the proposed antenna on single substrate

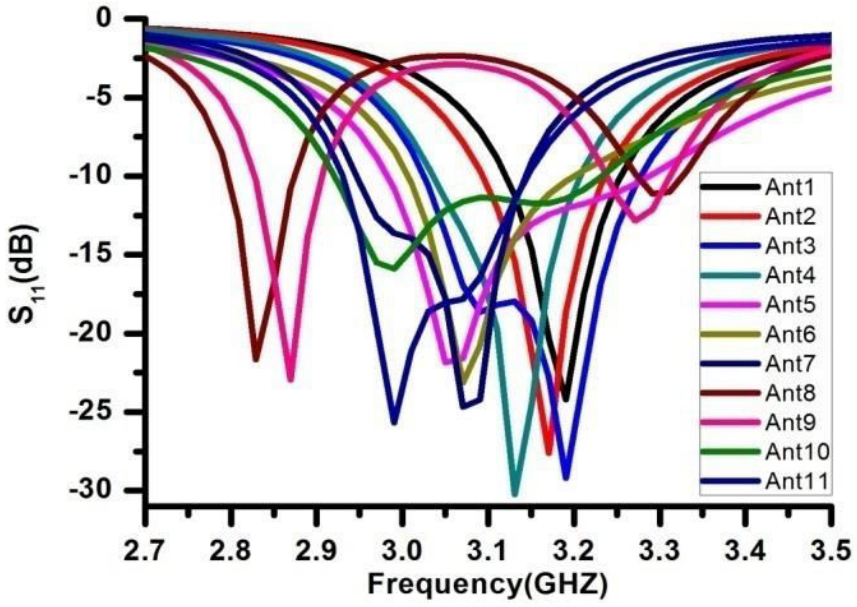

Fig. 6.12 Simulated return loss characteristics of Antennas Ant1 - Ant11

Table 6.8: Impedance bandwidth values

Antenna	IRs (in mm)		Impedance Bandwidth
	Rx	Ry	
Ant1	--	--	(3.13- 3.25) 3.76%
Ant2	1	2	(3.11- 3.23) 3.78%
Ant3	1	3	(3.03- 3.27) 7.61%
Ant4	2	3	(3.05- 3.19) 4.56%
Ant5	1	4	(2.98- 3.27) 9.29%
Ant6	2	4	(3.01- 3.19) 5.80%
Ant7	3	4	(2.94- 3.13) 6.27%
Ant8	1	5	(2.80- 2.86) 2.12%
Ant9	2	5	(2.82- 2.88) 2.10%
Ant10	3	5	(2.92- 3.23) 10.26%
Ant11	4	5	(2.94- 3.13) 6.27%

To get widened impedance bandwidth with circular polarization at Wi-Fi band the same antenna is implemented on HIS which is given in the Fig. 6.13. HIS is made of planar array of 3x3 fractal mushroom unit cells. Each unit cell has 8x8 mm^2 square patch and 0.5 mm radius VIA where all unit cells connected to ground through VIAs. The semi circle fractal curves are inserted into each square mushroom unit cell to make required HIS. Finally Ant20 is the proposed antenna with wide bandwidth.

The 10-dB return loss characteristics of all simulated antennas on fractal mushroom HIS are shown in the Fig. 6.14 and the impedance bandwidth of each antenna is listed in Table 6.10.

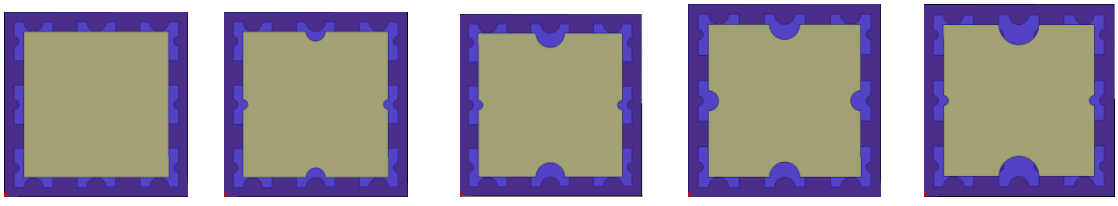

Ant12 Ant13 Ant14 Ant15 Ant16

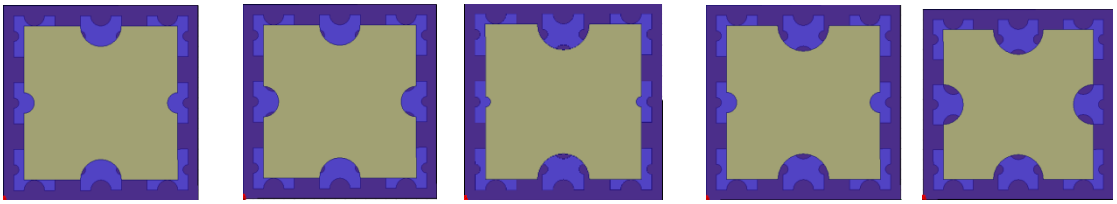

Ant17 Ant18 Ant19 Ant20 Ant21

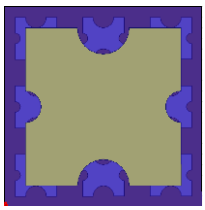

Ant22

Fig. 6.13 Evaluation of the proposed antenna on HIS

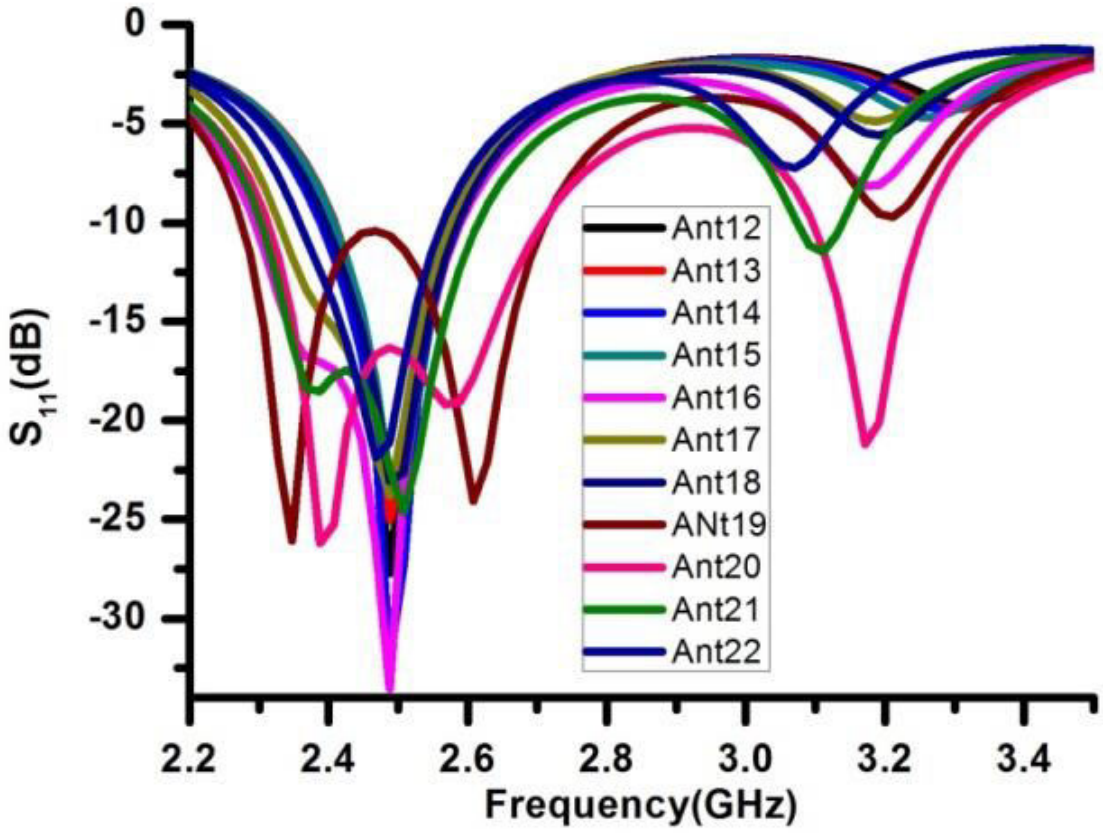

Fig. 6.14 Return loss characteristics of HIS antennas

Table 6.9: Impedance bandwidth values

Antenna	IRs (in mm)		Impedance Bandwidth
	Rx	Ry	
Ant12	--	--	(2.40- 2.56) 6.45%
Ant13	1	2	(2.42- 2.56) 5.60%
Ant14	1	3	(2.40- 2.58) 7.22%
Ant15	2	3	(2.42- 2.58) 6.45%
Ant16	1	4	(2.30- 2.58) 11.47%
Ant17	2	4	(2.34- 2.56) 8.90%
Ant18	3	4	(2.40- 2.56) 6.45%
Ant19	1	5	(2.28- 2.70) 16.86%
Ant20	2	5	(2.32- 2.70) 15.13%
Ant21	3	5	(2.30- 2.60) 12.24%
Ant22	4	5	(2.36- 2.54) 7.34%

The simulated radiation efficiency of the proposed antenna is shown in the Fig. 6.15. The efficiency is good at 2.4 GHz (98%).

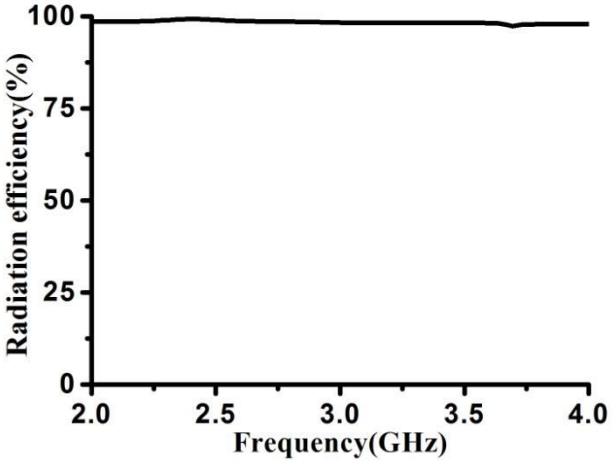

Fig. 6.15 Simulated Radiation efficiency characteristics of the proposed antenna

6. 5 EXPERIMENTAL RESULTS

The proposed antenna (Ant20) is fabricated on Rogers RT/Duroid substrate which is shown in Fig. 6.16. Fractal mushroom HIS and fractal patch antenna are individually fabricated. HIS is printed on bottom substrate and patch antenna is placed on top substrate without ground. The VIAs are fabricated with the help of through hole copper plating technique. Both the substrates are attached with the help of paper tape. The dimensions of both the substrates are 38 x 38 x 1.6 mm^3. The return loss characteristics are measured using Agilent 8719A microwave network analyzer. Radiation pattern measurements are taken in an anechoic chamber having physical dimensions 22.5 x 12.5 x 11.5 m^3. The operating frequency range of the anechoic chamber is 400 MHz to 18 GHz. The input power given to transmitter is -40dBm.

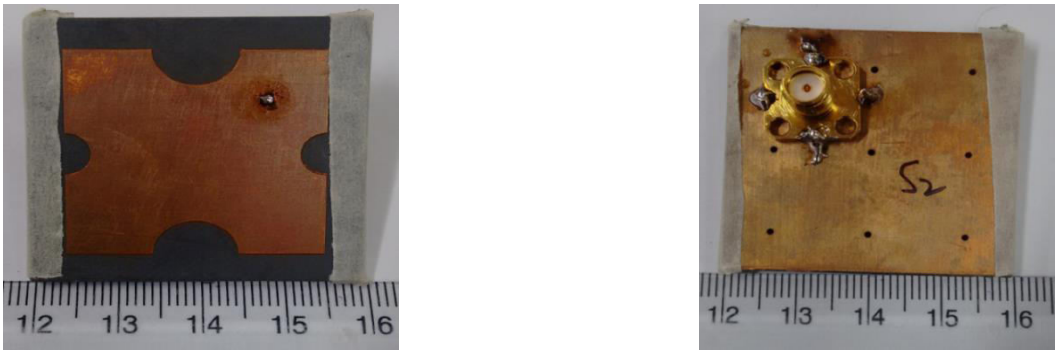

(a) (b)

Fig.6.16 photos of fabricated Ant20 (a) top view (b) bottom view

The measured return loss characteristics along with simulated data are given in Fig. 6.17. Measured results are in close agreement with simulated results. The 10-dB return loss bandwidth is 15.13% (2.32- 2.70 GHz). The discontinuity at patch mode band indicates that possibility of circular polarization radiation. The Axial ratio characteristics are given in Fig. 6.18. The 3-dB Axial Ratio bandwidth is 4.11% (2.38 GHz- 2.48 GHz). The minimum Axial Ratio value of 0.5 dB is occurred at the centre frequency.

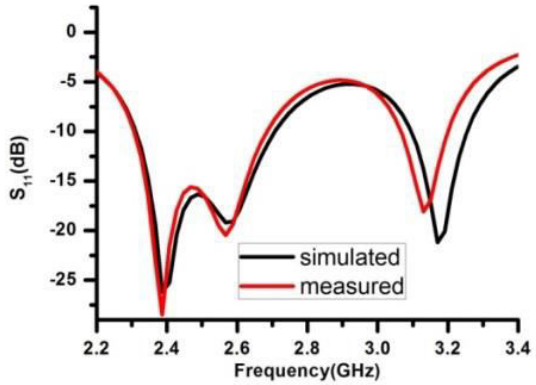

Fig. 6.17 Simulated and measured return loss characteristics of Ant20

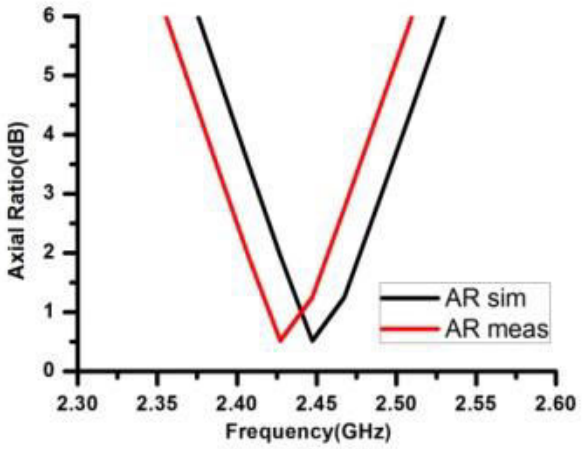

Fig. 6.18 Simulated and measured axial ratio characteristics of Ant20

The radiation patterns of the proposed antenna are depicted in Fig.6.19. The measured and simulated gains of the presented antenna are given in Fig. 6.20.

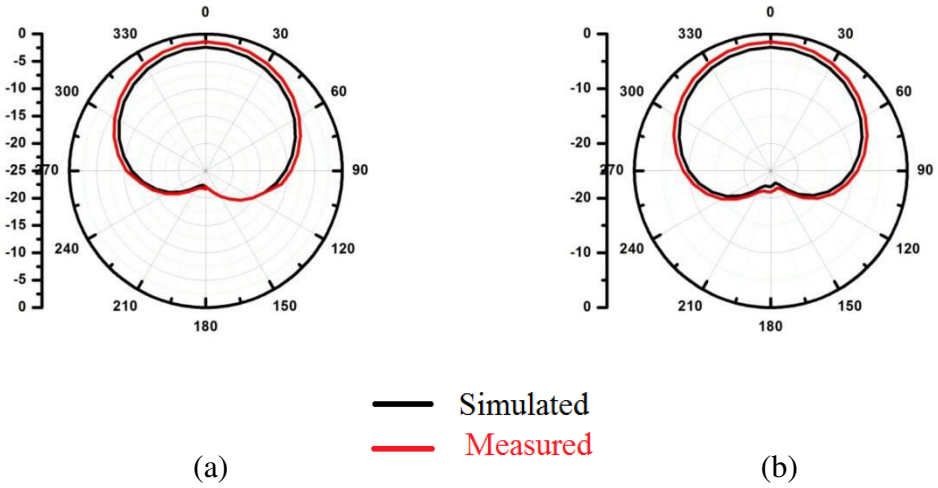

Fig. 6.19 Simulated and measured radiation patterns at 2.4 GHz (a) E Plane (b) H Plane

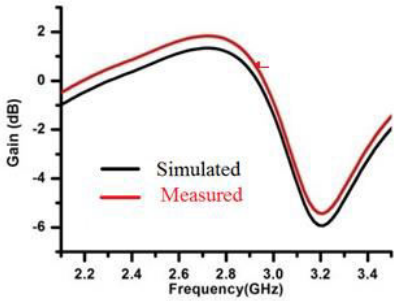

Fig. 6.20 Simulated and measured Gain of the proposed antenna

Comparison between the results of the proposed antenna and the antennas which already exist in the literature are given in the Table 6.9. The proposed antenna is more compact and producing wide bandwidth compared to remaining antennas listed in Table 6.9.

Table 6.10 Comparison between the proposed antenna and the existing literature

Antenna	Patch Size (mmxmm)	Board size (mmxmmxmm)	10- dB return loss bandwidth at corresponding centre frequency
proposed	30x30	40x40x1.6 40x40x1.6	(2.18- 2.56) 16.03%
[81]	27.5x27.5	45x45x2.47	(2.36- 2.45 GHz) 3.75%
[89]	33x41		(2.25- 2.3 GHz) 2.2%
[90]	27x27	40x40x0.5 40x40x1.5 40x40x2.5	(5.19- 7.08 GHz) 31.5%
[91]	49x55.1	150x150x10 150x150x1.57	(1.9- 2.7 GHz)

6. 6 Conclusions

Compact wide band patch antennas based on HIS are presented. Various fractal antennas using Minkowski, Koch, poly and semi circle fractal curves are studied for single wide band operation. By varying the feed point position wide band antennas which resonate at 2.4 GHz are designed. The 3-dB CP bandwidth obtained at patch mode band is more than 3%. These antennas are useful for systems operating at Wi-Fi standards IEEE 802.11. These antennas are fabricated and performance is measured. A good comparison is obtained. A very compact antenna with good impedance bandwidth and Axial Ratio bandwidth is presented with the blend of two recent concepts: fractals and metamaterials for the first time.

Chapter 7

Conclusions and Future Scope

7.1 Conclusions

This thesis is aimed at developing new compact dual band and wide band patch antennas based on metamaterials. Several antennas of above type are studied by applying different types of metamaterials. The edges of all the square patch antennas are replaced by the asymmetrical fractal curves to get CP radiation at patch mode band.

As first part of the contribution the new dual band patch antennas based on CSRR have been studied, simulated, fabricated and tested experimentally. The dimensions of the patch are 27mm x 27 mm so that the upper band (patch mode band) is resonating at 3.3 GHz. The second band (left hand band) along with patch mode band can be achieved by etching CSRR from the radiating element. The left handed nature of CSRR is the main cause for generation of second band. The dimensions and position of the CSRR are adjusted to generate left hand band exactly at 2.4 GHz. The impedance bandwidth is poor at left hand band and is good at patch mode band. By varying the parameters of the fractal curves like indentation angles and indentation depths, parametric study has been carried out. Later by replacing the sides of the square patch with asymmetrical fractal boundary curves, required perturbation is introduced in the patch structure to generate good circular polarization at patch mode band. It is concluded that the asymmetrical fractal curves along two perpendicular directions x and y – axes yield more CP bandwidth than other asymmetrical conditions. The best performed antennas are fabricated and the experimental results are in good agreement with simulated results. The maximum obtained 3-dB axial ratio CP bandwidth is about 2.50% and the 10-dB return loss bandwidth is 8.22% at patch mode band.

As the second part of the contribution, the Mushroom Unit Cell loaded dual band patch antennas have been studied, simulated, fabricated and tested experimentally. The dimensions of the patch are 27mm x 27 mm so that the upper band (patch mode band) is resonating at 3.3 GHz. The second band (left hand band) along with patch mode band can be achieved by loading Mushroom Unit Cell into the radiating element. The left handed nature of MUC is the main cause for generation of second band. The dimensions and position of the MUC are

optimized to generate left hand band exactly at 2.4 GHz. The impedance bandwidths at left hand band as well as at patch mode band are good. By varying the parameters of the fractal curves like indentation angles and indentation depths, parametric study has been carried out. Later by replacing the sides of the square patch with asymmetrical fractal boundary curves, required perturbation is introduced in the patch structure to generate good circular polarization at patch mode band. It is concluded that the asymmetrical fractal curves along two perpendicular directions x and y – axes yield more CP bandwidth than other asymmetrical conditions. The best performed antennas are fabricated and the experimental results are in good agreement with simulated results. The 10-dB return loss bandwidth is 2.51% at left hand band and is 6.23% at patch mode band. The maximum obtained 3-dB axial ratio CP bandwidth is about 2.35% at patch mode band.

As the third part of the contribution, the ENGTL metallic VIAs loaded dual band patch antennas have been studied, simulated, fabricated and tested experimentally. The dimensions of the patch are 30 mm x 30 mm so that the upper band (patch mode band) is resonating at 3.3 GHz. The second band (left hand band) along with patch mode band is achieved by loading VIAs into the radiating element. The left handed nature of VIAs is the main cause for generation of second band. The dimensions and positions of the VIAs are modified to generate left hand band exactly at 2.4 GHz. The impedance bandwidths at left hand band as well as at patch mode band are impressive. By varying the parameters of the fractal curves like indentation angles and indentation depths, parametric study has been carried out. Later by replacing the sides of the square patch with asymmetrical fractal boundary curves, required perturbation is introduced in the patch structure to generate good circular polarization at patch mode band. It is concluded that the asymmetrical fractal curves along two perpendicular x and y – axes yield more CP bandwidth than other asymmetrical conditions. The antennas with good performance are fabricated and the experimental results are in good agreement with simulated results. The 10-dB return loss bandwidth is 4.83% at left hand band and is 9.22% at patch mode band. The maximum obtained 3-dB axial ratio CP bandwidth is about 2.37% at patch mode band.

As fourth part of contribution, compact dual band patch antennas are proposed based on RIS for 2.4 GHz and 3.4 GHz wireless applications. The antenna structure consists of two substrates where RIS elements are placed on grounded bottom substrate and the MUC loaded asymmetrical fractal boundary patch is placed on top substrate without ground plane. Both substrates are combined to achieve dual band operation with good return loss bandwidth at

both the bands. The radiating patch size is 18 mm x 18 mm. For better CP characteristics, properties of fractal curves and dimensions of RIS elements are optimized. The 10-dB return loss bandwidth is 2.59% at left hand band and is 8.40% at patch mode band. The 3-dB axial ratio bandwidth is 2.12% at upper band. Likewise, several dual band RIS antennas have been studied using various fractal boundary curves.

As fifth part of contribution, HIS based wide band patch antennas are presented for wireless applications in the range of 2–3 GHz frequency. The antenna structure is made up of asymmetrical half circled fractal boundary patch over a High impedance surface (HIS). The simulations of single-layer Koch fractal antenna, dual layer with square and fractal HIS elements are carried out in a systematic way for broadband CP radiation and corresponding results are presented. For better CP characteristics, properties of fractal curves and dimensions of HIS elements are optimized. The antenna with fractal HIS iteration order one (iteration1) is experimentally studied. The 10-dB return loss bandwidth is 15.13%, whereas 3-dB axial ratio bandwidth is 4.11%, which indicate that by applying fractals concept to HIS technique, with a single probe feed, wide band CP radiation can be obtained. Likewise, several wideband HIS antennas have been studied using various fractal boundary curves.

Many antennas are fabricated and the measured results are compared with simulated results (using commercial simulation software: Ansoft HFSS). A close agreement is observed between experimental and simulated data. All the measurements are carried out with standard equipment.

Applications of Proposed Metamaterial based dual band Antennas

The latest developments in the field of wireless communication require compact and portable antennas. One of the best options for this is the use of antennas based on metamaterials, as they have the left hand wave propagation capability. All the proposed antennas in this thesis are designed at, Wi-Fi and Wi-MAX wireless applications. These types of antennas find applications in RFID, personal hand held wireless devices like cell phones, laptops etc.

7.2 Future Scope

Still more compact dual band antennas can be designed by adopting the combination of different types of metamaterials and fractals. In this thesis only single band antennas are implemented over HIS, but multiband antennas can also be designed on HIS.

References

[1] Balanis, Constantine A., ed. Modern antenna handbook. John Wiley & Sons, 2011.

[2] Garg, Ramesh, et al. Microstrip antenna design handbook. Artech house, 2001.

[3] Caloz, Christophe, and Tatsuo Itoh. Electromagnetic metamaterials: transmission line theory and microwave applications. John Wiley & Sons, 2005.

[4] Eleftheriades, George V., and Keith G. Balmain, " Negative-refraction metamaterials: fundamental principles and applications," John Wiley & Sons, 2005.

[5] Barnsley, Michael F. Fractals everywhere. Academic press, 2014.

[6] Marqués, Ricardo, Francisco Mesa, Jesus Martel, and Francisco Medina, "Comparative analysis of edge-and broadside-coupled split ring resonators for metamaterial design-theory and experiments," IEEE Transactions on antennas and propagation ,vol.51, no.10, pp.2572-2581, 2003.

[7] Baena, Juan Domingo, Jordi Bonache, Ferran Martin, R. Marqués Sillero, Francisco Falcone, Txema Lopetegi, Miguel AG Laso, "Equivalent-circuit models for split-ring resonators and complementary split-ring resonators coupled to planar transmission lines," IEEE transactions on microwave theory and techniques, vol 53, no.4, pp.1451-1461, 2005.

[8] Lee, Yoonjae, and Yang Hao, "Characterization of microstrip patch antennas on metamaterial substrates loaded with complementary split- ring resonators," Microwave and Optical Technology Letters, vol.50, no.8, pp. 2131-2135, 2008.

[9] Zhang, Hui, You-Quan Li, Xi Chen, Yun-Qi Fu, and Nai-Chang Yuan, "Design of circular/dual-frequency linear polarization antennas based on the anisotropic complementary split ring resonator," IEEE Transactions on Antennas and Propagation, vol. 57, no.10, pp.3352-3355, 2009.

[10] Niu, J-X, "Dual-band dual-mode patch antenna based on resonant-type metamaterial transmission line," Electronics letters,vol.46, no.4, pp.266-268, 2010.

[11] Joshi, J. G., Shyam S. Pattnaik, Swapna Devi, and M. R. Lohokare, "Electrically small patch antenna loaded with metamaterial," IETE Journal of Research, vol.56, no.6, pp.373-379, 2010.

[12] Cao, Wenquan, Yang Xiang, Bangning Zhang, Aijun Liu, Tongbin Yu, and Daosheng Guo, "A low-cost compact patch antenna with beam steering based on CSRR-loaded ground," IEEE Antennas and Wireless Propagation Letters, vol.10, pp.1520-1523, 2011.

[13] Dong, Yuandan, and Tatsuo Itoh, "Miniaturized patch antennas loaded with complementary split-ring resonators and reactive impedance surface," Antennas and Propagation (EUCAP), Proceedings of the 5th European Conference on. IEEE, 2011.

[14] Ortiz, N., F. Falcone, and M. Sorolla, "Enhanced gain dual band patch antenna based on complementary rectangular split- ring resonators," Microwave and Optical Technology Letters, vol.53, no.3,pp. 590-594, 2011.

[15] Xie, Yihong, Long Li, Cheng Zhu, and Chang-Hong Liang, "A novel dual-band patch antenna with complementary split ring resonators embedded in the ground plane," Progress In Electromagnetics Research ,vol.25, pp.117-126, 2012.

[16] Ha, Jaegeun, Kyeol Kwon, Youngki Lee, and Jaehoon Choi, "Hybrid mode wideband patch antenna loaded with a planar metamaterial unit cell," IEEE Transactions on Antennas and Propagation, vol.60, no.2, pp.1143-1147, 2012.

[17] Ortiz, Noelia, Francisco Falcone, and Mario Sorolla, "Gain improvement of dual band antenna based on complementary rectangular split-ring resonator," ISRN Communications and Networking, vol.3, 2012.

[18] Malik, Jagannath, and Machavaram Venkata Kartikeyan, "Metamaterial inspired patch antenna with L-shape slot loaded ground plane for dual band (WiMAX/WLAN) applications," Progress In Electromagnetics Research, vol.31, pp.35-43, 2012.

[19] Dong, Yuandan, Hiroshi Toyao, and Tatsuo Itoh, "Design and characterization of miniaturized patch antennas loaded with complementary split-ring resonators," IEEE Transactions on Antennas and Propagation,vol. 60, no.2, pp. 772-785, 2012.

[20] Basaran, S. C., Ulgur Olgun, and Kubilay Sertel. "Multiband monopole antenna with complementary split-ring resonators for WLAN and WiMAX applications," Electronics Letters, vol.49, no.10, pp.636-638, 2013.

[21] Sarkar, Debdeep, Kushmanda Saurav, and Kumar Vaibhav Srivastava,"Design of a novel dual-band microstrip patch antenna for WLAN/WiMAX applications using complementary split ring resonators and partially defected ground structure," Progress In Electromagnetics Research Symposium proceedings, 2013.

[22] Liang, J.G., Song, Z.J., Yu, L.J. and Zhang, X.F, "A Novel Tri-band Patch Antenna Based on Complementary Triangle Split Ring Resonator Pair," PIERS Proceedings, 2014.

[23] Ortiz, Noelia, Juan Carlos Iriarte, Gonzalo Crespo, and Francisco Falcone, "Design and implementation of dual-band antennas based on complementary split ring resonators." Waves in Random and Complex Media 25.3 (2015): 309-322.

[24] Ali, Wael, Ehab Hamad, Mohamed Bassiuny, and Mohamed Hamdallah, "Complementary split ring resonator based triple band microstrip antenna for WLAN/WiMAX applications," Radioengineering, vol.26, no.1, pp. 78-84, 2017.

[25] Bassiuny, Mohamed A., Ehab KI Hamad, Wael A. Aly, and Mohamed ZM Hamdallah, "Dual-band microstrip antenna for WiMAX applications using complementary split ring resonators," Radio Science Conference (NRSC)- 2016 33rd National. IEEE, 2016.

[26] Tang, Ming-Chun, Hao Wang, Li Guo, Xiaoping Zeng, Hong Liu, and Youbing Pang, "A Compact Dual-Band Patch Antenna Design Based on Single-Ring Split Ring Resonator," Applied Computational Electromagnetics Society Journal, vol.31, no.3 ,2016.

[27] Lai, Anthony, Tatsuo Itoh, and Christope Caloz, "Composite right/left-handed transmission line metamaterials," IEEE microwave magazine, vol.5, no.3, pp.34-50, 2004.

[28] Park, Jae-Hyun, Young-Ho Ryu, Jae-Gon Lee, and Jeong-Hae Lee, "Epsilon negative zeroth-order resonator antenna," IEEE Transactions on Antennas and Propagation, vol. 55,no.12, pp.3710-3712, 2007.

[29] Herraiz-Martinez, Francisco Javier, Vicente Gonzalez-Posadas, Luis Enrique Garcia-Munoz, and Daniel Segovia-Vargas, "Multifrequency and dual-mode patch antennas partially filled with left-handed structures," IEEE Transactions on Antennas and Propagation, vol.56,no.8, pp.2527-2539, 2008.

[30] Xiong, Jiang, Hui Li, Yi Jin, and Sailing He, "Modified ${\rm TM} _ {020} $ Mode of a Rectangular Patch Antenna Partially Loaded With Metamaterial for Dual-Band Applications," IEEE Antennas and wireless Propagation letters, vol.8, pp. 1006-1009, 2009.

[31] Dong, Yuandan, Hiroshi Toyao, and Tatsuo Itoh, "Compact circularly-polarized patch antenna loaded with metamaterial structures," IEEE transactions on antennas and propagation, vol.59, no.11, pp.4329-4333, 2011.

[32] Lee, Cherl-Hee, Jonghun Lee, Dong-Sik Woo, and Kang-Wook Kim, "Design of a composite right/left-handed transmission line unit-cell for a U-shaped mushroom ZOR antenna based on left-handed metamaterials," Journal of the Korean Physical Society, vol. 61, no.10, pp. 1633-1635, 2012.

[33] Seung-Tae, Byung-Chul Park, and Jeong-Hae Lee. "Dual-band circularly polarized patch antenna with first positive and negative modes." IEEE Antennas and Wireless Propagation Letters, vol. 12, pp: 1165-1168, 2013.

[34] Nasimuddin, Qing Xianming, and Zhi Ning Chen, "A compact circularly polarized slotted patch antenna for GNSS applications," IEEE Transactions on Antennas and Propagation, vol.62, no.12, pp.6506-6509, 2014.

[35] Saurav, Kushmanda, Debdeep Sarkar, and Kumar Vaibhav Srivastava, "Dual-polarized dual-band patch antenna loaded with modified mushroom unit cell," IEEE Antennas and Wireless Propagation Letters, vol.13, pp.1357-1360, 2014.

[36] Seung-Tae, and Jeong-Hae Lee. "Hybrid Zeroth-Order Resonance Patch Antenna with Broad E Plane Beamwidth." IEEE Transactions on Antennas and Propagation, vol. 61, no. 1, pp: 19-25, 2013.

[37] Zong, Binfeng, Guangming Wang, Cheng Zhou, and Yawei Wang, "Compact low-profile dual-band patch antenna using novel TL-MTM structures," IEEE Antennas and Wireless Propagation Letters, vol.14, pp.567-570, 2015.

[38] Dai, Xi-Wang, Tao Zhou, and Guan-Feng Cui, "Dual-band microstrip circular patch antenna with monopolar radiation pattern," IEEE Antennas and Wireless Propagation Letters, vol.15, pp.1004-1007, 2016.

[39] Basilio, Lorena I., Jeffery T. Williams, David R. Jackson, and Michael A. Khayat, "A comparative study of a new GPS reduced-surface-wave antenna," IEEE Antennas and wireless propagation letters, vol.4, no.1, pp. 233-236, 2005.

[40] Lai, Anthony, Kevin MKH Leong, and Tatsuo Itoh, "Infinite wavelength resonant antennas with monopolar radiation pattern based on periodic structures," IEEE transactions on antennas and propagation, vol.55, no.3, pp.868-876, 2007.

[41] Park, Jae-Hyun, Young-Ho Ryu, Jae-Gon Lee, and Jeong-Hae Lee, "Epsilon negative zeroth-order resonator antenna," IEEE Transactions on Antennas and Propagation, vol.55, no.12, pp.3710-3712, 2007.

[42] Lee, Jae-Gon, and Jeong-Hae Lee, "Zeroth order resonance loop antenna," IEEE Transactions on Antennas and Propagation, vol.55, no.3, pp.994-997, 2007.

[43] Tang, Hangfei, and Xiaopeng Zhao, "Center- fed circular Epsilon- negative zeroth- order resonator antenna," Microwave and Optical Technology Letters, vol.51, no.10, pp. 2423-2428, 2009.

[44] Yoo, Seongryong, and Sungtek Kahng, "CRLH ZOR antenna of a circular microstrip patch capacitively coupled to a circular shorted ring," Progress In Electromagnetics Research, vol.25, pp. 15-26, 2012.

[45] Hou, Quanwen, Hangfei Tang, Yahong Liu, and Xiaopeng Zhao, "Dual-frequency and broadband circular patch antennas with a monopole-type pattern based on epsilon-negative transmission line." IEEE Antennas and Wireless Propagation Letters, vol.11, pp.442-445, 2012.

[46] Majedi, Mohammad Saeed, and Amir Reza Attari, "Dual-band resonance antennas using epsilon negative transmission line," IET Microwaves, Antennas & Propagation, vol.7, no.4, pp. 259-267, 2013.

[47] Wan Y. T, F. S Zhang, "Dual-band dual-polarised square patch antennas using shorting metallic cylinder." Electronics letters, vol. 48, no.13, pp. 747-749, 2012.

[48] Hong, Youngtaek, Jinpil Tak, and Jaehoon Choi, "Dual-band dual-mode patch antenna for on–on–off WBAN applications," Electronics Letters, vol.50, no.25 pp. 1895-1896, 2014.

[49] Saghanezhad, Seyed Amir Hossein, and Zahra Atlasbaf, "Miniaturized dual-band CPW-fed antennas loaded with U-shaped metamaterials," IEEE antennas and wireless propagation letters, vol.14, pp. 658-661, 2015.

[50] Jimenez-Martin, Jose L, Angel Parra-Cerrada, Raul Fernandez-Recio, Daniel Segovia-Vargas, Lino Garcia, and Vicente Gonzalez-Posadas, "Dual band and dual polarization short-circuited ring patch antenna," Journal of Electromagnetic Waves and Applications, vol.30, no.9, pp. 1198-1206, 2016.

[51] Banerjee, Soumen, Biswarup Rana, and Susanta Kumar Parui. "SIW based compact and dual-band equilateral triangular antennas." Journal of Electromagnetic Waves and Applications, vol.30, no.5, pp.637-650, 2016.

[52] Cao, Wen-Quan, "Compact dual-band dual-mode circular patch antenna with broadband unidirectional linearly polarized and omnidirectional circularly polarized characteristics," IET Microwaves, Antennas & Propagation, vol.10, no.2, pp.223-229, 2016.

[53] Zhang, Xiao, and Lei Zhu, "Gain-Enhanced Patch Antenna without Enlarged Size via Loading of Slot and Shorting Pins," IEEE Transactions on Antennas and Propagation, vol.65, no.11, pp.5702-5709, 2017.

[54] Pal, Arpan, Amit Mehta, Dariush Mirshekar-Syahkal, and Hisamatsu Nakano, "A Twelve-Beam Steering Low-Profile Patch Antenna With Shorting Vias for Vehicular Applications," IEEE Transactions on Antennas and Propagation, vol.65, no.8,pp. 3905-3912, 2017.

[55] Cao, Wen-quan, Qian-qian Wang, Bang-ning Zhang, and Wei Hong, "Capacitive probe-fed compact dual-band dual-mode dual-polarization microstrip antenna with broadened bandwidth," IET Microwaves, Antennas & Propagation, vol.11, no.7 pp.1003-1008, 2017.

[56] Guo, E., Juhua Liu, and Yunliang Long, "A Mode-Superposed Microstrip Patch Antenna and Its Yagi Array with High Front-to-Back Ratio," IEEE Transactions on Antennas and Propagation, vol.65, no.12, pp.7328-7333, 2017.

[57] Liu, Ankang, Yilong Lu, and Ling Huang. "Low-profile patch antennas with enhanced horizontal omnidirectional gain for DSRC applications." IET Microwaves, Antennas & Propagation, vol. 12, no. 2, pp. 246-253, 2017.

[58] Buell, K., D. Cruickshank, H. Mosallaei, and Kamal Sarabandi, "Patch antenna over RIS substrate: A novel miniaturized wideband planar antenna design," Antennas and Propagation Society International Symposium, 2003. IEEE. Vol. 4. IEEE, 2003.

[59] Mosallaei, Hossein, and Kamal Sarabandi, "Antenna miniaturization and bandwidth enhancement using a reactive impedance substrate," IEEE Transactions on Antennas and Propagation, vol.52, no.9, pp. 2403-2414, 2004.

[60] Goussetis, George, Alexandros P. Feresidis, and John C. Vardaxoglou, "Tailoring the AMC and EBG characteristics of periodic metallic arrays printed on grounded dielectric substrate," IEEE Transactions on Antennas and Propagation vol.54, no.1, pp.82-89, 2006.

[61] Hosseini, Mehdi, and Mohammad Hakkak, "Characteristics estimation for jerusalem cross-based artificial magnetic conductors," IEEE Antennas and wireless propagation letters vol.7, pp.58-61, 2008.

[62] Dong, Yuandan, Hiroshi Toyao, and Tatsuo Itoh, "Compact circularly-polarized patch antenna loaded with metamaterial structures," IEEE transactions on antennas and propagation vol.59, no.11, pp. 4329-4333, 2011.

[63] Chen, Hsing-Yi, and Yu Tao, "Performance improvement of a U-slot patch antenna using a dual-band frequency selective surface with modified Jerusalem cross elements," IEEE Transactions on antennas and Propagation vol.59, no.9, pp.3482-3486, 2011.

[64] Bernard, Loïc, G. Chertier, and Ronan Sauleau, "Wideband circularly polarized patch antennas on reactive impedance substrates," IEEE Antennas and Wireless Propagation Letters vol.10, pp.1015-1018, 2011.

[65] Agarwal, Kush, and Arokiaswami Alphones, "RIS-based compact circularly polarized microstrip antennas, " IEEE Transactions on Antennas and Propagation vol.61, no.2, pp.547-554, 2013.

[66] Agarwal, Kush, Tanuja Mishra, Muhammad Faeyz Karim, Michael Ong Ling Chuen, Yong Xin Guo, and Sanjib Kumar Panda, "Highly efficient wireless energy harvesting system using metamaterial based compact CP antenna," Microwave Symposium Digest (IMS), 2013 IEEE MTT-S International. IEEE, 2013.

[67] Xu, He-Xiu, Guang-Ming Wang, Jian-Gang Liang, Mei Qing Qi, and Xi Gao, "Compact circularly polarized antennas combining meta-surfaces and strong space-filling meta-resonators," IEEE Transactions on Antennas and Propagation vol.61, no.7, pp. 3442-3450, 2013.

[68] Agarwal, Kush, and Arokiaswami Alphones, "Triple-band compact circularly polarised stacked microstrip antenna over reactive impedance meta-surface for GPS applications," IET Microwaves, Antennas & Propagation vol.8, no.13, pp.1057-1065, 2014.

[69] Cai, Tong, Guang-Ming Wang, Xiao-Fei Zhang, and Jun-Peng Shi,"Low-profile compact circularly-polarized antenna based on fractal metasurface and fractal resonator," IEEE Antennas and Wireless Propagation Letters vol.14, pp.1072-1076, 2015.

[70] Ta, Son Xuat, and Ikmo Park, "Low-profile broadband circularly polarized patch antenna using metasurface," IEEE Transactions on Antennas and Propagation vol.63, no.12, pp.5929-5934, 2015.

[71] Rajesh, Galaba Sai, K. Venkata Kishore, and Vijay Kumar, "Multiband microstrip patch antenna design using metamaterial for airborne SAR system," Signal Processing, Informatics, Communication and Energy Systems (SPICES), 2015 IEEE International Conference on. IEEE, 2015.

[72] Nasimuddin, N., Zhi Ning Chen, and Xianming Qing, "Bandwidth Enhancement of a Single-Feed Circularly Polarized Antenna Using a Metasurface: Metamaterial-based wideband CP rectangular microstrip antenna," IEEE Antennas and Propagation Magazine vol.58, no.2, pp.39-46, 2016.

[73] Ren, Junyi, Shuxi Gong, and Wen Jiang, "Low-RCS Monopolar Patch Antenna Based on a Dual-Ring Metamaterial Absorber," IEEE Antennas and Wireless Propagation Letters vol.17, no.1, pp.102-105, 2018.

[74] Gupta, Krashnkant, and Binod Kumar Kanaujia, "Miniturization and bandwidth enhancement of microstrip patch antenna using artificial ground structure," Industrial and Information Systems (ICIIS), 2014 9th International Conference on. IEEE, 2014.

[75] Ren, C., Loïc Bernard, and Ronan Sauleau, "Investigations and design of small-size printed antennas on a reactive impedance substrate," Antennas and Propagation (EuCAP), 2010 Proceedings of the Fourth European Conference on. IEEE, 2010.

[76] Jarchi, S., J. Rashed-Mohassel, and R. Faraji-Dana, "Analysis of microstrip dipole antennas on a layered metamaterial substrate," Journal of Electromagnetic Waves and Applications vol.24, no.5-6, pp.755-764, 2010.

[77] Sievenpiper, Dan, Lijun Zhang, Romulo FJ Broas, Nicholas G. Alexopolous, and Eli Yablonovitch, "High-impedance electromagnetic surfaces with a forbidden frequency band," IEEE Transactions on Microwave Theory and techniques vol.47, no.11, pp. 2059-2074, 1999.

[78] Bao, Xiu Long, Giuseppe Ruvio, and Max J. Ammann. "Directional dual-band slot antenna with dual-bandgap high-impedance-surface reflector." Progress In Electromagnetics Research, vol. 9, pp. 1-11, 2009.

[79] Moustafa, Lina, and Bernard Jecko, "Design of a wideband highly directive EBG antenna using double-layer frequency selective surfaces and multi feed technique for application in the Ku-band," IEEE Antennas and Wireless Propagation Letters vol.9 pp.342-346, 2010.

[80] Cao, W.Q., Zhang, B.N., Yu, T.B., Liu, A.J., Zhao, S.J., Guo, D.S. and Song, Z.D, "Single-feed dual-band dual-mode and dual-polarized microstrip antenna based on metamaterial structure," Journal of Electromagnetic Waves and Applications vol.25, no.13, pp.1909-1919, 2011.

[81] Roseline, A. Ameelia, K. Malathi, and A. K. Shrivastav, "Enhanced performance of a patch antenna using spiral-shaped electromagnetic bandgap structures for high-speed

wireless networks," IET microwaves, antennas & propagation vol.5, no.14, pp.1750-1755, 2011.

[82] Costa, Filippo, Olli Luukkonen, Constantin R. Simovski, Agostino Monorchio, Sergei A. Tretyakov, and Peter M. de Maagt, "TE surface wave resonances on high-impedance surface based antennas: Analysis and modeling," IEEE Transactions on Antennas and Propagation vol.59, no.10, pp.3588-3596, 2011.

[83] Sarrazin, Julien, Anne-Claire Lepage, and Xavier Begaud, "Circular high-impedance surfaces characterization," IEEE Antennas and Wireless Propagation Letters vol.11 pp.260-263, 2012.

[84] SalarRahimi, Marzieh, J. Rashed-Mohassel, and M. Edalatipour, "Radiation properties enhancement of a GSM/WLAN microstrip antenna using a dual band circularly symmetric EBG substrate," IEEE Transactions on Antennas and Propagation vol.60, no.11, pp.5491-5494, 2012.

[85] Cao, Wenquan, Bangning Zhang, Aijun Liu, Tongbin Yu, Daosheng Guo, and Xiaofei Pan, "Multi-frequency and dual-mode patch antenna based on electromagnetic band-gap (EBG) structure," IEEE Transactions on Antennas and Propagation vol.60, no.12, pp.6007-6012, 2012.

[86] Ghosh, Soham, Thanh-Ngon Tran, and Tho Le-Ngoc, "Dual-layer EBG-based miniaturized multi-element antenna for MIMO systems," IEEE Transactions on Antennas and Propagation vol.62, no.8, pp.3985-3997, 2014.

[87] Liu, Wei, Zhi Ning Chen, and Xianming Qing, "Metamaterial-based low-profile broadband mushroom antenna," IEEE Transactions on Antennas and Propagation vol.62, no.3, pp.1165-1172, 2014.

[88] Jaglan, Naveen, and Samir Dev Gupta, "Surface waves minimization in Microstrip Patch antenna Using EBG substrate," IEEE International Conference on Signal Processing and Communication (ICSC), 2015.

[89] Chandrasekaran, Karthik T., Muhammad Faeyz Karim, and Arokiaswami Alphones. "CRLH structure-based high-impedance surface for performance enhancement of planar antennas," IET Microwaves, Antennas & Propagation vol.11, no.6, pp.818-826, 2016.

[90] Wenwen yang, Jianyi Zhou, Zhiqiang yu "Single-fed low profile broadband circularly polarized stacked patch antenna." IEEE Transactions on Antennas and Propagation, vol. 62, no.10, pp. 5406-5410, 2014.

[91] Kovitz, Joshua M., Harish Rajagopalan, and Yahya Rahmat-Samii. "Circularly polarised half E-shaped patch antenna: a compact and fabrication-friendly design." IET Microwaves, Antennas & Propagation, vol. 10, no. 9, pp. 932-938, 2016.

[92] Luo, J. Y., A. Alphones, and C. Jin. "Microstrip square patch antenna with arc shaped edges for circular polarization." IEEE Asia-Pacific Microwave Conference Proceedings (APMC), 2011.

[93] Anjani, Y. S., and A. Alphones. "A wide-beam circularly polarized asymmetric-microstrip antenna." IEEE Transactions on Antennas and Propagation, vol. 63, no. 8, pp. 3764-3768, 2015.

[94] Karim, Muhammad Faeyz, and A. Alphones. "A low-profile dual-band circularly polarized GPS antenna." IEEE Asia-Pacific Microwave Conference Proceedings (APMC), 2016.

[95] http://sci-hub.tw/http://link.springer.com/chapter/10.1007/978-3-319-66044-8_1.

[96] http://www.emtalk.com/tut_3.htm.

[97] https://www.slideshare.net/cocho/metamateriales.

[98] Yan, Sen, Ping Jack Soh, and Guy AE Vandenbosch. "Compact all-textile dual-band antenna loaded with metamaterial-inspired structure." IEEE Antennas and Wireless Propagation Letters, vol. 14, pp. 1486-1489, 2015.

[99] Wang, Jin, et al. "Crashworthiness behavior of Koch fractal structures." Materials & Design, vol. 144, pp. 229-244, 2018.

[100] Sankaralingam, S., et al. "Use of Minkowski Fractal Geometry for the Design of Wearable Fully Fabric Compact Antenna." (2014).

List of Publications

International Journals

1) **Nelaturi, Suman,** and N. V. S. N. Sarma**. "CSRR based patch antenna for Wi-Fi and WiMAX Applications."** Advanced Electromagnetics 7.3 (2018): 40-45.

2) **Nelaturi, Suman,** and Nookala Venkata Satya Narasimha Sarma**. "A Compact Microstrip Patch Antenna Based on Metamaterials for Wi-Fi and WiMAX Applications."** Journal of Electromagnetic Engineering and Science 18.3 (2018): 182-187.

3) **Nelaturi, Suman**, and N. V. S. N. Sarma. "**Dual Band Circular Patch Antenna based on Metamaterials**." International Journal of Advances in Microwave Technology 3 (2018).

International Conferences

1) Suman Nelaturi, NVSN Sarma"**HIS Based Circularly Polarized koch Fractal Boundary Microstrip Antenna**" has been published in Proceedings of "International conference on Telecommunication Technology and Management (**ICTTM-2015**) held at **IIT Delhi**, April 2015.

2) Suman **Nelaturi**, NVSN Sarma "**HIS Based Poly Fractal Boundary Microstrip Antenna"** has been published in Proceedings of IEEE Indian Antenna Week **2015 (IAW 2015)** held at **Government Engineering College Ajmeer**, Rajasthan, India May 2015.

3) Suman Nelaturi, NVSN Sarma"**HIS Based Asymmetrical Fractal Boundary Microstrip Patch Antenna"** has been published in Proceedings of **INCEMIC 2015** held at **Andhra University**, Visakhapatnam, India July 2015.

4) Suman **Nelaturi**, NVSN Sarma"**Dual band dual polarized circular patch antenna loaded with circular mushroom unit cell"** " has been published in Proceedings of "9th International conference Antenna Test & Measurement Society **(ATMS 2016)**" during Feb 2^{nd}-3^{rd} 2016 held at Goa, India.

5) Suman **Nelaturi**, NVSN Sarma"**HIS based dual band dual polarized Minkowski fractal patch antenna"** has been published in Proceedings of "**APMC -2016**" held at Delhi, India during 5^{th} – 9^{th} Dec 2016.

6) Suman **Nelaturi**, NVSN Sarma"**Dual Band Dual Polarized Koch fractal boundary patch antenna based on Metamaterials**" has been published in Proceedings of "10^{th} International conference Antenna Test & Measurement Society (**ATMS 2017**)" held at Hyderabad, India during 6^{th} -8^{th} Feb 2017.